A REVIEW OF AERONAUTICAL FATIGUE INVESTIGATIONS IN SWEDEN DURING THE PERIOD JUNE 1999 TO MAY 2001

EDITED BY ANDERS F. BLOM AND BJÖRN PALMBERG

Swedish Defence Research Agency, FOI
The Aeronautics Division, FFA, Sweden

(FOI-R--0138--SE)

CONTENTS

3.1 INTRODUCTION

In this paper a review is given of the work carried out in Sweden in the area of aeronautical fatigue during the period June 1999 to May 2001. The review includes aircraft loading actions, basic studies of fatigue development in metals and composites, stress analysis and fracture mechanics, studies of crack propagation and residual strength, testing of joints and full-scale structures, and fatigue life predictions. A reference list of relevant papers issued during the period covered by the review is included. Throughout this review references are made to the earlier Swedish ICAF review, Ref. [1].

Contributions to the present review are from the following sources:

- The Swedish Defence Research Agency (FOI), Aeronautics Division, FFA
  Sections 3.4.1, 3.6.1, 3.6.2, 3.6.3, 3.6.4, 3.7.1, 3.7.2, 3.7.3, 3.7.4, 3.8.1, 3.8.2, 3.8.5, 3.8.6, 3.8.7, 3.8.8, 3.8.9, 3.8.10, 3.8.11, 3.8.12, 3.8.13

- The SAAB Company
  Sections 3.2.1, 3.3.1, 3.5.1, 3.5.2, 3.5.3, 3.5.4, 3.5.5, 3.5.6, 3.8.3 and 3.8.4

- The Royal Institute of Technology (KTH)
  Section 3.4.2

3.2 AIRCRAFT LOADS

3.2.1 Service Life Monitoring of Gripen Aircraft

The expected usage variability and the fact that the airframe is designed for one specific usage spectrum makes up an urgent need for procedures to monitor the actual usage of individual aircraft. The aspect of a loads monitor system affects both flight safety requirements and cost efficient maintenance procedures. There are several methods and procedures in use to handle the tracking of real service loads. There are two main principles for service loads monitoring. One is founded on direct measurements of loads using calibrated strain gauge installations while the other makes use of recorded flight parameters and a theoretical model to calculate the loads indirectly. The first method has its advantage in the direct recording of loads in pre-selected vital structures. The main disadvantage is that other structures are not monitored at all. The main advantage with the second method is that the whole structure covered by the loads model can be handled. The disadvantages are that the load model can be unreliable for some structures or load cases and that it does not to pick up unpredicted vibrations. A mix of the two systems is sometimes preferred.

The loads monitor system for Gripen is shown in Figure 1. The measured structure and load entities are:
- Vertical load factor in the c.g. of the aircraft
- Wing root bending moment measured in the forward attachments of the left wing
- Canard bending moment measured in the left pivot
- Canard torque measured in the left pivot
- Fin bending moment measured in the rear attachments
- Elevon torques
- Pylon loads

The wing, canard and fin bending moments are all measured by strain-gauge bridges while the other loads are derived from sampled flight parameter data. It should be pointed out that all measured entities are global loads and not local hot-spot stresses.

The analogue signals from the strain-gauge bridges are amplified and low-pass filtered. The signals are subsequently sampled and digitized and thereafter scaled and discretisized into specified intervals. Range-pair-range cycles are identified and counted and stored into a matrix for each entity. The matrixes are finally down-loaded after a certain number of flights, typically 3 to 5.

The service experience from the strain-gauge installations is so far very good. One might be concerned about mechanical failures of the gauges but so far have no breakdowns at all occurred in the current fleet of about 90 aircraft and 10,000 flh. The strain-gauge installation on one of the wing attachments is shown in Figure 2.

The strain-gauge bridges need however to be regularly calibrated. For Gripen this is done during flight every 200 hours of flying. The pilot activates a calibration mode of the loads monitor system while flying specified manoeuvres. New strain-gauge factors are calculated which replace the previous ones. The calibration manoeuvres were defined during flight tests with the test aircraft (#2) dedicated to load measurements. The strain-gauge bridges on the wing and canard foreplane are calibrated during turning manoeuvres with increasing load factor and the bridges on the fin while flying in a knife-edge attitude.

The initial attempt was to use strain-gauge bridges also for monitoring the elevon loading. The idea was to obtain the elevon loading by using the torque of the wing, measured in a vertical wing shear link in a rear intersection with the fuselage. This way turned out to be difficult to accomplish due to several reasons of which one was to define a suitable calibration manoeuvre. Other attempts to measure the elevon torque in a more direct manner, e.g. by measuring the actuator force, did also turn out to be impractical.

The way forward was instead to shift to flight parameter monitoring and a loads model to calculate the elevon loading. The model has been developed and verified by data from instrumented actuators in the loads test aircraft.

The pylons need also to be monitored. The pylon loads are however almost impossible, and very impractical to record directly by means of strain-gauge bridges. Several loads and moments contribute to the primary loading conditions in critical sections of the individual pylons. The only way forward has been to develop load models with flight parameters and other logistic parameters as input. The development and verification work of the models is not yet finished but besides typical flight parameters, logistic parameters such as stores in each pylon, release of stores, amount of fuel in individual tanks etc. play important roles.

The above description of Gripen loads monitor system is extracted from reference [2]. The reference contains also a general discussion about load spectrum variability to be expected in 4:th generation combat aircraft.

3.3 FATIGUE LIFE TESTING AND PREDICTION

3.3.1 Fatigue of HSM Aluminium Specimens

Fatigue tests of notched HSM (High Speed Machining) specimens of plate alloy AA7010-T74 have shown fatigue strength lower than that of conventionally milled specimens. The difference at HSM cutting speed 1800 m/min was minus 15 % on stress in constant amplitude loading, which is similar to what was found on flat specimens sectioned from frame pocket walls into plates made by down cut milling. The tested notch was simulating the bottom radius of the frame pockets. Loading with FALSTAFF spectrum, the HSM had about one third of the No of Flights achieved by the conventional milling. Loading with a symmetrical spectrum of fin bending, the difference was reduced to almost zero. Characterization of the microstructure in the surface layers by residual stress measurements and other laboratory methods are used to explain the fatigue degradation by HSM. Figures 3 and 4.

3.4 JOINTS

3.4.1 Mechanical Joints

In a number of Swedish national ICAF reviews the results of the quasi-static and fatigue testing of different mechanical joints have been reported. The aim of the testing has been to measure directly or indirectly a number of parameters, which influence the fatigue life of joints with shear loaded fasteners. Joints with low, medium and high load transfer have been studied as well as joints with low and high secondary bending. Different fastener systems have been investigated.

In these experiments there are parameters which are not possible to measure during the testing. One such parameter is the local relative motion between the mating surfaces of the joined plates. In order to investigate the effect of fastener clamping force, fastener fit and surface friction on the load transfer, first principal stress and energy dissipation from local slipping in the faying surface a finite element model was developed, Ref. [3].

A simple lap joint with two fastener columns and two fastener rows was used for the analysis. The aluminium alloy 2024-T3 was selected for the plates and the fasteners were assumed to be of titanium alloy. The same joint configuration had previously been tested extensively. The fasteners, in the model, were countersunk using a ∅5 mm Hi-Lok fastener as reference. The plate thickness was 3 mm and the plate width 50 mm. Symmetry was assumed with respect to the longitudinal centre line of the lap joint.

The finite element model was built from 3D brick elements. Contact modelling was applied to all mating surfaces using the small-sliding formulation available in ABACUS. Isotropic friction was assumed using a Coulomb friction model with the same coefficient of friction in all directions. However, the coefficient of friction was initially set to 0.65 for the area close to the fastener hole and to 0.25 for all the other areas in contact. The specification of clearance or grip inside fastener holes is made through a clearance option in ABACUS which ramps the relative distance between the master and slave surfaces from zero to the desired grip during the first load step.

The tightening of the fasteners was based on an ABACUS function called pre-tension. This function allows the axial load in the fastener to change during the external loading. As for the fastener grip the fastener tightening is achieved during the first load step and fixed at the beginning of the second load step. The first load step refers to a linearly increasing fastener load which reaches its maximum after one second. The second load step refers to the external loading on the lap joint. The external load was increased linearly from zero to 30 kN introducing a far field stress of 200 MPa. This process took 1 second. Finally, during the third load step, which also took 1 second, the lap joint was unloaded to zero external load. The time scale has no influence on the results since none of the constitutive parameters used was time dependent. The time scale was just used as a way to increment the loading.

Firstly, a linear elastic analysis was made using a fastener clamping force of 5 kN, 50 μm interference fit and a coefficient of friction equal to 0.65 for the area close to the fastener hole. This analysis was the referred to as the reference case. For elastic material properties the load transfer by the fasteners at maximum external load was nearly the same, 36 %, for the two fastener rows. Using elastic ideally plastic material properties the load transfer at maximum external load was slightly higher, 41 % for the first row and 39 % for the second row. Furthermore, it was primarily in the regions close the holes that the first principal stress was influenced by the choice of material properties. Also, it was concluded that the elastic ideally plastic material model was not stiff enough for the maximum load level and that a strain hardening model should have been included.

The fastener clamping force influences the load transfer. Using the elastic material model the load transfer for a clamping force of 2 kN became 44 % for each fastener row. The first principal stress distribution, close to the holes, is influenced by the fastener clamping force. However, the change in first principal stress distribution does not explain the change in crack initiation site due to differences in clamping force, observed in the experiments.

The coefficient of friction influences the load transfer. Increasing the coefficient of friction, in the region close to the holes, from 0.65 to 1.0 resulted in a reduction of the load transfer by the fastener rows from 36 % to 28 %. The first principal stress distribution is changed mainly in front of and behind the fastener holes as a result of changing the coefficient of friction.

The fastener fit influences the load transfer. A neat fit results in a load transfer of 41 % for each fastener row as compared to the 36 % obtained with a 50 μm interference fit. The regions on the faying surface where the change in fastener fit influences the first principal stress field are mainly behind and at each side of the fastener holes.

The influence of the different parameters on the fastener row load transfer has been summarised in Figure 5.

The contact pressure, in the faying surface, near each fastener hole and in absence of the external load has been studied for two different fastener clamping forces, 0.5 kN and 5.0 kN. The maximum contact pressure became 17.5 MPa for the low clamping force and 193MPa for the high clamping force. In both cases the radius of the circular area, in the faying surface, which is influenced by the clamping force is approximately twice the hole radius.

The displacement fields, in the faying surface, for two successive time steps have been subtracted from each other such that an average incremental displacement field was created. This displacement field was then multiplied by the average shear stress for the corresponding time step. The result is a measure of the incremental energy dissipation. During loading, at 46 % of the maximum external load, the maximum energy dissipation (for the assumed friction model and selected clamping force of 5 kN) is located slightly in front of and to the two sides of the fastener hole. These two locations almost coincide with the locations where crack initiation has occurred during fatigue loading.

3.4.2 Fatigue of Composite Joints

Since modern aircraft composite structures often are fastened by means of bolted joints, the structural integrity of such connections has to be validated according to the certification requirements. The behaviour of full-scale composite structures can be represented on sub-structural elements including mechanically fastened joints. Therefore, the behaviour of composite joints during static and fatigue loading has to be well understood. Two projects on the static strength and fatigue performance of composite bolted joints have been completed recently. The main objectives of the projects were to obtain experimental data on the joint resistance to quasi-static and fatigue loading. The influences of different configurations of joints, lay-ups, fastener systems on the joint static strength and fatigue performance were studied. Strain gauge measurements were carried out in order to measure strain distribution and to calculate load transfer between bolt rows. Bolt-movement measurements were done in order to study the local behaviour of the bolt and the surrounding composite. Fractographic SEM and optical microscopy were employed to investigate fracture and damage developed in the joint system during static and fatigue loading.

The first project deals with CFRP laminates joined by protruding-head bolts (hexagon bolts). Four different configurations of these joints are shown in Figure 6.

Specimens shown in Figure 6(a) were manufactured using two lay-ups, that is quasi-isotropic ($[\pm45/0/90]_{3s}$ and $[\pm45/0/90]_{6s}$ for the outer and middle parts, respectively) and 0^{o}-dominated ($[\pm45/0/90/0_4/90/0_3]_s$ and $[\pm45/0/90/0_4/90/0_3]_{2s}$ for the outer and middle parts, respectively). The other types of joints had only the above quasi-isotropic lay-up. Elastic modulus in load direction, E_x, was equal to 51 and 99 GPa for composite plates with quasi-isotropic and 0^{o}-dominated lay-ups, respectively.

Three joints with the configuration shown in Figure 6(a) and two specimens of each one of the other configuration types were tested by tensile loading until failure of the joints occurred. One specimen of each configuration was subjected to compression loading. The other specimens were tested by fatigue loading with the stress ratio, $R = \sigma_{min}/\sigma_{max}$, equal to –1. The frequency of the fatigue loading cycles was limited by the maximum temperature limit of +33°C in the bolts. In order to prevent specimen bending, the joints were tested mounted in a lateral support consisting of two aluminium plates which were fastened by bolts and nuts to a finger tight torque.

The obtained quasi-static tensile and fatigue test results are presented in Figure 7(a) and (b). The obtained results from the compression tests together with detail information about the test procedure and other achieved results can be found in Ref.[4].

The obtained results suggest that the joints with six bolts and with a quasi-isotropic lay-up had the highest static strength and the longest fatigue life. The lowest quasi-static strength and fatigue durability were shown by the single-row joints. In the quasi-static tensile tests the dominant failure mode was net-section failure; whereas during the fatigue tests most of the joints failed due to fatigue fracture of bolts. As can be seen, the fatigue resistance of single and double lap joints bolted by six fasteners was similar. Specimens with more than two bolts usually failed after that at least two of the bolts had broken. The fatigue life results for those joints which failure mode was bolt fracture are re-plotted in Figure 7(c) in terms of the average bearing stress on one bolt versus number of cycles to failure. These results suggest a linear relationship between the number of bolts and the fatigue strength of joints. The linear dependence opens the possibility to calculate the fatigue life of composite joints. Once a specific configuration of joints has been tested, the fatigue life for other configurations can be estimated from the experimental curves (see Fig. 7(c)). However, the bolt diameter has to be the same for all configurations. This method works for all lay-ups as long as the failure mode is bolt failure since the specimens tested quasi-statically did not show the above relationship between the joint strength and their configuration (see Fig. 7(c)). This is due to the joint failure mode during the static tensile tests not being bolt failure, Ref.[4]. The interaction between two dominant failure modes, that is in static and fatigue, is discussed in Ref.[5].

As the obtained results on the load transfer between different bolt rows in Figure 8(a) show, one of the outer bolt rows (that is the first bolt row in the plot and the left row in Fig. 6(a)) was transferring a slightly larger part of the applied load during quasi-static loading than the other bolt rows, Ref.[4].

The same distribution of applied load between the bolt rows was found at the beginning of fatigue testing (see Fig. 8(b)). However, fatigue damage accumulated in the joints during the cyclic loading affected the load transfer of the bolt rows. It was observed that a reduction in the initial pre-stress in the bolts, fatigue degradation of the bolt holes, increase and decrease in the initial coefficient of friction between the composite plates, and fatigue failure of bolts had a significant influence on the load transfer in the bolted joints, Refs.[5,.6] The increased volume of damage at a bolt row would reduce the load transfer of this bolt row, and as a result, the other bolt rows would start to transfer more load than they did at the beginning of the fatigue loading.

As the achieved results on bolt-movement measurements showed, the bolt behaviour represented well the overall behaviour of composite joints. Using this method of measurements it was possible to analyse the influence of friction forces between the composite parts, bolt presence and its behaviour, and fatigue degradation of bolt holes on the joint behaviour during fatigue loading, Refs.[6, 7]. Optical fractography displayed that different bolt holes were subjected to different degrees of fatigue damage during the testing. This is due to the behaviour of individual bolts depending on the degree of fatigue degradation of the particular fastener, Ref.[6].

In the second project the quasi-static and fatigue behaviour of composite joints with three different types of countersunk fasteners was studied. The joint configuration and the fastener systems are shown in Figure 9.

The joint plates had a quasi-isotropic lay-up ($[\pm45/0/90]_{3s}$ and $[\pm45/0/90]_{6s}$ for the outer and middle parts, respectively). The nominal bolt diameter was 6 mm for all types. Specimens with Torque-set bolts were fastened by 9 Nm torque. The Huck-comp fasteners were installed with the minimum preload of 6 kN according to the specification requirements. The average torque of the composite bolts was 2.7 Nm. The composite bolts were manufactured from PEEK/carbon long fibre reinforced composite material, which was supplied by Textron Aerospace Fasteners.

One specimen of each type was quasi-statically tested to obtain the ultimate tensile strength data. One specimen with each metal fastener system was tested in compression, Ref.[5]. In general, the highest static tensile strength was obtained by the specimens with titanium fasteners, whereas the joint with composite bolts yielded the lowest ultimate tensile strength, see Figure 10. During the tensile tests, both joints with metal fastener failed in the net-section failure mode, whereas the joint with composite bolts broke in the bolt failure mode. The composite bolts displayed a low capacity to support shear loading, Ref.[8].

Four joints with composite bolts, five joints with Torque-set bolts, and six specimens with Huck-comp fasteners were tested in fatigue at different load levels with the stress ratio equal to –1, Ref.[6]. The obtained fatigue test results are presented in Figure 10 together with the fatigue life results of joints having the same geometry, but fastened by protruding-head bolts Ref.[9].

In general, the highest fatigue resistance was shown by the joints with Huck-comp fasteners. The shortest fatigue life was obtained for the joints with composite bolts. In comparison to the joints with protruding-head bolts (i.e., hexagon bolts in the plot), the joints with Huck-comp fastener showed slightly better fatigue strength at low load levels (less than σ = 250 MPa). The dominant failure mode of joints with countersunk fasteners was due to fatigue fracture of fasteners.

As the obtained results on the load transfer in joints with countersunk fasteners showed, the outer plate with countersunk holes transferred less of the applied load compared to the plate with ordinary holes, see Figure 11, Ref.[9]. This is due to only the cylindrical part of the bolt holes being involved in the load transfer of the fasteners, which obviously is shorter in the countersunk holes than in the ordinary holes.

From the achieved test results, several conclusions can be drawn. Increasing the number of bolt rows to the joint configuration improves its ability to support static and fatigue loading. A linear dependence was found between the number of bolt rows and the fatigue life of those joints, which failure mode was due to fatigue fracture of bolts. This makes it possible to estimate the fatigue life of composite joints with different configurations. It has the potential in the future to reduce the required number of fatigue tests, and thus, the total experimental expenses associated with designing composite bolted structures. When comparing quasi-isotropic and 0^o-dominated lay-ups in terms of applied strain, joints with the latter lay-up yielded lower static and fatigue strength than joints with the quasi-isotropic lay-up. Load-transfer measurements of bolt rows showed that the outer bolt rows appeared to be transferring a slightly larger amount of the applied load than the inner one. In composite joints with countersunk fasteners the outer plate with countersunk holes transferred less load than the outer plate with ordinary holes. The joint configuration, the level of pre-stress in the bolts, load transfer of the applied load between the joined parts, and the extent of damage developed during loading are very important issues which should be considered during the design procedure of composite mechanically fastened joints.

3.5 STRUCTURAL EVALUATION

3.5.1 The Saab 340 Full Scale Fatigue Test

General

The SAAB 340 Full Scale Fatigue test has presently been tested for 192000 simulated flights. The first 180000 flights of testing completed the fatigue phase of the test. This corresponds to twice the current design life of 90000 flights. Artificial damages were embodied after the fatigue testing in order to verify the damage tolerance characteristics of the airframe structure. This damage tolerance phase testing is ongoing and presently 12000 flights have been simulated. The aim is to continue the damage tolerance testing until 24000 flights have been achieved, which constitutes two times of the longest inspection interval outlined in the Maintenance Review Report.

An interim testing of the empenage structure of the SAAB 340 Full Scale Fatigue is also ongoing in order to verify the consequences of implementing some cold working of specific structural elements.

Damage tolerance phase

The damage tolerance testing is conducted to verify and correlate the damage tolerance analysis of SAAB 340 in accordance with requirements presented in FAR/JAR 25.571.

A total of 21 artificial damages were introduced before the start of the damage tolerance testing. The test specimen will be subjected to fatigue testing for at least 24000 flights. The damages can be divided into two different types:

- Damages where the intention is to study the crack growth rate.
- Damages in fail safe structures, where the primary load path is removed. In this case the ”residual fatigue life” of the remaining load paths, i.e. the time to initiation of secondary cracks, is of interest. The subsequent crack growth rate of possible secondary cracks will also be studied.

The following structural parts have been furnished with artificial damages:

- Wing: lower panels, lower spar caps, front and rear spar web, wing centre splice, wing to fuselage attachment.
- Fuselage: skin panels, skin splices, skin cut-outs
- Cockpit: pilot window posts
- Stabiliser: stabiliser spar/skin, stabiliser/fuselage attachment.
- Nacelle: upper longeron

The selected damages are considered to cover the relevant types of spectra, crack types and materials, in order to be a substantiation for the complete damage tolerance analysis of the SAAB 340.

The experiences from the damage tolerance testing will be taken into consideration in the damage tolerance analysis and the existing in service inspection program will be updated if necessary.

Cold working testing

Cold working technique is introduced on the interface between the horizontal stabiliser spars and the fuselage of SAAB 340 Full Scale Fatigue test specimen. A limited number of fastener holes are cold worked and modification will be verified by additional fatigue testing of the horizontal stabiliser structure.

The purpose of this modification is to improve economic life of some of the components and thereby avoid future time and cost consuming repairs.

A service bulletin is released for all SAAB 340 aircraft which calls out the implementation procedure of the cold working as retrofit modification.

3.5.2 The Saab 2000 Full Scale Fatigue Test

General

For the SAAB 2000, no complete airframe will be tested due to the commonality with the SAAB 340.

Consequently, a number of full scale component tests are used. At the present time, three fatigue tests with subsequent damage tolerance testing are ongoing.

Stabiliser fatigue test

The stabiliser fatigue test includes the horizontal stabilisers and the attachment structure to the rear fuselage.

The fatigue phase of this test is completed comprising 150000 flights which corresponds to two times of the design life of 75000 flights. The subsequent damage tolerance testing is ongoing. The damage tolerance testing phase is performed in order to verify and correlate the damage tolerance analysis in accordance with the requirements in FAR/JAR 25.571.

A total number of four artificial damages have been embodied on the test specimen. The damages can be classified into two types as follows :

- Damages where the intention is to study the crack growth rate.
- Damages in fail safe structures, where the primary load path is removed. In this case the ”residual fatigue life” of the remaining load paths, i.e. the time to initiation of secondary cracks, is of interest. The subsequent crack growth rate of possible secondary cracks will also be studied.

The following structural elements of the horizontal stabiliser have been subjected to artificial cracks. This was made by mechanical means in terms of sawing, grinding or cutting.

- Stabiliser/fuselage attachment
  Study of crack growth rate for a crack in the stabiliser spar cap, from a fastener hole at the attachment to the fuselage frame.

- Rear spar web
  Study of crack growth rate for a crack growing from an inspection hole.
- Upper skin panel
  Study of crack growth rate for a crack growing from a fastener hole towards the honey comb core.
- Mid hinge
  Study of crack growth rate for a crack growing from a fastener hole (LHS), study of residual fatigue life and crack growth of possible secondary cracks after complete failure of one of two parts in the mid hinge (RHS).

The rationale for selecting the aforementioned damages is that the damages shall cover relevant types of spectra, crack types and materials in order to constitute a justification of the damage tolerance analysis of the SAAB 2000 horizontal stabilisers.

At the moment, 9000 flights have been simulated with artificial cracks present and the aim is to verify at least 24000 flights. In that case, the highest inspection interval (12000 flights) is verified.

Residual strength tests will be carried out for those damages which are considered to require substantiation of the residual strength as a result of complex geometry and/or loading.

Detailed visual inspections are carried out each 500 flights where lengths of the cracks are recorded. NDT inspections in terms of X-ray and Eddy Current inspections are performed at each 3000 flights. On the basis of the interim inspections up to 9000 flights, it can be concluded that the cracks in general have shown a small propagation.

The experiences from the damage tolerance testing will be taken into consideration in the damage tolerance analysis and the existing in service inspection program will be updated if necessary.

Wing/fuselage fatigue test
The test in question includes the centre and the rear part of the fuselage, the complete wing torque box and the rear part of the engine nacelles.

The wing detail design is changed compared to the SAAB 340 (machined spars with integral spar caps), and the wing/fuselage interface also. Furthermore the cabin pressurisation spectrum is more severe. The flight and landing loads on the fuselage is also more severe due to the slender fuselage of SAAB 2000.

The Wing/Fuselage Fatigue test will be tested to 150000 flights of fatigue loads with a subsequent damage tolerance testing. At the current date 110000 flights of fatigue testing have been completed.

Engine Mount structure fatigue test
The SAAB 2000 engine mounting structure is completely different in design compared to the SAAB 340. The structure is basically built up by eighth steel struts attaching the forward engine mounts to the nacelle structure. Each one of those eight struts is redundant in terms of continuing airworthiness if a strut fails.

The fatigue phase of the testing is completed (verification of 150000 flights from fatigue point of view). A number of fail safe situations with respect to the fatigue behaviour are tested in order to check the fail safe characteristics of the truss-grid.

The damage tolerance phase with artificial cracks will be the final phase of this test programme.

3.5.3 JAS39 Gripen Fatigue Testing

The strength verification programme concerning large components was completed during 1994. The full scale fatigue test of the twin seater, 39B, was completed last year (2000). The only ongoing structural test at the moment is the full scale fatigue test of the single seater, 39A. Test planning is ongoing for a full scale fatigue test of the twin seater export version, 39D.

3.5.4 Full Scale Fatigue Test of the Single Seater, 39A

The configuration of the major fatigue test is almost identical to that of the major static test, both with regard to the structure and the test arrangement, Figure 12. The test set-up has about 90 control channels and is monitored by acoustic emission in addition to the inspection by conventional methods. The test article has more than 1000 strain gauges installed and has been subjected to 22000 flight hours (30800 flights) testing today (May -01). The test will continue to at least 24000 flight hours.

Fatigue cracks have been found:
- in a lug for the attachment of the actuator for the main landing gear door.
- in parts belonging to the air brakes.
- at hole edges in webs of formed sheet frames.
- at tool holes in the web of a machined fin attachment frame.

The outcome of the test has been used to retrofit operational aircraft and to redesign parts for batch 3 for the Swedish airforce as well as for export aircraft. The lug for the main landing gear door actuator and the parts for the airbrake are redesigned. The formed sheet frames are replaced by high speed machined integral frames and the web of the machined fin attachment frame is made thicker.

The cracking is not a flight safety issue but the rectifying actions have been made in order to avoid any cracking at all during the design life.

3.5.5 Full Scale Fatigue Test of the Twin Seater, 39B

The configuration of the major fatigue test of the twin seater is designed to reflect the differences with respect to the single seater. The test object is thus a fuselage consisting of the structure between the front of the engine bay and the radome, Figure 13. Attachment loads from the wings are applied via dummies. The whole test set-up has about 50 control channels and the structure is equipped with about 600 strain gauges.

The test has completed the goal of 16000 hours (22400 flights) of fatigue testing. The only crack found during inspections was a crack in a lug for the attachment of the actuator controlling the main landing gear door. After the fatigue test, the test object was subjected to a strength check to 200% limit load (L.L.) for 11 load cases. No abnormalities were discovered.

3.5.6 Full Scale Fatigue Test of the Twin Seater Export Version, 39D

The test object is a complete fuselage, Figure 14. Attachment loads from the wings, fin, foreplanes, landing gears etc. are applied via dummies. The whole test set-up has about 90 control channels (actuators and pressure valves) and the structure is equipped with more than 1000 strain gauges.

The test is made in order to verify:
- Increased service life (8000 flh)
- Changes due to part count reduction (e.g. introduction of high speed machined integral parts)
- Changes due to world wide climate adaptation (WWC)
- Increased cabin pressure
- Increased basic design mass
- Changes due to Air-to-Air Refuelling installation (AAR)
- Changes due to Radar Cross Section reduction (RCS)

A number of unit load cases and balanced load cases will be subjected to the test object before fatigue testing in order to measure strains. Some of the load cases will be measured after every 1000 flight hour of fatigue testing as well.

The repetition test sequence consists of about 400 flights representing 500 flight hours. The initial goal is to exceed 16000 flight hours of test simulation. Start of testing is scheduled for spring 2003.

3.6 STRESS ANALYSIS AND FRACTURE MECHANICS

3.6.1 Accurate Stress Intensity Functions for Corner Cracks at a Hole

Stress intensity functions, K, for un-symmetric corner cracks at a hole subject to general loading (Figure 15) were determined [10] using an *hp*-version of the finite element method (FEM) in conjunction with a mathematical splitting scheme to enable efficient and accurate calculations with control of error in calculated stress intensity functions. For details about the splitting method see section 3.5 in [1]. The work was a joint project between Wright-Patterson Air-Force Research Laboratory, Ohio, U.S. and the Aeronautical Research Institute of Sweden.

In traditional applications of the FEM, mesh generation is labour intensive, however using the splitting scheme, stress intensity functions are obtained without explicitly including the crack in the FE-mesh of the global structure. By using the *hp*-version of FEM, a set of K solutions converging exponentially fast to the exact mathematical solution is obtained

(Figure 16). The crack is analysed in the local domain with easily generated FE-meshes. All structurally significant crack shapes were considered, specifically, crack depth to crack length ratios (*a/c*) of 0.1-10.0, crack depth to sheet thickness ratios (*a/t*) of 0.10-0.99 and hole radius to sheet thickness ratios of (*r/t*)=0.2-10.0. The loading conditions were remote tension, remote bending and simulated pin loading (bearing). In addition, all combinations of *a/c*, *a/t* and *r/t* are analysed at each side of the hole, thus, more than 900 000 geometries were analysed with control of the errors in computed stress intensity functions. Calculated relative errors are generally much smaller than 1% along the entire crack front including the vertex regions. Laboratory test and in-service experience show fatigue cracks at holes exhibit un-symmetric growth, thus, the need for new solutions is paramount. Comparisons are made to solutions in the open literature.

The new K-solutions show that the literature solutions are in general accurate for all three loading conditions, however, for more extreme cases of *a/c*, *a/t* and *r/t* the literature solutions are in error as much as 30%.

3.6.2 Stress Intensity Factors for a Centre Crack Plate

Very accurate closed form stress intensity factor (SIF) expressions exist for a centre crack in a sheet of finite width subjected to a remote uniform, uniaxial stress. In the case the sheet has both a finite width and a finite height, stress intensity factor solutions exist but only in tabular and graphical form. Also, in the case of different crack surface loading conditions, instead of the remotely applied stress, solutions exist and some closed form expressions have been proposed without verification of their accuracy.

The purpose of this study was to assess the accuracy of some stress intensity factor expressions for the centre crack in a sheet and to develop an expression for the case of both finite width and height, Ref.[11]. The latter objective was easily accomplished by the aid of existing SIF solutions and expressions combined with the method of least squares. The resulting expression is presented below where 2a is the crack length from tip to tip, E is the distance from the crack centre to the sheet edge and H is the total height of the sheet.

$$K_I = \sigma\sqrt{\pi a}\, f_W f_H \tag{1}$$

where the finite width correction is given by,

$$f_W = \left(1 - 0.025\alpha^2 + 0.06\alpha^4\right)\left[\cos(\pi\alpha/2)\right]^{-\frac{1}{2}} \tag{2}$$

and the finite height correction is assumed to be

$$f_H = 1 + A_1\alpha + A_2\alpha^2 \tag{3}$$

with

$$A_1 = \gamma(C_1 + C_2\gamma) \quad ; \quad A_2 = \gamma(C_3 + C_4\gamma) \tag{4}$$

and

$$\alpha = a/E \quad ; \quad \gamma = E/H \tag{5}$$

The coefficients C became,

$$C_1=0.170218 \; ; \; C_2=0.43604 \; ; \; C_3=-0.55270 \; ; \; C_4=1.68076 \tag{6}$$

The accuracy of the proposed expression compared to the result presented as a table in the handbook by Murakami is better than 7 % for all $\alpha \leq 0.7$ and $\gamma \leq 1.25$, see Figure 17. On the average the accuracy is better than 2.1 % and since the table is said to have an accuracy better than 1 % the total error in the expression should, on the average, be better than 3.1 %.

Using the approximate weight function technique the stress intensity factor for a centre crack subjected to a symmetric partial crack surface pressure was obtained. The above expression for the stress intensity factor was selected as reference solution. Based upon a closed form weight function solution for the centre crack in a sheet of infinite height, developed by Tada, an expression for the stress intensity factor for the partially loaded crack was obtained as,

$$K_I = \frac{2}{\pi} p\sqrt{\pi a}\left[f_W + \left(1-\frac{\kappa}{\alpha}\right)\frac{B_1\alpha^2 + B_2\alpha^4}{\sqrt{\cos(\pi\alpha/2)}}\right]\sin^{-1}\left(\frac{\sin(\pi\kappa/2)}{\sin(\pi\alpha/2)}\right) \tag{7}$$

where f_w and α are given above and $\kappa = b/E$. The crack surface pressure, p, acts over the range x=-b to x=b where x is a co-ordinate system having its origin in the crack centre. The coefficients, B_i, were found from a least squares fit with respect to the numerical result obtained using the approximate weight function technique. The numerical values of B_i became,

$$B_1=0.321549 \; ; \; B_2=-0.324864 \tag{8}$$

The maximum absolute error in the expression above as compared to the weight function solution is 3.3 % for $\alpha \le 0.9$ and any κ. Comparisons of values obtained using Eq.(7) to values obtained using finite element computations showed that the relative difference was less than 5 %. A finite height correction factor was developed according to,

$$f_H = 1+\gamma\left(D_1 + D_2\gamma + \frac{(\alpha-\kappa)}{1-\kappa}(D_3 + D_4\gamma)\right) \tag{9}$$

where γ is defined above and the coefficients D_i are functions of κ, such that,

$$\begin{aligned} D_1 &= 0.0894194\left(1-4.330e^{-0.458/\kappa}\right) \; ; \; D_2 = -0.111202\left(1-21.01e^{-0.518/\kappa}\right) \\ D_3 &= -0.499953\left(1-0.352e^{-0.633/\kappa}\right) \; ; \; D_4 = 3.024540\left(1-1.262e^{-0.756/\kappa}\right) \end{aligned} \tag{10}$$

The numerical values of the coefficients were obtained using the method of least squares. Compared to the stress intensity factors obtained using the approximate weight function technique the proposed equation gives stress intensity factors with an accuracy better than a few percent for $\alpha \le 0.9$, any κ and E/H<1,see Figure 18.

A stress intensity factor equation for a centre crack subjected to a single pair of splitting forces, in a sheet of finite width, has been developed by Tada, 1973, using asymptotic interpolation. The force pair acts at the location x=b on the crack surfaces. The equation which is said to have an accuracy better than 1 % is as follows,

$$K_I^{\substack{A\\B}}(\alpha,\rho) = \frac{P}{\sqrt{\pi a}}\sqrt{\frac{\pi\alpha}{2}\tan\left(\frac{\pi\alpha}{2}\right)}\cdot\left[1+\frac{\left(\pi-\sqrt{\pi^2-4}\right)\sqrt{1-\rho^2}\left(1-\cos\left(\frac{\pi\alpha}{2}\right)\right)}{\sqrt{\pi^2-4}}\right] f^{\substack{A\\B}} \tag{11}$$

with

$$f^{\substack{A\\B}} = \frac{\cos\left(\frac{\pi\kappa}{2}\right)\left(\sin\left(\frac{\pi\alpha}{2}\right)\pm\sin\left(\frac{\pi\kappa}{2}\right)\right)}{\sin\left(\frac{\pi\alpha}{2}\right)\sqrt{\sin^2\left(\frac{\pi\alpha}{2}\right)-\sin^2\left(\frac{\pi\kappa}{2}\right)}} \tag{12}$$

where α and κ are the same as above and ρ=b/a. The superscript identifies the crack tip considered and is related to the plus/minus sign in the last term.

A comparison between stress intensity factors calculated using Eq.(11) and corresponding stress intensity factors calculated using an equation developed by Chen et. al., 1993, based upon the force-balance method, showed very large relative differences for crack tip B (when the splitting force pair acts nearest to crack tip A). Therefore, some finite element analyses were made using the in-house code STRIPE. The finite element analyses confirmed that Eq.(11) results in stress intensity factors, for crack tip B, which are erroneous. The relative difference between the stress intensity factors calculated using Eq.(11) and corresponding stress intensity factors obtained from the finite element analyses are shown in Figure 19.

3.6.3 Stress Intensity Factors for Radial Cracks at a Circular Hole in a Plate of Finite Dimensions

The stress intensity factor for a single radial crack, two symmetrical radial cracks or two radial cracks of un-equal lengths at a circular hole in a plate of infinite dimensions can be obtained for various loading conditions by solving a singular integral equation. This technique, developed by Tweed and Rooke in the late 70:th, is rather simple to implement in a computer programme and the method converge quickly to very accurate stress intensity factors.

During the years several equations have been proposed in order to describe the stress intensity factor as function of crack length. These equations are generally valid for a single crack or two symmetrical cracks. In the present investigation, Ref.[12], the stress intensity factors obtained by these equations were compared to the numerical data found in tables, in the literature, and computed by using the technique developed by Tweed and Rooke.

Very often the stress intensity factor equations according to above are combined with correction factors for finite width or eccentric location of the hole in a sheet of finite width. The accuracy of the end result has not been very well established. Furthermore, in many applications it is advantageous to have an equation to calculate the stress intensity factor compared to interpolating in tables or reading values from graphs. This is particularly true when their are many parameters involved, as is the case for cracks at a hole in a plate of finite dimensions.

Through the comparisons made in this investigation it was concluded that the following equation for the normalized stress intensity factor,

$$F_{OH}^{2} = \frac{1}{0.539 + 1.93\frac{a}{R} + 2\left(\frac{a}{R}\right)^{2}} + \frac{\lambda + 2}{2} \tag{13}$$

suggested by Schijve for two symmetrical cracks, diametrically located at the hole, was the most accurate. The equation refer to cracks at an open hole in a sheet of infinite dimensions loaded with a uniaxial, uniform stress acting perpendicular to the crack line at a remote distance from the cracks. The parameter λ is defined as,

$$\lambda = 1/(1 + a/R) \tag{14}$$

where a is the crack length measured from the hole edge and R is the hole radius. The maximum relative difference compared to the numerical data is 0.2 %. The normalized stress intensity factor is defined as,

$$F_{OH} = \frac{K_I}{\sigma\sqrt{\pi a}} \tag{15}$$

Also, in the case of a single crack at the hole the normalized stress intensity factor equation according to Schijve turned out to be the most accurate. This equation can be written as the equation for two cracks multiplied with a conversion factor according to,

$$F_{OH}^{1} = F_{OH}^{2}\sqrt{\frac{\lambda + 1}{2}}\left[1 + \frac{a}{R}\frac{\lambda^{3}}{5}\right] \tag{16}$$

The maximum relative difference compared to the numerical data in this case is less than 0.4 %. In the case of two cracks of unequal lengths the following equation for the normalized stress intensity factor at crack tip A is proposed,

$$F_{OH}^{A} = \left(\frac{1}{0.539 + 1.93\frac{a_1}{R} + 2\left(\frac{a_1}{R}\right)^2} + \frac{\lambda_1 + 2}{2} \right) f_c^A \tag{17}$$

where a_1 is the length of the crack having the crack tip denoted A and $\lambda_1 = 1/(1 + a_1/R)$. The conversion (interpolation) factor is given by,

$$f_c^A = \sqrt{\frac{1}{2}\left(1 + \frac{\lambda_1}{\lambda_2}\right)\left[1 + \frac{a_1}{R}\frac{\lambda_1^3}{5}\left(1 - \frac{4}{\pi}\tan^{-1}\left(\frac{a_2}{a_1}\right)\right)\right]} \tag{18}$$

where a_2 is the length of the crack, diametrically located to a_1, having the crack tip denoted B and $\lambda_2 = 1/(1 + a_2/R)$. The stress intensity factor for crack tip A is written,

$$K_I^A = \sigma\sqrt{\pi a_1} F_{OH}^A \tag{19}$$

Correspondingly, the stress intensity factor for crack tip B is written,

$$K_I^B = \sigma\sqrt{\pi a_2} F_{OH}^B \tag{20}$$

where F_{OH}^B is identical to F_{OH}^A but with the crack length indices shifted. For $\lambda_1/\lambda_2 \leq 1$ the maximum relative difference between the values calculated using the equation and the numerical results obtained using the solution technique by Tweed and Rooke is less than 1.6 % for crack tip A, see Figure 20. For crack tip B the maximum relative difference occurs in cases where the crack length a_2 is small and increases as the crack length a_1 increases, see Figure 21. The largest relative difference found in the investigation was 7.8 %. The numerical results obtained using the solution technique according to Tweed and Rooke were also compared to the more recent numerical results of Lai et. al.. The maximum relative difference found in this case was 1.7 %.

The investigation also showed that the finite width correction proposed by Newman, Jr.,

$$F_W^A = \left[\cos\left(\frac{\pi}{2}\frac{1}{E/R}\right)\cos\left(\frac{\pi}{2}\alpha_{eq}^A\right)\right]^{-\frac{1}{2}} \tag{21}$$

was sufficiently accurate. E is the distance from the centre of the hole to the nearest edge of the sheet ($E \leq W/2$, where W is the total width of the sheet). The equivalent crack length, for crack tip A, is given by,

$$\alpha_{eq}^A = \frac{a_{eq}}{E_{eq}} = \frac{2R + a_1 + a_2}{2E - (a_1 - a_2)} \tag{22}$$

For crack tip B a corresponding correction factor is,

$$F_W^B = \left[\cos\left(\frac{\pi}{2}\frac{R/W}{(1 - E/W)}\right)\cos\left(\frac{\pi}{2}\alpha_{eq}^B\right)\right]^{-\frac{1}{2}} \tag{23}$$

where

$$\alpha_{eq}^{B} = \frac{a_{eq}}{W - E_{eq}} = \frac{2R + a_1 + a_2}{2(W - E) + a_1 - a_2} \tag{24}$$

In the case of a single crack $a=a_1$ and $a_2=0$. For two symmetrical cracks $a=a_1=a_2$. The finite width corrections above implies that the cracks and the hole are viewed as an internal line crack of length a_1+a_2+2R from tip to tip. The distance from the centre of this line crack to the edge of the sheet at the crack tip A side has been denoted E_{eq}, which in general is different from W/2. This means that a correction for the eccentric location of the crack centre is made if the cracks a_1 and a_2 are of different lengths and/or the hole is displaced from the sheet centre line. Furthermore, the finite width corrections imply that the total width of the sheet becomes $2E_{eq}$ at the crack tip A side and $2(W-E_{eq})$ at the crack tip B side, which is incorrect. To adjust for this error an additional correction for eccentricity is introduced. For the stress intensity factor at crack tip A this correction is written,

$$F_E^A = \sin\left(\pi \frac{E_{eq}}{W}\right) + \left[\frac{1 + \sqrt[4]{\cos\left(\frac{\pi}{2}\alpha_{eq}^{A}\right)}}{2}\right]^2 \left[1 - \sin\left(\pi \frac{E_{eq}}{W}\right)\right] \tag{25}$$

if $E_{eq}/W \leq 0.5$ and

$$F_E^A = \left(\frac{\dfrac{1}{\sqrt{\cos\left(\dfrac{\pi}{14}\alpha_{eq}^{A}\left(\dfrac{3 + E_{eq}/W}{1 - E_{eq}/W}\right)\right)}} - 1}{1 + 0.21\sin\left[8\tan^{-1}\left(\left(2\dfrac{E_{eq}}{W} - 1\right)^{0.9}\right)\right]} + 1 \right) \sqrt{\cos\left(\frac{\pi}{2}\alpha_{eq}^{A}\right)} \tag{26}$$

if $E_{eq}/W \geq 0.5$. Similar correction can be obtained for the stress intensity factor at crack tip B.

To account for a finite height of the sheet a first suggestion is the same finite height correction as used for the centre line crack in a sheet of finite dimensions.

The complete stress intensity factor equation for a single, two symmetrical or two cracks of unequal lengths at a circular hole in a sheet of finite dimensions subjected to a uniform, uniaxial stress may, thus, be written,

$$\begin{aligned} K_I^A &= \sigma\sqrt{\pi a_1}\, F_{OH}^A F_W^A F_E^A F_H^A \\ K_I^B &= \sigma\sqrt{\pi a_2}\, F_{OH}^B F_W^B F_E^B F_H^B \end{aligned} \tag{27}$$

These stress intensity factors were compared to literature data and to the results of some complementing finite element (FE) computations. The FE analyses were made using the in-house computer code STRIPE, which uses the p-version of adaptive technique and an optimized meshing close to the crack tip. The accuracy of these analyses should be better than ±2 %.

During these comparisons it became obvious that the equations yielded poor results when the dimensional ratio E/H became large (E/H>0.25). An additional finite height correction factor was therefore developed. This was done by studying the stress distribution in the ligament for a fixed ratio E/R=2 and 7 different ratios H/R. Based on the approximate weight function technique using the above stress intensity factors as reference solutions new stress intensity factors were calculated. The quotient between these new stress intensity factors and the reference solutions then yielded the additional correction factors. These correction factors were fitted with closed form expressions according to,

$$F_{HR}^{A} = -e^{B_{11}(H/R)+B_{12}}\left(\frac{a_1}{E-R}\right) + e^{e^{B_{21}(H/R)+B_{22}}}$$
$$F_{HR}^{B} = -e^{B_{11}(H/R)+B_{12}}\left(\frac{a_2}{W-E-R}\right) + e^{e^{B_{21}(H/R)+B_{22}}} \quad (28$$

where the constants B became,

$$\begin{matrix} B_{11} = -0.733 \\ B_{12} = 2.096 \end{matrix} \; ; \; \begin{matrix} B_{21} = -0.817 \\ B_{22} = 2.374 \end{matrix} \quad (29)$$

For a single crack or two symmetrical cracks with a/(E-R)□0.8 in a sheet having E/H□0.25 the accuracy of the complete stress intensity factor, including the additional finite height correction, is generally between –4 % and 7 %. In a sheet having E/H>0.25 the accuracy is not so good, -11 % to 22 %.

For two cracks of unequal lengths the accuracy of the complete stress intensity factors is in most cases better than 8 % if E/R□4 and E/H□0.25, see Figures 22 and 23. However, for $a_2/a_1>1$ the accuracy becomes poor for small crack lengths a_1. For E/R=2 the accuracy at tip A is generally better than 11 % if $a_2/a_1>1$ but for a_2/a_1□1 the accuracy decreases with increasing crack length at tip A. For E/H>0.25 the accuracy is better than 18 %.

It should be noted that the effect of the corrections made for the finite height is almost negligible for E/H□0.25. Also, the effect of the correction for eccentricity is rather small, a few percent, in most cases of practical interest.

3.6.4 Multiaxial Fatigue

In a lot of modern constructions where fatigue loading is the limiting factor in the dimensioning, the load state at critical parts is not uniaxial but multiaxial. This can be exemplified by fasteners in aeroplanes. A major part of the fatigue research has historically concerned uniaxial loading why most design rules are bases on uniaxial fatigue testing. Alternatively, simple multiaxial design criteria are used but the criteria have been tested in a limited amount of situations. This might lead to a conservative design in order to make the constructions safe. However, there is also a risk that the multiaxial load is underestimated leading to an unconservative design.

Starting during 1999 a project on multiaxial fatigue was initiated. The project covers both experimental and theoretical aspects of multiaxial fatigue, mainly in metals. A literature survey presenting different aspects such as experimental techniques, initiation mechanisms, initiation criteria and crack propagation was made, Ref.[13].

In a general multiaxial load situation not only the amplitudes of the different loading components but also the principal directions will vary in time. While for uniaxial random loading, cycle counting methods such as rain flow counting and range-pair counting are well established, no such generally accepted method exists for the multiaxial case, though a couple of algorithms have been proposed. One objective of the project was to compare three of these approaches for multiaxial cycle counting, test them on different load sequences and evaluate them with respect to factors such as total damage, computational efficiency and physical basis, Ref.[14]. Two cycle counting methods has been taken from the literature and one is newly developed. Two sequences of in-plane load with different degree of complexity have been used. The load situation is limited to the case of plain stress, corresponding to the assumption that a crack is initiated on a surface. A critical plane criterion has been used to quantify and summarise the damage predicted by each cycle counting algorithm. The estimated total damage of the cycle counting methods varied within maximum 20 % which is a rather small difference compared to the normal spread in fatigue tests. In the algorithm that gave the lowest damage sum, the multiaxial load sequence is projected to an axis in a critical plane where a rain flow cycle counting is performed. All possible critical planes are surveyed to find the plane that gives the highest damage. In the algorithm that got the highest damage, for each cycle the critical plane with the maximum damage is detected.

An experimental series has been started. The fatigue testing is performed on cruciform specimen set to a biaxial in-plane load state. Unfortunately the testing has been hampered by technical problems why no results can be presented.

3.7 FATIGUE CRACK PROPAGATION AND RESIDUAL STRENGTH

3.7.1 FFA-Work in European Joint Project SMAAC 1996-1999

FFA participated 1996-99 in the three year European research project "Structural Maintenance of Ageing Aircraft", SMAAC. The work which mainly involved development of computational methods for analysis of multiple 3D fatigue crack growth, and residual strength analysis of aircraft shells with widespread fatigue is reviewed in [15].

For 3D multiple fatigue crack growth analysis, a mathematical splitting scheme was developed which was described in section 3.5 in Ref. [1]. The splitting method was during the year 2000 implemented on a cluster of SMP-computers and used for statistical fatigue crack growth analysis of a fuselage side. In the study over 200 rivets, skin, doublers and stiffeners where modelled as 3D objects and multiple fatigue crack propagation, linkup etc were studied using a Monte Carlo type of statistical analysis (compare Ref.[16]. Figure 24 exemplifies one type of results obtained from this type of analysis. The figure, shows the distribution function for the number of load cycles from detection of the first 1 mm crack in a double-lap joint until the first link-up has taken place. The graph shows (assuming cracks >= 1 mm can be found at inspection) that 22 kcycles after inspection the probability of finding two cracks that have linked up is 1%. After 43 kcycles, the probability is 50%.

The results are based on 3D fatigue crack growth analysis of 8000 double-lap samples. The figure shows that the high accuracy solution *p=4* is very close to *p=3* solution hence demonstrating that convergence is obtained. In all 10^7 3D fracture mechanics solutions were derived in the analysis of the fuselage side where a FE-mesh having 10 Mdofs was used. For flapping cracks where the mode II component is large, crack face sliding over rivets were found to significantly increase K_I. A new version of the splitting method, with which 3D contact problems in riveted joints can be solved very efficiently is currently being developed.

A yield-strip model for residual strength analysis was developed in the SMAAC-project. Damage propagation was assumed to take place under the condition that cracks propagate with a constant crack opening angle α.

Onset of crack growth is assumed to occur when the crack-tip opening attains a critical value δ_0 (Figure 25). The two fracture parameters α and δ_0 were determined from basic fracture tests (Figure 26). The smaller MSD cracks in the damaged joint were assumed to follow the same crack propagation law as the lead crack. As an effect of the crack growth resistance behaviour, not only the lead crack but also smaller MSD cracks embedded in the plastic zone were usually found to propagate before a crack link-up. The structural model used is built up of beam and shell elements with an elastic behaviour (yielding is accounted for by the yield strip model). Shell and beam finite elements are used to represent the skin, the stiffeners and the rivets. Geometrically non-linear effects were considered in the FE-analysis.

The validity of the model was verified against test data for four different types of joint structures where each joint had at least two different damage patterns. Figure 27 shows half of a typical FE-mesh used in analysis of a panel with an initial lead crack of length 76 mm.

MSD-cracks were in some of the experiments artificially introduced at each fastener hole [16]. In Figure 28 calculated and measured residual strength curves are compared. Illustrated are also the computed location of the lead crack tip and the plastic zones for a few key events. The agreement with experimental data is good, despite the complexity of the problem. An old aircraft fuselage side was tested by another partner in the SMAAC project. Analysis of this situation (where all data are not open) showed also good agreement between experiment and analysis.

3.7.2 Initial Flaw Concept and Short Crack Growth

In February 2000 a GARTEUR action group, AG26, was formally established to work on the topic, “Initial Flaw Concept and Short Crack Growth”. The group had already been active about a year, preparing the proposal for forming the action group. The partners in the project are EADS Airbus SA, EADS CCR, EADS Airbus GmbH, Airbus UK, DERA, NLR and FOI.

The current practice in determining fatigue thresholds for components in the Airbus aircraft is based on classical fatigue analyses, i.e. using Palmgren-Miner´s rule and SN-data. In a draft to a new Advisory Circular of FAR/JAR 25.571 (presented in Long Beach in 1997) the definition of the fatigue threshold was changed or, rather, the implicated method to obtain the fatigue threshold was changed to one based on fracture mechanics. Furthermore, in contrast to the MIL-A 83 444 no specific initial flaw sizes were given. Instead the draft defined a rogue flaw of maximum probable size where the size depends upon the area being investigated, the manufacturing process, the ability to detect the flaw at the time of manufacture and the susceptibility of the area to corrosion. The rogue flaw is assumed to exist at a critical location, either at the time of manufacture, representative of manufacturing damage, or as a result of the operating environment.

Also, a quality flaw was defined as a flaw assumed to exist at most of the locations at the time of manufacture, representative of the initial quality.

As a part of the GARTEUR project a round robin exercise was initialised. The exercise consisted of determining the equivalent initial flaw size (EIFS) distribution given the experimental fatigue lives of coupon test specimens, the constant amplitude crack growth rate as function of the stress intensity factor range for the material and the loading conditions. Two specimen types were considered. Firstly, a flat rectangular bar and, secondly, a flat dog-bone specimen having a circular hole in the centre. Both specimen types had a width of 25.4 mm and a thickness of 6.0 mm in the test section. The circular hole in the dogbone specimen had a radius of 2.5 mm. The material for both specimen types was the aluminium alloy 7010-T7651 and the loading condition was constant amplitude cycling with a stress ratio of 0.1.

The FOI contribution to the round robin exercise involved 3 different methods to obtain the equivalent initial flaw size distributions. Firstly, a Paris´ law was fitted to the crack growth rate data. Using the stress intensity factor equations for a corner crack at an edge and a corner crack at a circular hole, proposed by Newman, Jr, the crack growth from a guessed initial flaw size to failure was computed. The procedure was repeated until the computed number cycles to failure matched the experimental fatigue life of each test specimen. Log-normal distributions were then fitted to the initial crack sizes of each group of the specimens tested at the same stress level.

Secondly, an inverse hyperbolic tangent relation was fitted to the crack growth rate versus the stress intensity factor range. For each stress level and specimen type the number of cycles for the crack growth from an initial quarter-circular flaw of radius 0.1 mm to failure was computed. The computed number of cycles were then subtracted from the corresponding experimental fatigue lives. This gave sets of data (cycles, crack length) for the crack growth in the range 0.1 mm to 0.25 mm, which were fed into a computer programme based upon the US Airforce initial fatigue quality models. Two models were selected for the computation of equivalent initial flaw sizes, the fully stochastic model and the fully deterministic model. Log-normal distributions as well as Weibull compatible distributions were fitted to the equivalent initial flaw sizes obtained for the whole set of data for each specimen type and for sets of data representing each stress level.

Thirdly, a Paris´ law was fitted to the collapsed crack growth rate data approximately corresponding to the stress ratio 0.7. Again the equations proposed by Newman, Jr were used to evaluate the stress intensity factors and to obtain the crack opening displacement based upon the approximate weight function technique. A strip yield model, based upon the model by Newman, Jr, was applied. The equivalent initial flaw sizes were obtained by guessing an initial flaw size and computing the number of cycles to failure trying to match the experimental fatigue lives. Again, log-normal distributions were fitted to the equivalent initial flaw sizes for each stress level.

It was found that the log-normal EIFS distributions obtained for different stress levels were different, see Figure 29. They were entirely different for the same stress level when the different methods of computing the EIFS were compared, see Figure 30. Thus, non of the methods used were able to remove the stress dependence in the crack growth. All the EIFS distributions obtained were purely hypothetical and had very little to do with the real initial quality of the test specimens.

3.7.3 Deterministic and Probabilistic Analyses of the Initiation of Wide Spread Fatigue Damage for SMAAC Test Panels

A detailed analysis, Ref. [17], has been performed on the onset of multiple site damage at mechanical joints. The crack initiation is analysed based on a non-linear stress analyses and a crack closure model. It has been found in Ref. [17] that the stress-strain response in the joint can have a stabilised linear relation under fatigue loading even if considerable plastic yield has occurred. This makes it possible to analyse the post yield multiple crack initiation based on fracture mechanics solutions for the crack growth in a residual stress field. A weight function method has been used to solve stress intensity factors and Green's functions for the crack growth analyses according to a strip yield crack closure solution. In this analysis, the small crack behaviour as well as the post yield effect have been accounted for. Intrinsic material parameters have been extensively used such that the method is not limited to the specified problem. Together with the crack growth analyses, a probabilistic model has been developed to account for uncertainties in initial flaw size, stochastic crack propagation, geometrical inconsistencies, as well as variation in the fatigue loading. According to the probabilistic solution, important information about the onset of multiple site damage, e.g. the probability of crack occurrence, and the probability of crack break-through etc., are predicted as a function of the stress and the joint configuration. One example is provided to illustrate the procedure and to highlight problems in dealing with the onset of multiple site damages at mechanical joints.

The test specimens, shown in Fig.31, were analysed. The specimens were used in a multiple site fatigue test program for the fuselage lap joints in a European co-operated project. Various detailed finite element models were created for the stress analyses. One example is shown in Fig.32. Contact conditions, friction, non-linear material and geometry effects are included in the model.

The finite element analyses revealed that the stress-state in the joint is severe. However, an elastic shakedown condition may be achieved under fatigue loading for all the interested stress levels, see Fig.33. The shakedown condition is strongly spectrum related, see Fig.34. The extreme load levels in the spectrum determines the final shakedown stress condition, see Fig.35.

The effective contact area between the sheets is very stable at various fatigue load levels, see Fig.36 for the contact areas at different fatigue levels as shown in Fig.34. At the shakedown condition, half the hole circumference is almost free from contact, see Fig.36. The major friction boundary correlates well with the crack initiation locations.

Various parameters are investigated such as the coefficient of friction and the strain hardening. The results are shown in Fig.37. The general trend shows that reduction in the friction can reduce the residual strain and increase slightly the local stress range. As a result, the fatigue life may be reduced. The increase in strain hardening may increase the friction and the residual strain. The increase in strain hardening does not, however, significantly increase the stress range, which is considered to be a major crack growth driving force. A low coefficient of friction and reasonable strain hardening is preferred in finite element models since they may provide a more realistic situation.

A qualitative evaluation of the effect of the parameters is shown in Fig.38 as a total fatigue map. In this map, the envelope of fatigue life is determined by the physical condition of material behaviour, the static material strength. Approximately, equal fatigue life curve may be plotted in the figure. Locations of various material and friction assumptions are shown in the figure. The coefficient of friction can systematically reduce the fatigue life while strain hardening may slightly reduce the fatigue life.

The effect of the fatigue load levels is also analysed. Some results are shown in Fig.39. It is remarkable to see that significant plastic yielding can occur at the critical location for fatigue load levels which often give adequate fatigue lives. Many "ordinary" lap joints can experience severe plasticity at critical locations even though their fatigue lives are relatively long. The elastic finite-plastic analyses are apparently required for the detailed stress analyses even at low fatigue load levels. The reason is that the stress concentration factor can be very high in the lap joint (as high as a factor of 10).

There is no linear relation between the applied fatigue load level and the magnitude of the local stress due to the strong plasticity at the critical location of the joint, see the stress range results shown in Fig. 40. The local stress ratio is considerably different from the fatigue load ratio. While the remote fatigue load ratio is the same for all the load levels shown in Fig. 40 (R=0.1), the local stress ratio is less than R=-1. Also, the local stress ratio seems to be load level related, see Fig.40.

The elastic shakedown stress is used to evaluate stress intensity factors at the critical location according to initial flaws in the material matrix and possible machine scratches. This analysis revealed a major fault in the project for the baseline rate of fatigue crack growth. The original crack growth rate is determined using CCT specimens made of the same sheet. The Paris crack growth rate is determined using fatigue test results for long through cracks. When the same Paris Law is extrapolated into the regime of initial cracks, the crack growth rate is overestimated by more than one order of magnitude, see the comparison shown in Fig.41. This fault is remedied based on the widely published 2024-T3 crack growth data, see Fig.41 as the "best guess".

The strip yield crack closure model is used to analyse the fatigue crack growth. Some results are shown in Fig.42 of the crack growth initiated from different initial flaws. The strip yield model is capable of dealing with the small crack growth effect. The prediction results showed that, on the contrary to what might be expected from other models, the fatigue life has almost a linear relation to the initial crack size. The sizes of the initial cracks effectively affect the crack growth rate, as shown in Fig.43 as a function between the crack size and the crack growth rate. There is a strong "small crack" effect such that the crack growth rate depends both on the load levels and the initial crack sizes.

The predictions of fatigue lives give a good description of the general trend. However, the fatigue life seems to be overestimated. It is understood that the state of stress may be more severe at the joint due to fretting, wear and tear etc., which can not be considered in the finite element analyses. An empirical modification is made in the finite element stress results to account for this shortage.

Obviously, the success in fatigue life analyses for individual cracks may not guarantee a satisfactory solution for the multiple site crack initiation problem. When many cracks are considered at the same time, the initiation crack size may be different, the crack growth rate may be different, and the stress condition at the critical locations may also be different. A much more realistic solution should be based on the probabilistic consideration of both the crack initiation and propagation where random effects in material, stress, and surface condition should be considered.

Since the stochastic fatigue crack growth is conditional on the initial crack size, see Fig.44, the previously developed stochastic crack growth model, which is based on material variation and damage accumulation, is used to evaluate the initiation of multiple site fatigue cracks as shown in Fig.45. The probabilistic material data is based on the small crack growth data published previously for the aluminium alloy of 2024-T3.

Based on fatigue test results, parameters used to characterise the production consistency were determined. The comparison between analytical and test results is shown in Fig.46. The extension of the analyses shows that the MSD initiation can be significantly reduced for low load levels. The initiation of MSD is non-linear with respect to the load level. Combined with the threshold based crack initiation analyses, the prediction of crack initiation is shown in Fig.47 as a function of load level. The prediction shows that, while the increase in MSD is not significant for a 20% higher load, based on a stress level of 100 MPa , the decrease in MSD is substantial for a 20% reduction of the load.

The analytical model has various uses. For example, a very practical extension of the analyses is that the effect of production consistency may be analysed as shown by the example in Fig.48. This example shows that for a given detail, fatigue life can be significantly increased without changing the geometry or load level. The increase in production quality, in terms of production consistency, can increase the fatigue life for a given risk level. The shortcoming of such a method is that the MSD initiation can be very rapid at the end of the fatigue life. This means that many cracks may be initiated “suddenly” everywhere.

A single piece of specimen, can benefit from the analysis as well. Fig.49 shows an example for the number of breaking-through cracks as a function of the fatigue cycles. It is possible to compute how many cracks may be initiated for a given number of fatigue cycles. This is very useful in order to determine the severity of an MSD scenario. Another thing is that the distribution of the size of leading crack may be evaluated as shown in Fig.50. This evaluation can be very practical in determining inspection and maintenance procedures since there should be detectable cracks when the inspection is performed in order to avoid the waste of time and money.

The probabilistic onset of multiple site damage has been analysed for cracks initiated at mechanical joints. The crack initiation is analysed based on detailed stress analyses, fracture mechanics methods, and probabilistic solutions. It has been shown that the stress distribution in mechanical joints is very complicated. To achieve reasonable estimations of stress conditions at the joints, contact conditions, friction, plastic yield, and non-linear geometrical deformations should be considered. It is demonstrated that the greatest challenge in the analysis is to evaluate the dynamic effect of fretting and friction occurring in the joints. Analyses involving tear and wear, and oxidation may be required for the stress at the joints under the fatigue loading condition.

The fatigue load sequence has an observable effect on the local stresses in the joints since significant plastic yield occurs even under a relatively low remote load. A very important result from the stress analyses is that the stress-strain response in the joint may achieve a “saturated” linear state depending on the load sequence and the load level. The stress-strain response may behave linearly, after the initial plastic yield has occurred due to the fatigue load sequence, with a stress concentration range smaller than what could be expected from the linear-elastic considerations. The stabilised stress-strain response has, however, a different stress ratio compared to the remote load. For example, the local stress-strain has a stress ratio less than –2.5 compared to the remote fatigue stress ratio of 0.1 for the test panels in the example.

In spite of complexity in stresses at the joints, it is feasible to analyse crack initiation as long as correct considerations have been made regarding the stress and the strain in the joint. For example, the three-dimensional weight function method can be used to evaluate stress intensity factors according to the stabilised linear stress-strain distribution at the critical locations. The weight function solutions also provide Green’s functions for a crack closure model to evaluate crack initiation and growth before the break-through of the thickness of the sheet. Since the crack closure model is used, the intrinsic crack growth rate can be used to evaluate the crack growth without involving many empirical parameters.

Together with an intrinsic crack growth threshold value and a probabilistic solution of the stochastic crack propagation, the probability of crack occurrence, and the probability of the crack breaking-through are evaluated for the multiple site damage scenario. In the probabilistic solution, uncertainties due to initial flaw, stochastic crack growth, geometrical inconsistency, and load severity etc., are separately considered so that their individual effects can be analysed for the estimation of the onset of multiple site damage.

3.7.4 Effect of Environmental Crack Growth Acceleration on Initiation of Wide Spread Fatigue Damage at Mechanical Joints

An advanced analytical procedure has been developed to predict multiple site fatigue crack initiation in mechanical joints where environmental pitting and crack growth acceleration have been considered. The fatigue crack growth is analysed taking into account contact areas, friction, plastic deformation and non-linear geometrical deformation etc.,. The fatigue crack growth analyses are based on the plasticity induced crack closure model. Uncertainties in pitting, fatigue crack propagation, production quality, loading, and material data are considered in a probabilistic solution combined with deterministic predictions. Monte-Carlo solution technique is used to simulate the fatigue crack initiation and to determine uncertainties in the initiation of fatigue cracks. One example is used throughout the paper to illustrate the procedure and to demonstrate capability of the method.

It is widely accepted that environmental attacks have detrimental effect on the fatigue of many metallic materials. Aluminium alloys, though being better corrosion resistant than steel alloys, suffer still from the environmental elements. While fatigue is load cycle related, environmental damage is time related. When the material is unprotected the fatigue life can be significantly reduced based on how frequent the component is exposed to the environmental attacks. Various mechanisms have been proposed as explanation to the fatigue life reduction. In this paper, two predominant mechanisms the pitting crack initiation and the corrosion assistant crack growth are considered since there are established models published in the open literature for these two mechanisms.

For the MSD panels investigated in [18], fatigue lives are evaluated according to published pitting and corrosion fatigue crack growth models. One example is shown in Fig.51. Depending on the exposure frequency, fatigue life can be reduced up to orders of magnitude if environmental attacks occur. The environmental attacks cause a rapid increase in the crack growth rate and the fatigue crack growth becomes much faster as the example in Fig.52 shows.

The scatter in pitting and crack growth acceleration is large. From the open literature, an example of a pitting model is shown in Fig.53. A single day exposure to environmental attacks may create pits with sizes ranging from 10 μm up to 100 μm. After 6000 days of exposure, the pits can range from 100 μm up to millimetres.

A probabilistic model is preferred for the analysis. The Monte-Carlo method is used to simulate the pitting and fatigue crack initiation. Some results are shown in Fig.54 as a comparison between the stochastic fatigue crack growth and the environmental assisted fatigue crack growth. Similar to the deterministic solution, the environmental attacks show a significant effect in reducing the fatigue crack growth even for a relatively high frequency of exposure.

The simulation can be very useful in determining the inspection interval since the distribution of fatigue damage may be evaluated. Fig.55 shows an example of the distribution of fatigue damage sizes compared to the probability of detection curves based on the simulations shown in Fig.55. According to the analytical results, it may be determined that the initial inspection should be arranged after 1000 days of service for the average crack based on a method with a(90/95)=2 mm, since the POD can be larger than 50% (the probability of discovering cracks are larger than the probability of missing cracks). Such an arrangement of the inspection may be much more rational. Another consideration may be made for the leading crack instead and a shorter inspection interval may be used.

For a general management, to assume environmental attacks occurring at every critical detail is not a rational way to solve the problem. Environmental attacks may or may not occur at a specific detail. Often, another consideration should be added to the solution of the probability of environmental attacks. Such a consideration yields the results shown in Fig.56. While a full environmental attack on all the critical details results in a very high MSD initiation, controlled environmental exposure may significantly reduce the MSD risk even though there can be a small number of part of the total number of details showing early fatigue damage, see Fig.56.

Even though the mechanisms may be very complicated in the initiation of MSD at mechanical joints, reasonable predictions may be realised based on the advanced analyses of the fatigue crack growth when the non-linear effect of friction, contact area, material, and deformation are considered together with the environmental effect. It is very effective to consider the plasticity induced crack closure in evaluating the fatigue crack growth in a complex stress field existing at mechanical joints.

The significant result in the present analyses is that when fatigue loading is considered, the material response may recover a linear relation after the peak loads. This makes it possible to analyse the crack growth according to the superposition principle of linear elasticity. The crack growth can be reasonably predicted according to the analyses of the fatigue crack growing in a residual stress field created by yield, contact and friction. Together with the strip yield model, which is also based on the linear solutions for plasticity, the prediction of fatigue crack growth can be realised based on a cycle-by-cycle evaluation of crack growth. This model makes it possible to analyse the fatigue crack growth under arbitrary fatigue loading conditions.

Combined with the crack closure analyses, the number of load cycles within different crack growth rate regimes can be separated. It is therefore possible to establish a probabilistic solution that can account for the small crack growth effect while disciplines developed according to the long crack growth tests are not violated. A total life probabilistic model can be established according to both small and long crack behaviours for the fatigue crack growth under spectrum loading condition when uncertainties in both loading and geometry are considered.

The pitting and environmental acceleration of crack growth can be accounted for according to their contribution to the process of fatigue in both the creation of initial cracks and the acceleration in the crack growth rate. Monte-Carlo simulations can be used to evaluate uncertainties in the crack initiation, in the MSD scenarios, by combining the crack growth analytical model with environmental crack growth acceleration and the pitting corrosion model. It has been shown that environmental attacks, when occurring at fatigue critical locations, may have a significant effect on the onset of MSD.

3.8 COMPOSITE MATERIALS

3.8.1 Measuring Shear Strength in Composites

A couple of methods to measure composite interlaminar shear strength (ILSS) are available. Unfortunately these methods all suffer from drawbacks of various kinds. The main problem is to achieve a state of pure and uniform shear over the test region. This usually leads to that the measured values are on the conservative side.

Four methods to determine ILSS have been evaluated, Ref.[19]. The work has been made in collaboration between FOI and KTH (Royal Institute of Technology, Stockholm). Particularly the recently devised inclined double notch shear test (IDNS), see Figure 57, was compared to three existing and more established methods: the Iosipescu test, the short three point bending test and the double notch compression test. The uniformity of strain field in the test region in a real test situation was investigated by strain mapping using the optical measurement technique "digital speckle photography". The measured strain fields were compared to FE-calculated strains representing ideal conditions and both known advantages and drawbacks of the different methods were confirmed. The IDNS-test had the most uniform strain fields and also consistently high ILSS values. The shear strain field close to failure is shown in Figure 58. It has a shear band, about 0.7 mm wide, with nearly constant shear strain between the notch ends. Fields of high strain have developed around the loading points opposite of the notches; these fields interfere slightly with the otherwise homogeneous shear band, a phenomenon that was observed only at the highest load levels close to failure.

A fractographic analysis indicated shear separation over a major part of the fracture surfaces of all specimen types: typical shear cusps were found over about 80% of the IDNS fracture surface and in about 50% to 70% in the other specimens. For the Iosipescu tests, failure initiation could be ascribed to initiation in tension at defects. Experimentally determined stress-strain responses in shear exhibited a distinct variation among the different methods. For the best methods, a notable material softening due to shear cusp formation was observed prior to failure in the composite material studied here.

3.8.2 Fatigue Testing of Impact Damaged Composite Specimens

An extensive fatigue testing programme on impact damaged carbon fibre/ epoxy composite laminates is ongoing at FFA in co-operation with SAAB. The objective is not only to evaluate the fatigue resistance of such structures but also to study the mechanisms that control the fatigue life. To aid this study two measurement techniques are used: Ultrasonic C-scan and Digital Speckle Photography (DSP). With the Ultrasonic measurements, one can see the distribution of delaminations after impact and which delaminations that grow during the fatigue life. The optical measurement technique DSP enables one to see the 3D displacement field as the specimen is loaded. DSP is used mostly to study the shape of the buckles during compressive load.

In Ref. [20] two layups, quasi-isotropic and 0°-dominated, were tested at constant amplitude loading. The experimental conditions were chosen to be representative of damages in aircraft structures. The fatigue results for specimens are shown in Figure 59. The R-value was found to have small influence on the fatigue life indicating that the compressive part of the load cycle has more importance than the tensile part, this because the compressive load caused local buckling around the damage zone. The buckling was inward on the impact side and outward on the backside with larger buckles on the backside. Also the backside buckles showed a larger growth during the fatigue life. Fatigue lives were compared to the results of an analytical model which was found to give conservative predictions.

The mechanisms leading to delamination growth and in the end fatigue failure in the specimens discussed above were analysed in Ref.[21]. The observations indicate that the fatigue life is controlled by delamination growth in the direction transverse to the load, though the final failure mechanism can be another one. More than half of the delaminations that grow are along plies in transverse direction. The delamination growth is driven by buckling that occurs during the compressive part of the load cycles; an indication of this is that the buckle on the backside usually had the same areal shape as some delamination. This is exemplified in Figure 60 showing the buckling shape and extension of the delaminations at two times during the fatigue life. The iso-contours shows that the main buckle goes inwards on the frontside and outwards on the backside.

In specimens run to fatigue limit, buckling and delamination growth occur only in the outer 2-3 layers on the backside. For the quasi-isotropic laminate it is suggested that a threshold compressive load exists, a threshold which is individual for each specimen. At loads higher than the threshold, the specimen buckles through the whole thickness and fatigue failure is probable.

3.8.3 Composite Fatigue

It has been shown previously, mainly for open hole specimens, and with reasonable accuracy that it is possible to map spectrum data on constant amplitude data if a characteristic number of cycles is considered, Refs. [22, 23, 24]. Another important issue is the effect of spectrum truncation and load cycle elimination on the composite life. For the mapping onto constant amplitude data the number of extreme values in a spectrum (N_{CC}). i.e., the number of range pairs that exceed a particular value e.g. 90% of the maximum range, times the number of actual blocks to failure are considered to be the equivalent number of cycles.

$$N_{CA} = N_{CC} \times N_{Block} \tag{30}$$

To investigate the effect on bolted joint specimens a rather extensive test program was outlined for panels with a quasi-isotropic layup, having the following stacking sequences $[(45/-45/\ 0/90/)_3]_s$ and $[(45/-45/0/90/)_6]_s$ for the thin and the thick part, respectively, Refs. [25, 26, 27, 28]. All the specimens were tested statically and in fatigue comprising spectrum and constant amplitude loading with R=-1, -0.2 and -5. Different elimination levels were also investigated for a symmetrical fin-spectrum.

A similar program was also conducted on fatigue after impact specimens with quasi-isotropic and zero-dominated lay-ups, with the following stacking sequences $[((0/45\text{-}45/90/)_s(90/\text{-}45/45/\ 0)_s)_2]$ and $[45/\text{-}45/0/90/45/\text{-}45/0/0/(45/\text{-}45/0/90/)_2(45/\text{-}45/0/0/45/\text{-}45/0/90)]_s$, respectively Ref. [24, 29]. All the panels were impacted with 30J, damage characterised, and tested statically and in fatigue comprising both spectrum and constant amplitude loading with R=-1 and -5. The spectrum used was a compression-dominated upper-wing spectrum, OVKB, which from a constant-amplitude point of view was close to R=-5. Elimination was also considered for one elimination level.

For both bolted joint and fatigue after impact specimens, it was possible to map spectrum data on constant amplitude data with reasonable accuracy, if only a characteristic number of cycles were taken into account. A previous investigation concerning typical open hole specimens led to the same conclusion. This means that the calculation procedure and the verification testing can be simplified. The number of cycles that are required for the mapping of spectrum fatigue data needs to be further investigated.

After Rain-Flow Counting (sorting in constant-amplitude events), the spectrum contains numerous loading conditions (R-values). For that reason it must be an advantage to have S-N curves covering both tension and compression loading but with different slopes. Also, the fatigue life is usually dominated by the highest loads in an absolute sense.

In Figure 61 constant-amplitude loading of bolted joints is depicted. To have a simplified approach, straight lines, in a least square sense, have been drawn. For many loading conditions, especially tension or compression dominated loading the S-N curve is very flat indicating the possible existence of a threshold value below which fatigue is not likely to result in failure of the composite.

This implies that in such structures a fatigue test is of limited value. A static test to a statistically established safe value should be enough. From the testing of the fatigue after impact specimens it can be concluded, based on the very flat S-N curve, that there is a threshold problem which means that for a suitable statistically safe static value, the structure also will be substantiated in fatigue.

The effect of spectrum truncation and elimination on composite fatigue life was studied in Ref. [23]. It was concluded that the elimination level could be set to 50% of the maximum range of the fatigue spectrum tensile or compressive stresses, where maximum or minimum stresses correspond to the material ultimate strain. The current investigation within the EDAVCOS program covering bolted joints and fatigue after impact specimens also indicate that a high degree of elimination can be adopted for that type of specimens, Refs. [22, 23, 26, 28]. The investigation needs to be expanded to more structure like type of specimens before any firm conclusions can be drawn. Anyhow performed investigations give a clear indication that this could be a fruitful way forward, in order to have a rational way to handle the fatigue substantiation of composite structures.

For bolted joints, single and double lap joints with various number of bolts, constant amplitude testing with tension or compression dominated loading results in rather flat S-N curves although, with a high degree of scatter. For compression dominated loading the fatigue life is longer than for tension dominated loading. This is probably due to the increased ability to transfer load through the fasteners in compression. As for open hole specimens it is likely that the elimination level can be set to at least 50% of the maximum peak or trough for both bolted joints and fatigue after impact specimens. Very few cycles in the sequence contribute to the overall damage. This means that the actual time to perform a verification test can be substantially reduced since only a few characteristic cycles contribute to the life. The R-value is dependent on the structural detail considered but generally R=-1 is the worst case and for other R-values simplifications can be made. Looking at a typical wing or fin spectra used in the current investigation, strain ranges less than 30 and 50% of ultimate strain range are eliminated. Depending on frequency, which typically is in the range of 0.2 to 0.5 Hz, the testing time can be reduced to 50% of the original testing time if the elimination level is set to 30%, see Fig. 62.

Despite the fact that current tests have been carried out on a coupon level and that the data base is limited, the indication is very clear that substantial time and money can be saved in this area.

The Sendeckyj analysis is a convenient way to address the reliability both for static and fatigue related problems in the certification process, see e.g. Refs. [30, 31, 32, 33]. For fatigue related problems the technique gives similar results as the traditional S-N curve representation. The technique is also very effective for establishment of e.g. load or life scatter factors, the so called load enhancement factor approach. Once the shape and scale parameters are established it is also very convenient to establish the B-value for the configuration at hand. The traditional well known load enhancement curve used in the certification process is established for a variety of configurations but fatigue after impact is not included and nor is bonded joint data. It should be pointed out that data determined within the EDAVCOS program and described in Ref. [34] is limited and that the database should be expanded.

The basic two-parameter wear-out equation introduced by Sendeckyj is given by

$$\sigma_s = \sigma_a \left[(\sigma_r / \sigma_a)^{1/S} + (N-1)C \right]^S \tag{31}$$

where

σ_s = the equivalent static strength
σ_a = maximum applied cyclic stress
σ_r = residual strength
N = number of fatigue cycles (test duration - life times)
S and C are fitting parameters

It can be shown that at each individual stress level that the fatigue life distribution, α_L, is also a Weibull distribution with a shape parameter

$$\alpha_L \approx S\alpha_S \tag{32}$$

where S is the slope, k, of the curve. Assuming C=1 and rewriting Eq.31 in terms of strain the following equation in a log-log scale is obtained, see also Fig. .63.

$$\log \varepsilon = \log \varepsilon_S + k \log(N) \tag{33}$$

Using the test results i.e. constant amplitude data for bolted joints, R=-1, -0.2 and -5 and for fatigue after impact specimens, R=-1 and -5, as well as spectrum data with and without elimination, the slopes and average static strains can be obtained, see Refs. [25, 26, 27 and 32].

Spectrum data are mapped on constant-amplitude data taking into account only the maximum number of troughs in the spectrum for fatigue after impact specimens. It should be remembered that only one level of energy has been considered, i.e. 30J. On the other hand, this energy level is rather high in relation to the thickness of the laminate, t=4.2mm.

For bolted joints the slope for tension and compression dominated loading is very flat and is associated with a high degree of scatter, but for tension and compression dominated loading, R=-1, the scatter is reduced and the slope is more pronounced, see Fig.63. For fatigue after impact specimens the slopes are almost identical for compression or tension-compression dominated loading indicating that compression loading rules the behaviour. The difference between bolted joints and fatigue after impact specimens in compression loading seems to be of minor importance. In Figure 64, all test results for fatigue after impact specimens are collected, constant amplitude data R=-1 and -5, and spectrum data including also results from tests with eliminated spectra.

The slopes are determined in a log-log scale in a least square sense. An iterative procedure is described in Ref. [30] taking into account both the slope and the constant *C* in Eq.(31). The one life time reliability, B-basis, can easily be determined as function of mean fatigue life knowing the shape and scale parameters.

In Fig.65 the load enhancement factor as function of mean fatigue test time for all test results, i.e. open hole specimens bolted joint specimens and fatigue after impact specimens, is shown and compared to the corresponding curve from Refs. [32, 33]. The various configurations covers both static and fatigue testing which was conducted as constant-amplitude loading but also as spectrum loading with different elimination levels. In the light of the very few test results the curves are very close. It should be noted that, the current curve, based on our testing and covering fatigue after impact, is covered by the reference curve up to almost 4 lives. Current curve gives α=1.12 in fatigue respectively and α=22.5 for static loading as compared to 1.25 respectively 20 as determined in Refs. [32, 33]. For constant amplitude loading (R=-1) and spectrum loading (BFKB and OVKB) the mean and B-basis strain versus number of cycles is shown in Figs.66 and 67 for bolted joints and fatigue after impact specimens respectively.

3.8.4 Equivalent Damage and Residual Strength for Impact Damaged Composite Structures

A number of stiffened wing-panels were manufactured and tested within the EDAVCOS- program (Efficient Design And Verification of Composite Structures BRPR-CT98-0611). The panels were flat with co-bonded and co-cured I-beam stiffeners, where the I-beams are built up from two C-beam stiffeners back-to-back. The panels were manufactured from HTA/6376C prepreg with a nominal thickness of 0.125 mm. The stacking sequence used in the skin was $[+45/-45/0/90]_{3s}$ giving a skin thickness of 3mm. The layup for the C-beams were $[45/-45/0_3/\ 90/0_3/-45/45]$. A general description of performed tests and geometry for the stiffened wing- panels can be found in Refs. [28, 29, 35], see Fig. 68 for a general description.

The panels were tested in compression with artificial delaminations and impact damage in mid-bay skin but also with this type of damage adjacent to the stringers. Material data used for residual strength prediction are presented in Table 1.

Basic room temperature material data used are given below, where the subscript 11 stands for the fiber direction and 22 is perpendicular to the fiber direction. Table 1 was used for current testing.

E_{11}=140 GPa	E_{22}=10.0 GPa	G_{12}=5.2 GPa
t_{nom}=0.13 mm	ν_{12}=0.3	

Table 1: Material data for HTA7/6376

For residual strength prediction a value of G_c= 300 N/m has been used for the critical strain energy release rate.

To predict the strength of the panel with the artificial delamination, Ø40mm, the analytical technique described in Ref. [36] was used. The method includes three different techniques to describe the actual damage size. In Fig.69 the initial buckling curve and three G_c curves are depicted. The G_c curves indicates the strain at which the sublaminate starts to grow or become critical. The critical energy release rate, G_c, is assumed mainly to be composed of G_I with a minor contribution of G_{II}. The high G_c curve indicates an alternative critical energy release rate mainly dominated by modus II and the lower one indicates a possible fatigue threshold value on the energy release rate. In the figure, the interrupted test results are also invoked. The predicted strain is roughly in the middle of the test results, covering initiation up to final failure. The interrupted tests are associated to increased damage size but also to an increase in energy release rate. That means to capture initiation a threshold value should be used and to capture final failure a higher critical value than

G_c=300N/m should have been used. The prediction also indicate that local delamination buckling will occur at a much lower strain than the critical strain associated with the G_c curve. Compared to the test results the predicted initial buckling curve is very close to where delamination buckling actually occurred. Damage evolution associated with increased loading meant that the damage area increased from 1199mm^2 to 2017mm^2 at final failure.

For impact damaged panels the same technique as for the case with artificial damage was used, see e.g. Ref. [36]. The energy-level at impact was 15J causing damage sizes in the range 380 to 460 mm^2. On the other hand, the predictions with current technique have turned out to be rather insensitive for various damage sizes, since mainly the same interface being critical for increasing damage size. With the same assumption on G_c=300N/m, as in the case for artificial damage, the result is shown in Fig. 70. In the figure the interrupted test results and the interrupted test results for local buckling are invoked. The interrupted test results are associated with increased damage size as the load successively increased. Despite that global skin buckling occurred before the local delamination buckling, technique two gives an conservative estimate of the initiation of delamination buckling. Taking the initial damage area, as detected by the scanning technique, and utilising technique 1 the predicted strain is 0.51% as compared to 0.58% at final failure. Considering the scatter in damage size that can occur a good prediction has been obtained.

3.8.5 Mass Criteria for Impact Response of Composite Plates

A unique mass criterion has been developed to distinguish the response types during impact on plates [37]. The criterion is based on the impactor/plate mass ratio. Relatively light impactors cause a response controlled by wave propagation independent of the boundary conditions of the plate, Fig. 71a. Relatively heavy impactors cause a quasi-static response, which is highly dependent on the entire stiffness of the impacted structure, Fig71b. For a given impact energy, a small mass impact causes a higher peak load and more extensive damage. The criterion may be used to simplify analytical and numerical modelling and to guide the selection of impact test matrices.

3.8.6 Prediction of Response and Damage Formation in Laminates Under Large Mass Impact

The quasi-static response and damage formation in laminates under large mass impact has been modelled by a spring-mass model, Fig. 72, which involves indentation, bending, shear and membrane effects [38]. Delamination growth is governed by the delamination threshold load and the number of delaminations. The threshold load is shown to be essentially independent of the size and boundary conditions of the plate and acts as a mechanical fuse for the load carried by out-of-plane shearing. The number of equivalent circular delaminations is at the present stage empirical and based on fractographical measurements of delamination area in typical laminates.

The model is compared with a number of instrumented impact tests on square laminates and rectangular laminates having different thickness, layup and boundary conditions [39]. The predicted independence of the delamination threshold load with respect to laminate size and boundary conditions is validated by the experiments. The load-deflection relation is predicted fairly accurately, Fig. 72b, while the predicted delamination size is highly dependent on the assumed number of delaminations.

3.8.7 Characterisation of Impact Damage in Composite Laminates

An extensive program has been initiated to characterise impact damage in composite laminates. The aim is to provide guidelines for improved models to predict strength after impact. The damage geometry has been characterised with respect to the distribution of matrix cracks, delaminations and fibre fracture in typical laminates of different width, thickness, boundary conditions and layup [40]. Fibre fracture was almost uniformly distributed through the thickness and was only found in a central region with a width of one third to one half of the delaminated region, Fig. 73. Delaminations were fairly uniformly distributed through the thickness, with the exception of single extended delaminations in the lowermost interface.

The constitutive properties of impact damage zones in two quasi-isotropic carbon/epoxy laminates have been studied in tension and compression at low strains [41]. Small coupons were cut at increasing distance from the impact centre, to allow determination of the spatial variation in stiffness. The experiments demonstrated a negligible influence of delaminations prior to local buckling. The stiffness reduction due to fibre fracture, which was primarily found in a central region of the thinner laminates, was larger in tension (80% reduction) than in compression (50% reduction), Fig. 74.

3.8.8 Prediction of Delamination Buckling and Growth

An in-house program (DEBUGS) has been developed to simulate growth of single delaminations due to interaction between local delamination buckling and global skin buckling [42, 43]. The program is based on buckling/post-buckling analysis with shell elements in a commercial FE code, which has been combined with routines for fracture mechanics calculations and a moving mesh to simulate delamination growth. An approximate method is used for fracture mode separation, and the crack front is automatically moved when a mixed mode fracture mechanics criterion is satisfied. The program was originally limited to local delamination buckling, but has later been extended to allow global skin buckling and panels with stiffeners.

DEBUGS has been validated by extensive tests with artificial circular delaminations at different depths, where load, out-of-plane deflections and delamination growth have been carefully monitored [42]. Two examples of results are shown in Fig. 75 The most recent tests were used to validate a predicted transition from growth perpendicular to the load for shallow delaminations to growth in the load direction for deeper delaminations [43]. The program has also been used to simulate buckling and delamination growth in skin-stringer panels tested by DERA (UK) in joint European programmes [44, 45, 46]. Initial attempts to predict the behaviour of impact damage in such panels are promising but also demonstrate the need to include additional factors [46]. Initial imperfections and softening due to damage and multiple delaminations are features addressed in ongoing work.

3.8.9 Delamination Growth in Laminates Under Fatigue

Previous studies of delamination growth under fatigue loading have been extended to study the effect of temperature (20º C and 100º C). Carbon fibre/epoxy laminates were loaded statically and in fatigue under pure and mixed Mode I/Mode II loading, by use of an MMB test rig in a climate chamber [47]. Delamination threshold toughness values were significantly lower than static values, and ranged from one fourth of the static toughness for mode I (DCB) to one tenth for mode II (ENF), Fig. 76. The elevated temperature only had a moderate effect on static toughness values but the delamination threshold values decreased by 30 to 50 %.

Fractography was used to explain differences in toughness under fatigue and static loading [48]. Similar shear cracks were observed ahead of the crack front in fatigue and static Mode II loading. In static loading such cracks were shown to appear at a much lower load than required for macroscopic crack growth. As an explanation of the lower Mode II toughness in fatigue it was suggested that the shear cracks may grow and coalesce in fatigue once the load for initiation of shear cracks has been reached. The resulting shear cusps just behind the crack front were similar, but in fatigue specimens the number of cusps further behind the crack front gradually decreased as a result of abrasion.

3.8.10 Residual Compressive Strength of Indented Sandwich Panels

This report [49] describes residual compressive tests performed on indented sandwich panels. Indentation damage was introduced statically, while load and indentation were recorded. Before compressive tests the damage were characterised by ultrasonic C-scan and by measuring the dent depth and width. During the compressive tests strain and out of plane displacements were measured using strain gauges and a full field optical system. The face sheets had a quasi-isotropic stacking sequence, with the nominal thicknesses varying from 1 to 3 mm. Three different cores were used, i.e. a Nomex honeycomb and a high and a low density aluminium honeycomb core.

The purpose of the program was to study the effect on compressive failure load and failure mode of the different materials employed for a specific damage, i.e. a 5 J indentation, a core crush damage with no delaminations and finally a damage with the delamination diameter of 25 mm

A reduction in residual compressive strength to less than 50 % compared to the undamaged panels was observed for these relatively small damage sizes. Similar results were obtained in a previous study on larger panels tested in four-point-bending [50].

Two different failure modes, in some cases in combination, were identified. The first was dent growth, transverse the load direction, followed by compressive failure, see Fig. 77, and the second was delamination buckling of a small portion of the damage above or below the centre of the dent, see Figs. 78 and 79. When delamination growth occurred the final failure did not coincide with the centre of the dent, but with the delaminated area. No effect on failure strain for the different failure modes could be observed. For the 192 kg/m^3 aluminium core only delamination growth was observed, since dent growth is unlikely with a stiffer core material. There is a tendency that indentation growth is more frequent in specimens with Nomex core than in specimens with 72 kg/m^3 aluminium core. This can be explained by the fact that the aluminium core has approximately five times higher stiffness in the undamaged region.

By evaluating the strains from the full-field optical system it was also shown that the damage did not introduce strain concentrations at the damage border in the same way as expected from an open hole. The strain concentrations are more pronounced in the centre of the damage, which can be explained by the fact that the damaged zone is supported by the core material which prevents buckling of the skin, whereas significant stresses can be transferred by the damaged material.

The results showed that the method to predict damage initiation and damage size developed at FFA gives good correlation with experiments [51, 52]. Failure due to delamination buckling will require modification of published methods to predict delamination growth.

3.8.11 Impact Damage Close to Bolted Joints

The purpose with this experimental program [53] was to determine the effect of impact damage close to bolted joints and to a substructure. It is known that impact damage close to clamped boundaries results in a larger damage than impacts far from the boundaries, and that such an impact will reduce the buckling load of the impacted laminate [54]. However, the effect of impact close to a bolted joint has so far not been investigated.

Specimen dimensions and boundary conditions during impact are presented in Fig. 80. During impact, the load and displacement of the plate under the impact point were recorded. Specimens were impacted at five different distances, *r*, from the joint. After impact, the specimens were inspected with ultrasonic C-scan and a few specimens were fractographically inspected with respect to damage distribution.

A significant effect on both damage size and shape was demonstrated. The effect can mostly be related to the stiffness of the substructure, as bending of the panel during impact is smaller. When impacting close to a substructure more of the energy is available for damage formation and consequently both dent depth and damage width increased significantly. Extensive fibre fracture was also observed in the panels, see Fig 81.

3.8.12 Tests and Analytical Prediction of Compressive Strength of Impacted Composite Laminates

The purpose of this program [55] is to create experimental results with well-defined boundary conditions for the residual compressive strength of impacted CFRP laminates. Comparisons are made with analytical solutions for global buckling, delamination buckling and delamination growth. Damage smaller than a barely visible impact damage, i.e. damage without or with a small extent of fibre fracture are studied.

Square laminates, impacted with 17 J or 30 J, with different lay-ups are tested in compression, with two different boundary conditions, see Fig. 82. The lay-ups tested are cross-ply, quasi-isotropic and an orthotropic. During compressive tests load, displacement, out of plane displacements and strains are measured to detect local/global buckling. At intervals during compressive tests the specimens are unloaded and delamination growth is characterized by ultrasonic C-scan.

Regarding delamination size after impact no significant difference could be seen between 17 J and 30 J impact on the cross-ply laminates. For the quasi-isotropic laminates a 30 J impact causes larger delaminations than a 17 J impact. In the orthotropic laminates the difference was extremely large, as a 17 J impact caused a hardly detectable delaminations, whereas a 30 J impact caused a larger delaminations than in the isotropic laminates.

The global buckling characteristics of the panels have been demonstrated to be affected by an impact damage since the load for onset of nonlinearity is reduced by the damage. The delamination-buckling load was also shown to depend on the impact energy, although in some cases delamination size detected by ultrasonic C-scan only showed a small difference for the two different impact energies. This observation indicates an effect of fibre damage, multiple delaminations or increasingly connected delamination areas. For the case with clamped/free edges the effect on the maximum load was very small, whereas for the panels loaded with clamped/simply supported edges the differences were significant. Delamination growth detected by ultrasonic C-scan was more pronounced in panels impacted with 30 J than in those impacted with 17 J, except for the cross-ply laminates loaded with clamped/free edges in which delamination size after impact was very similar.

Analytical expressions for the global buckling gave nonconservative results for laminates tested with clamped/free edges. For panels tested with clamped/simply supported edges good agreement was obtained between experimental and analytical results.

Analytical expressions for delamination buckling are non-conservative for panels tested with free unloaded edges, but agree fairly well with the experimental results when the unloaded edges are simply supported. Analytical expressions for delamination growth are in all cases non-conservative. This can also be explained by additional stresses due to bending of the buckling laminates.

3.8.13 Compression Tests on Impacted Rectangular Composite Laminates With Various Lay-Ups

This experimental program [56] determines the residual failure loads and failure mechanisms of CFRP laminates impacted with 30 J. As composite structures presently are designed against buckling, there are two failure modes of interest, i.e. local/global buckling combined with delamination growth and compressive failure due to stress concentrations at the damage.

Compressive tests are performed with anti-buckling guides and with a combination of clamped/simply supported edges on panels with the dimensions 260 by 156 mm. Three quasi-isotropic and one orthotropic lay-up are studied. The quasi-isotropic lay-ups were either 48 or 32 plies thick, where double plies were used in one of the 32 ply lay-ups.

Load, out of plane displacements and strains are measured during tests to detect local/global buckling. Out-of-plane displacements are on some specimens measured with an optical full field system. At intervals the specimens are unloaded and delamination growth is characterised by ultrasonic C-scan to determine the site and amount of growth.

Significant effects of the 30 J impacts were found on both global buckling and residual compressive strength of the panels. In the impacted panels delamination buckling was observed at strain levels below 0.2 % independently of the boundary conditions.

Delamination growth was observed in all impacted panels except the 48-ply specimens tested with anti buckling guides. The nature of delamination growth was found to be highly dependent of the stacking sequence and also of the boundary conditions:

3.9 SWEDISH ICAF-DOCUMENTS DURING JUNE 1999 TO MAY 2001-05-30

2231 "Analysis Methodology for Fatigue Crack Propagation and Residual Strength of Joints with Widespread Fatigue Damage". Nilsson, K.F. and Andersson, B.

2240 "Accurate Stress Intensity Factor Solutions for Unsymmetric Corner Cracks at a Hole". Fawaz, S. and Andersson, B.

2266 "Fatigue Life Prediction and Load Cycle Elimination During Spectrum Loading". Schön, J. and Blom, A.F.

2267 "Spectrum Fatigue of Composite Bolted Joints". Schön, J. and Nyman, T.

2268 "Fatigue Testing and Buckling Characteristics of Impacted Composite Specimens". Melin, G., Schön, J. and Nyman, T.

ACKNOWLEDGEMENTS

This work was supported by the Defence Material Administration. The assistance of Ms. Inez Engström in preparing the manuscript is gratefully acknowledged. The editors are also indepted to the following individuals who helped to write parts of this review:

Hans Ansell	SAAB	(Sections: 3.2.1, 3.5.3, 3.5.4, 3.5.5, 3.5.6)
Lennart Magnusson	SAAB	(Sections 3.3.1)
Roman Starikov	KTH	(Sections: 3.4.2)
Stefan Thuresson	SAAB	(Sections: 3.5.1, 3.5.2)
Gunnar Melin	FOI	(Section: 3.6.4, 3.8.1, 3.8.2)
Geng-Sheng Wang	FOI	(Sections: 3.7.3, 3.7.4)
Tonny Nyman	SAAB	(Sections: 3.8.3, 3.8.4)
Sören Nilsson	FOI	(Sections: 3.8.10, 3.8.11, 3.8.12, 3.8.13)
Robin Olsson	FOI	(Sections: 3.8.5, 3.8.6, 3.8.7, 3.8.8, 3.8.9)
Börje Andersson	FOI	(Sections: 3.6.1, 3.7.1)

REFERENCES

1 Blom, A.F. (Ed), ”A Review of Aeronautical Fatigue Investigations in Sweden During the Period May 1997 to May 1999”, FFA TN 1999-44, Stockholm 1999.

2 Ansell, H. “The need for and use of a Life Monitor System on a Fourth Generation Combat Aircraft”. In proceedings from the 2000 USAF Aircraft Structural Integrity Program Conference, San Antonio, USA, 5-7 December 2000.

3 Änggård, J., “Parametric Study of Lap Joint”. FFA TN 2000-44, 2000.

4 R. Starikov and J. Schön. “Quasi-static behaviour of composite joints with protruding-head bolts“, Composite Structures 2001;51(4):411-425.

5 R. Starikov and J. Schön. “Experimental study on fatigue resistance of composite joints with protruding-head bolts“, accepted in Composite Structures 2001.

6 R. Starikov and J. Schön. “Local fatigue behaviour of CFRP bolted joints“, submitted to *Composite Science and Technology* 2001.

7 R. Starikov and J. Schön. “Fatigue behaviour of composite joints with hexagon bolts“, *the 13th International Conference on Composite Materials*, ICCM-13, Beijing, China, 25-29 June 2001, to be presented.

8 R. Starikov and J. Schön. “Quasi-static behaviour of composite joints with countersunk composite and metal fasteners“, Composites Part B: Engineering 2001;32(5):401-411.

9 R. Starikov and J. Schön. “Fatigue resistance of composite joints with countersunk composite and metal fasteners", accepted in International Journal of Fatigue 2001.

10 S Fawaz and B Andersson,"Accurate Stress Intensity Factor Solutions for Unsymmetric Corner Cracks at a Hole", Fourth Joint DoD,FAA,NASA Conference on Aging Aircraft, May 15-18, St Louis, Missouri, U.S.

11 Palmberg, B., “Stress Intensity Factor Formulae for a Through the Thickness Centre Crack in a Sheet of Finite Dimensions”., FOI-R—0091—SE, 2001 (in printing).

12 Palmberg, B., “A Stress Intensity Factor Equation for Cracks at an Open Hole in a Sheet of Finite Dimensions Subjected to a Uniform, Uniaxial Stress”. FOI-R—0061—SE , 2001 (in printing).

13 L. Gunnar Melin, "Multiaxial Fatigue: a Literature Survey", FFA TN 2000-41, (2000).

14 L. Gunnar Melin, " Cycle count in high cycle fatigue of a multiaxial random load: a comparison of different approaches", To be presented in "6th International Conference on Biaxial/Multiaxial Fatigue and Fracture", Lisbon, Portugal, (2001).

15 KF Nilsson, B Andersson, "Analysis Methodology for Fatigue Crack Propagation and Residual Strength of Joints with Widespread Fatigue", 1999 USAF Aircraft Structural Integrity Program (ASIP) Conference, San Antonio, Texas, USA, Nov 30-Dec 2, 1999, 45 pp

16 B. Andersson, “Statistical Analysis of 3D Multiple-Site Fatigue Crack Growth in Ageing Aircraft using a hp-version of FEM”, Keynote Lecture MSCOM 2000, Yamaguchi, Japan, Sept. 29-Oct. 3, 2000. In preparation.

17 G.S. Wang, “Deterministic and Probabilistic Analyses of the Initiation of Wide Spread Fatigue Damage for SMAAC Test Panels”, FFA TN 2000-11, February 2000.

18 G.S. Wang, ”Effect of Environmental Crack Growth Acceleration on Initiation of Wide Spread Fatigue Damage at Mechanical Joints”, FFA TN 2000-12, February 2000.

19 L.G. Melin, J.M. Neumeister, K.B. Pettersson, H. Johansson and L.E. Asp, "Evaluation of Four Shear Test Methods by Fractographic Analysis and Digital Speckle Strain Mapping", *J. of Composites Technol. & Research* 22 (3), 161-172, (2000).

20 L. G. Melin, J. Schön and T. Nyman, "Fatigue testing and buckling characteristics of impacted composite specimens", To be published in *Int. J. Fatigue*. Also: FFA TN 2000-48.

21 L. Gunnar Melin and Joakim Schön, "Buckling behaviour and delamination growth in impacted composite specimens under fatigue load: an experimental study", To be published in *Composite Sci. Technol*. Also: FFA TN 2000-80.

22 Nyman T., Ireman T. and Friberg M.," Appendix N.SAAB - Predict Strength and life of bolted joints", SAAB.T1.TR.7/ FKH-2000-0011.

23 Nyman T.," Appendix G.SAAB - Predict Residual Strength and Life of Stiffened Panels with Midbay Impact Damage", SAAB.T1.TR.8/ FKH-2000-0016.

24 Nyman T., Ansell H. and Blom A., "Effects of truncation and elimination on composite fatigue life", Composite Structures 48 (2000) 275-286.

25 Starikov R.,"Experimental Investigation of Fatigue Behaviour in Composite Bolted Joints", Report No. 97.39, Royal Institute of Technology (KTH), Department of Aeronautics.

26 Nyman T.,"Fatigue Testing of Bolted Joints in Composite Structures NFFP336+345", FKH P-98006.

27 Schön J. and Nyman T., " Experimental results from spectrum fatigue of composite bolted joints", FFAPH-1417.

28 Nyman T.,"Fatigue Testing of Impact Damaged Composite Structures NFFP336+345", FKH P-98005.

29 Melin G. L. and Schön J., "Experimental report from fatigue testing of impacted composite laminates", FFAPH-1416.

30 Sendecky G. P., " Fitting Models to Composite Materials Fatigue Data", Test Methods and Design Allowables for Fibrous Composites, ASTM STP 734, C. C. Chamis, Ed., American Society for Testing and Materials, 1981, pp. 245-260.

31 Nyman T., "Review of Certification Procedures at Saab", SAAB.T4.TR.1, FKH-1999- 080.

32 Whitehead R.S., Kan H.P. and Saether E.S.," Certification Testing Methodology for Composite Structure - Volume I-Data Analysis", NADC-87042-60, DOT/FAA/CT-86/39, October 1986.

33 Whitehead R.S., Kan H.P. and Saether E.S.," Certification Testing Methodology for Composite Structure - Volume II-Methodology Development", NADC-87042-60, DOT/FAA/ CT-86/39, October 1986.

34 Melin G. L. and Schön J., "Experimental report from fatigue testing of impacted composite laminates", FFAPH-1416.

35 Greenhalgh E., Clarke A. and Thatcher J. " Mechanical Evaluation of Stringer Stiffened Panels tested Under Compression - Contribution to EDAVCOS Deliverable D3.3.1 - UC", DERA.T3.TR4, DERA/MSS/MSMA2/TR002079, August 2000.

36 Nyman T., Bredberg A. and Schön J., " Equivalent Damage and Residual Strength for Impact Damaged Composite Structures". Journal of Reinforced Plastics and Composites, Vol. 19 No. 06/2000.

37 Olsson, R (2000) Mass criterion for wave controlled impact response of composite plates, Composites Part A, 31(8)879-887.

38 Olsson, R (2000) Analytical prediction of large mass impact damage in composite laminates, *FFAP H-1423*, FFA, Bromma, to appear in *Composites Part A* (2001).

39 Olsson, R (2000) Large mass impact tests on rectangular composite laminates with various layups, *FFA TN 2000-01*, FFA, Bromma.

40 Sjögren, A (1999) Fractographic characterization of impact damage in carbon fibre/epoxy laminates, *FFA TN 1999-17*, FFA, Bromma.

41 Sjögren, A, Krasnikovs, A and Varna, J (1999) Experimental determination of constitutive properties of impact damage in carbon fibre/epoxy laminates, *FFA TN 1999-53*, FFA, Bromma, to appear in *Composites Part A* (2001).

42 Nilsson, K-F, Asp, LE, Alpman, JE and Nystedt, L (2001) Delamination buckling and growth for delaminations at different depths in a slender composite panel, *Int. J. Solids Struct*., 38(17)3039-3071.

43 Nilsson, K-F, Asp, LE and Sjögren, A (2000) On transition of delamination growth behaviour for compression loaded composite panels, *FFA TN 2000-19*, FFA, Bromma.

44 Asp, L (1999) Preliminary analysis of DAMOCLES panels, *FFAP H-1412*, FFA, Bromma.

45 Asp, L (2000) Effects of code and geometry corrections on the DAMOCLES analysis results, *FFAP H-1423*, FFA, Bromma.

46 Olsson, R (2000) A summary of the FFA contribution to GARTEUR AG22, *FFAP H-1432*, FFA, Bromma.

47 Sjögren, A and Asp, LE (2000) Effects of temperature on delamination growth in a carbon/epoxy composite under fatigue loading, *FFA TN 2000-27*, FFA, Bromma.

48 Asp, LE, Sjögren, A and Greenhalgh, E (2001) Delamination growth thresholds in a carbon/epoxy composite under fatigue loading, *J. Compos. Technol. Res.,* 23(2)55-68.

49 Nilsson S., " Residual compressive strength of indented sandwich panels", FFA TN 1999-27, The Aeronautical Research Institute of Sweden, 1999.

50 Nilsson S., "Effect of impact damage in CFRP sandwich panels", *FFAP H-1338,* The Aeronautical Research Institute of Sweden, 1997.

51 Olsson R., "Prediction of Impact Damage in Sandwich Panels", *FFA TN 1995-35*, The Aeronautical Research Institute of Sweden, 1995.

52 Olsson R., "Methodology for Predicting the Residual Strength of Impacted Sandwich Panels", *FFA TN 1997-09*, The Aeronautical Research Institute of Sweden, Sweden, 1998.

53 Nilsson S., "Impact damage close to bolted joints", FFA TN 2000-75, The Aeronautical Research Institute of Sweden, 2000.

54 Nilsson S., "The effect of impact damages on the buckling characteristics of graphite fibre reinforced panels", FFA TN 1994-26, The Aeronautical Research Institute of Sweden, 1994.

55 Nilsson S., "Tests and analytical prediction of compressive strength of impacted composite laminates" FFA TN 2000-16, The Aeronutical Research Institute of Sweden, 2000.

56 Nilsson S., "Compression tests on impacted rectangular composite laminates with various lay-ups", FFA TN 2000-02, The Aeronautical Research Institute of Sweden, 2000.

Figure 1. Monitored structures and load entities for JAS 39 Gripen.

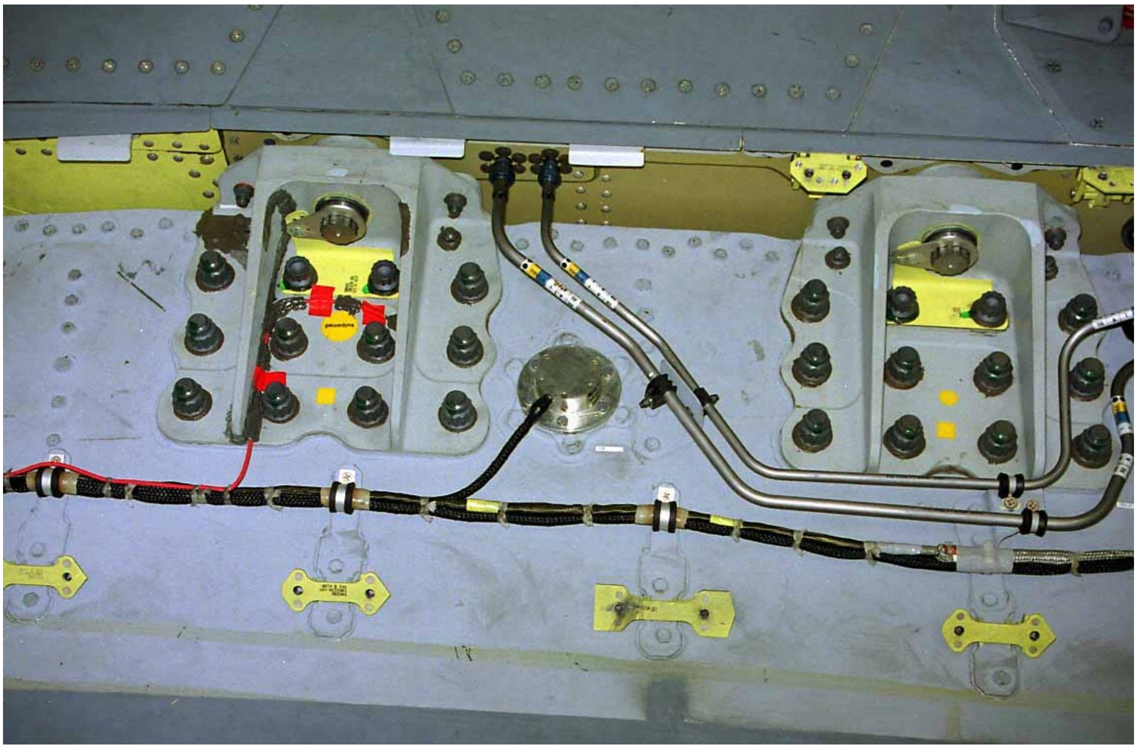

Figure 2. The strain-gauge installation on one of the wing attachments.

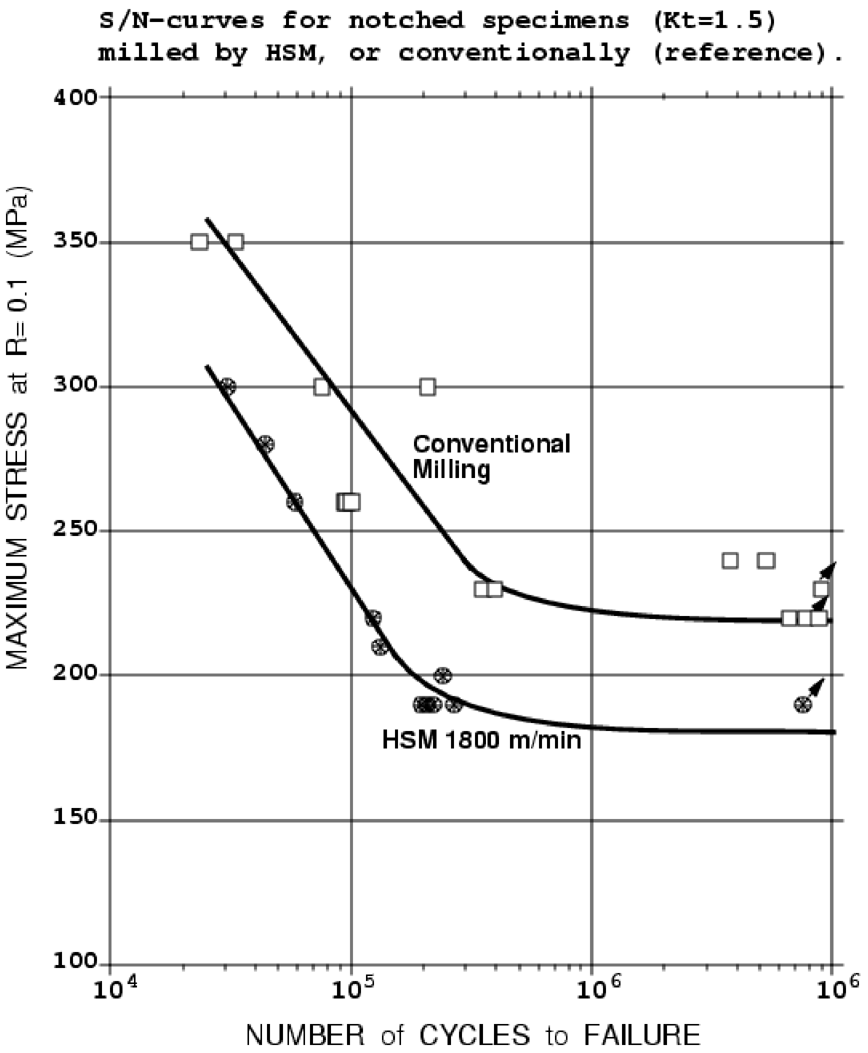

Figure 3

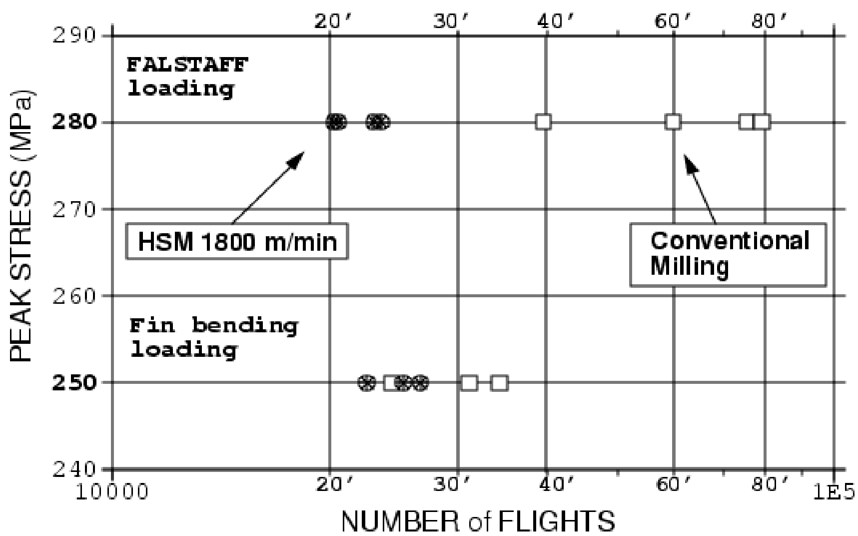

Figure 4.

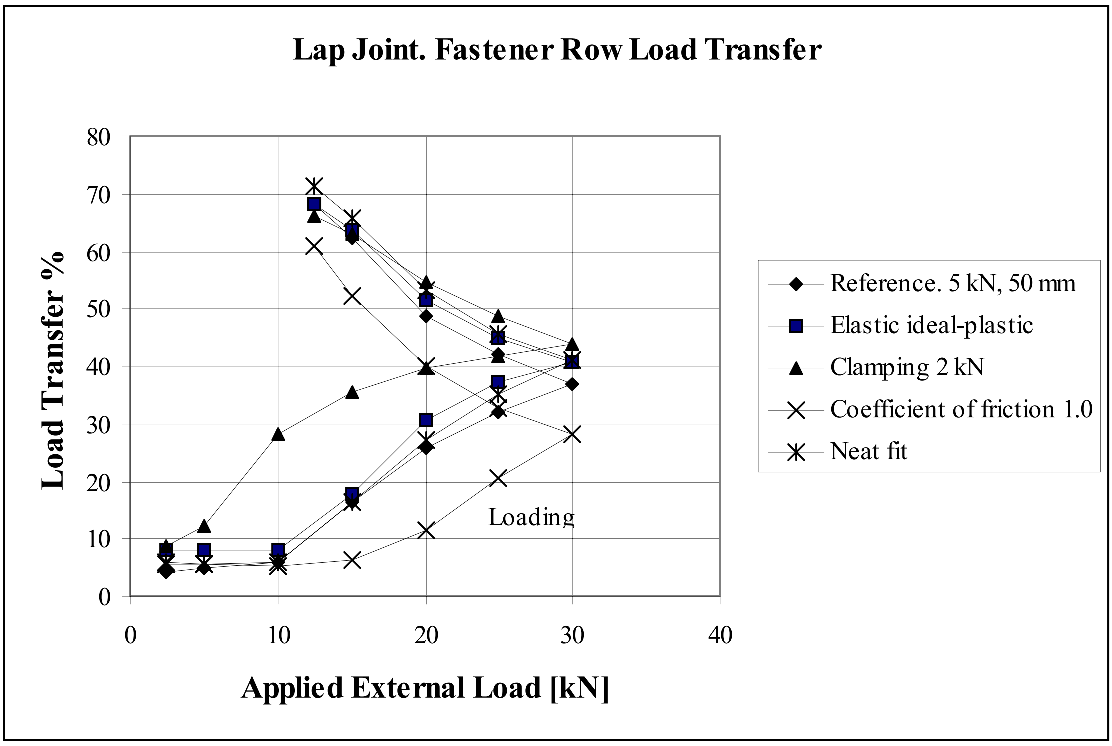

Figure 5. Influence of different parameters on the fastener row load transfer compared to the reference case.

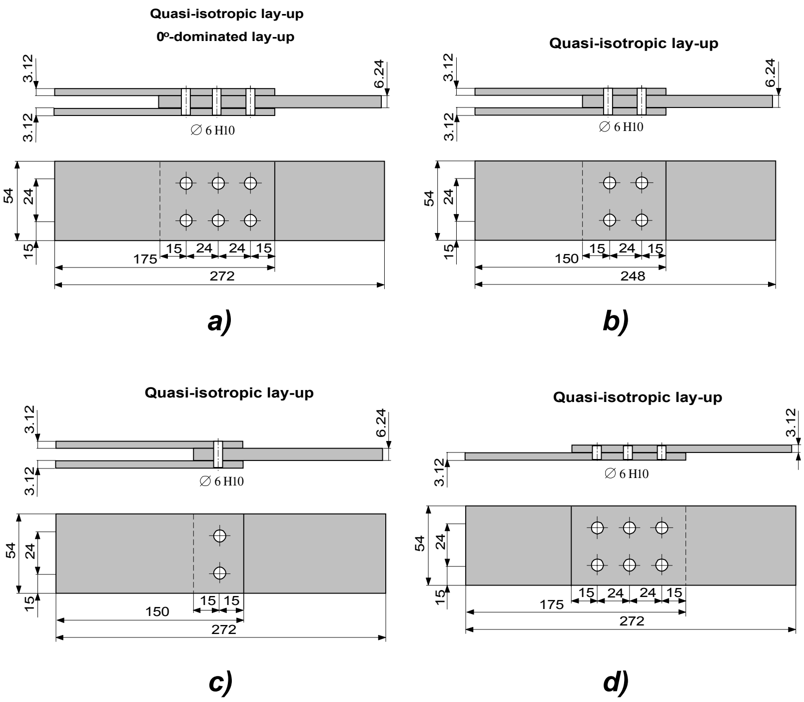

Figure 6. Specimens with (a) six bolts, (b) four bolts, (c) two bolts, (d) six bolts (single overlap).

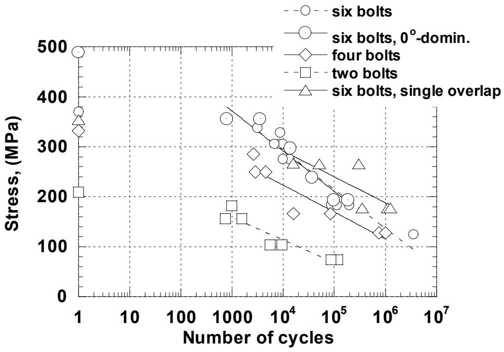

a)

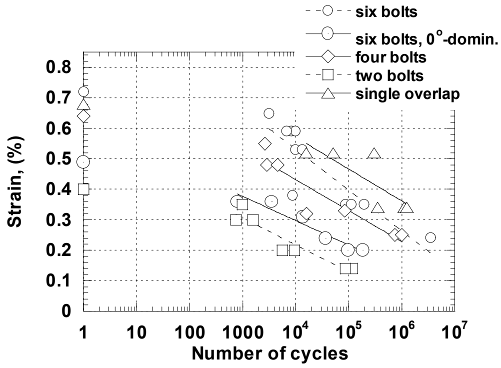

b)

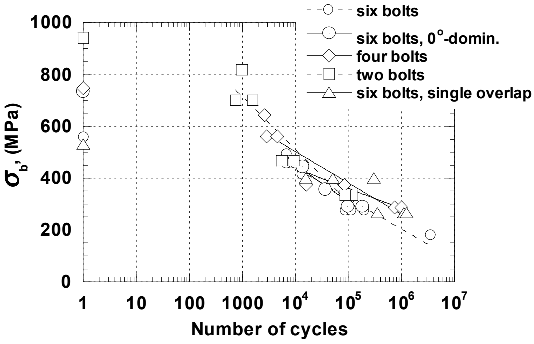

c)

Figure 7. Test results: (a) stress versus number of cycles; (b) strain versus number of cycles; (c) average bearing stress on one bolt for different specimen types.

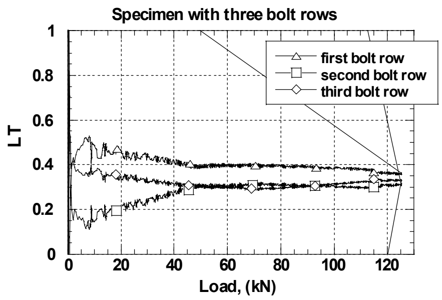

a)

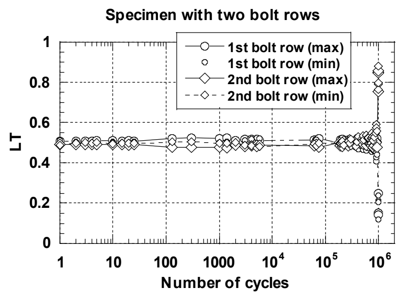

b)

Figure 8. Load transfer between different bolt rows: (a) joint with six bolts tested in static; (b) joint with four bolts tested in fatigue.

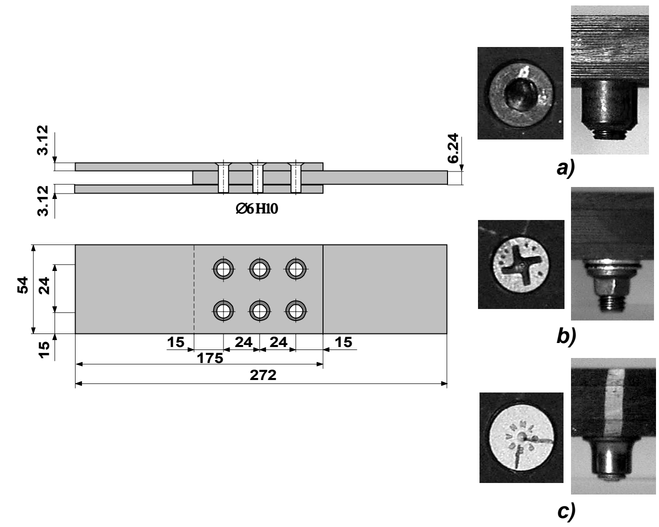

Figure 9. Specimen and fastener configurations: (a) composite bolt; (b) titanium Torque-set bolt; c) titanium Huck-comp fastener.

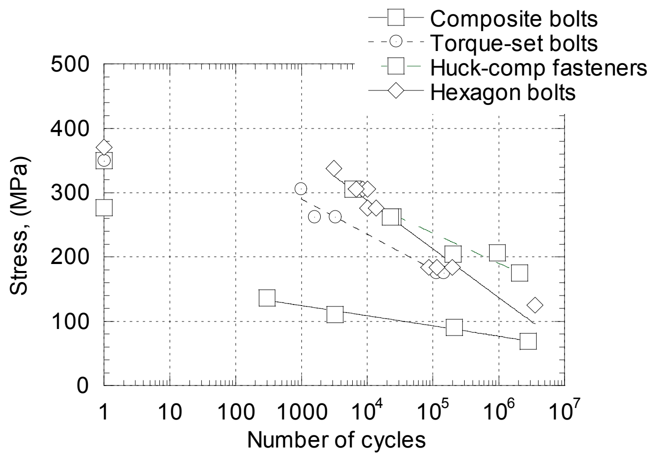

Figure 10. Fatigue life results.

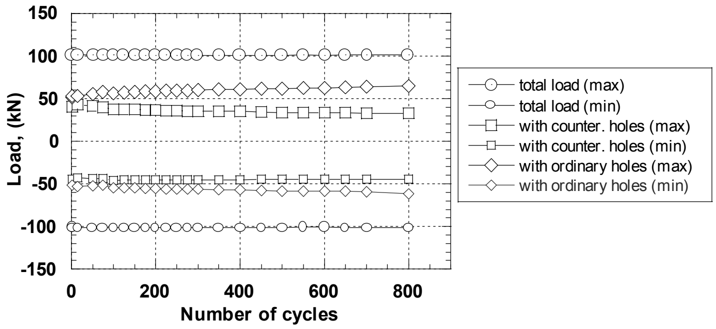

Figure 11: Distribution of applied load between outer plates in joint with countersunk bolts.

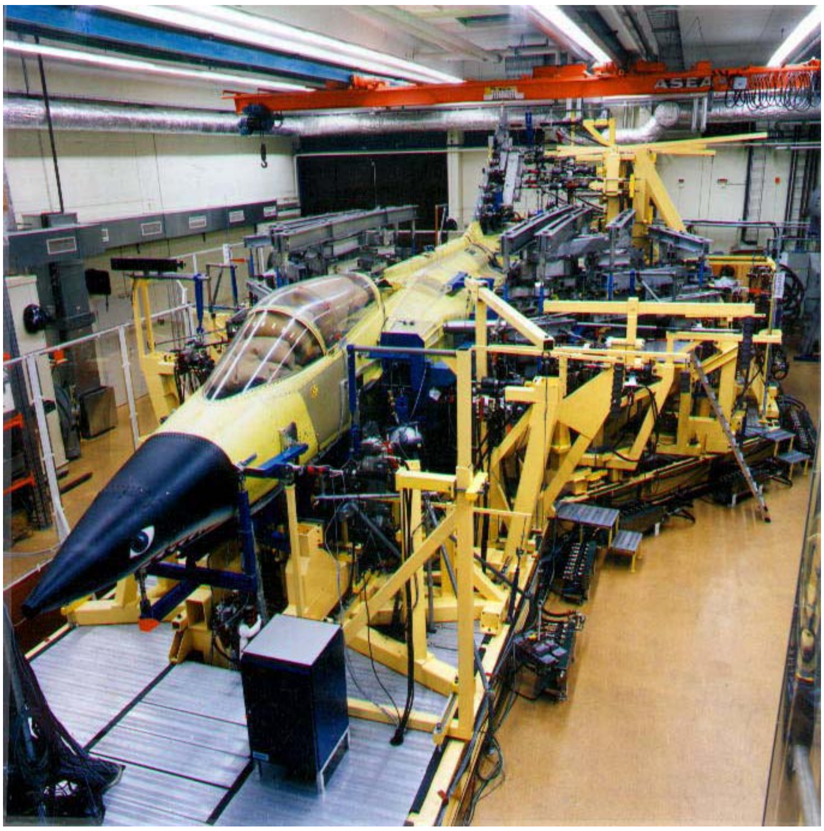

Figure 12. Photograph of the full scale fatigue test of the Gripen single seater, 39A.

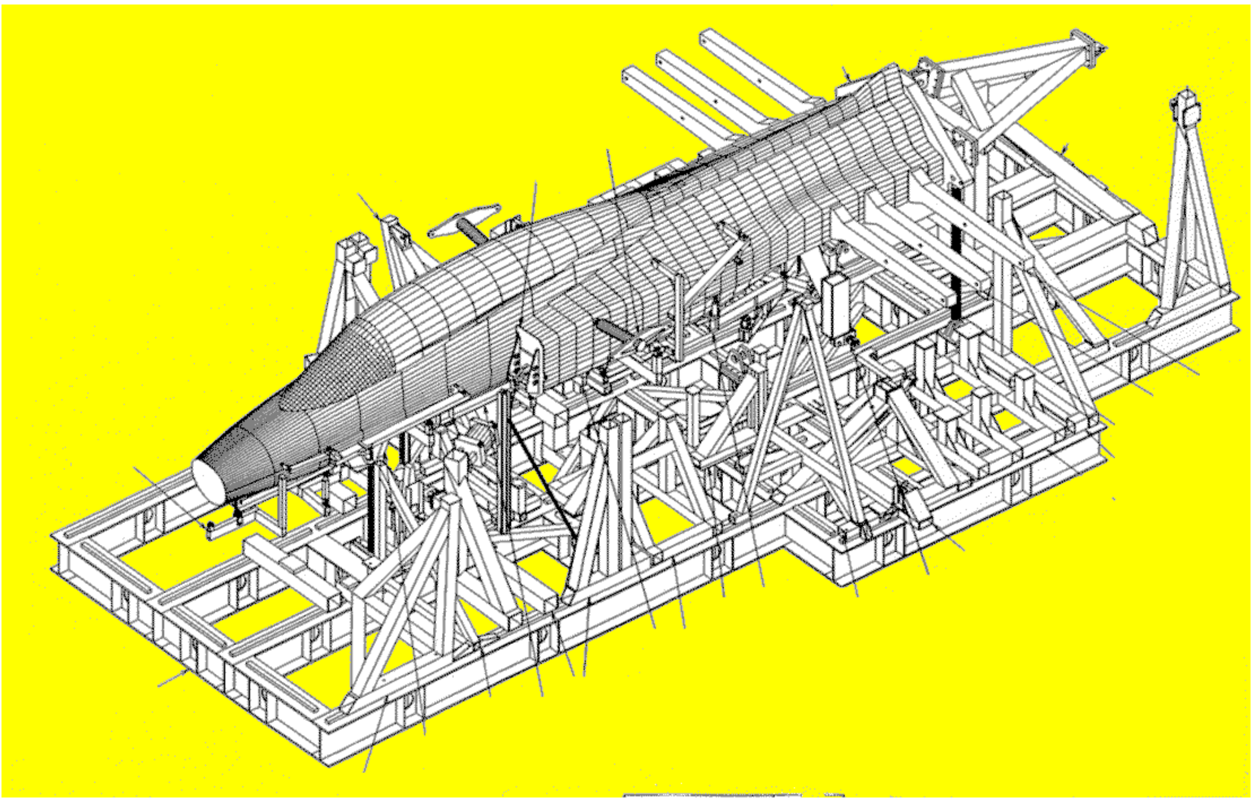

Figure 13. Schematic drawing of the full scale test of Gripen twin seater, 39B.

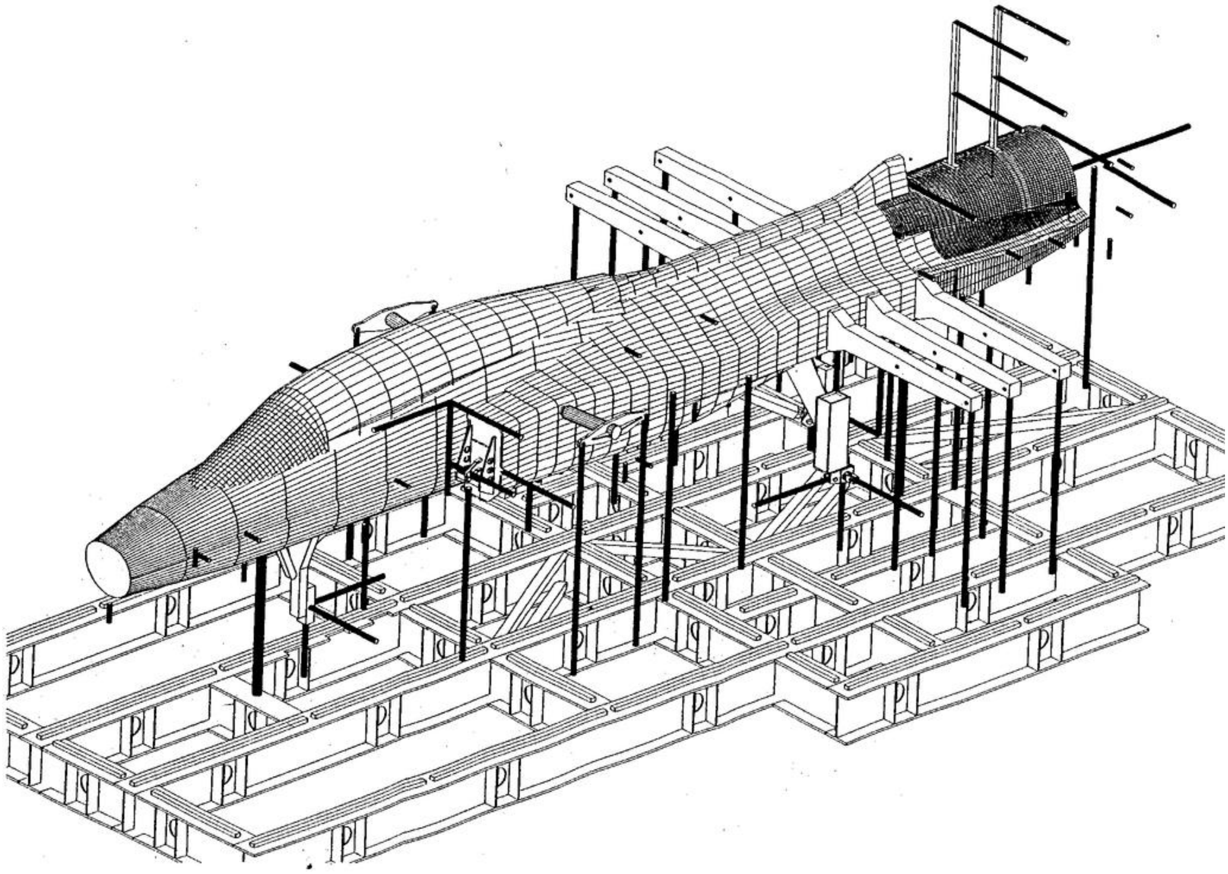

Figure 14. Schematic drawing of the full scale test of Gripen twin seater, export version (AAR dummy not shown in the drawing).

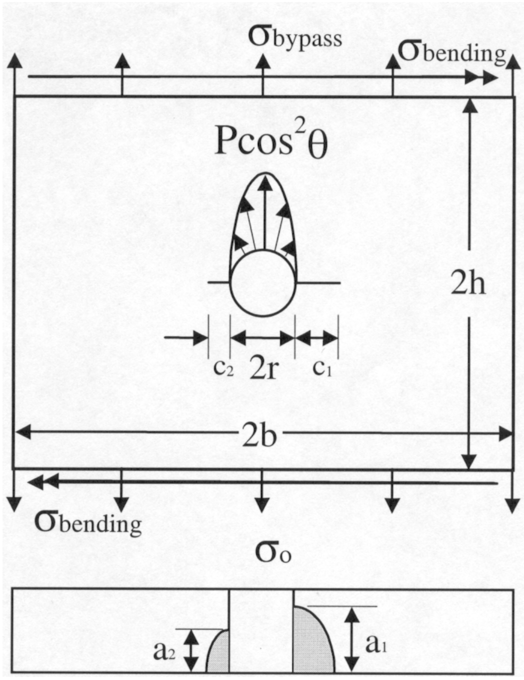

Figure 15. Parameter definition for two unequal corner cracks at centrally located hole in finite width sheet subject to general loading.

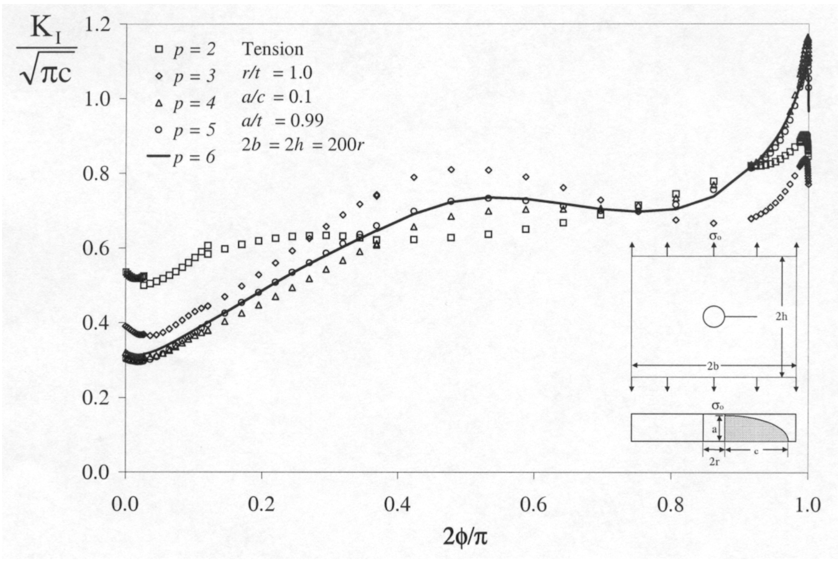

Figure 16 Convergence study for single deep corner crack (*a/t*=0.99, *c/a*=10, *r/t*=1.0) at hole subject to remote tension.

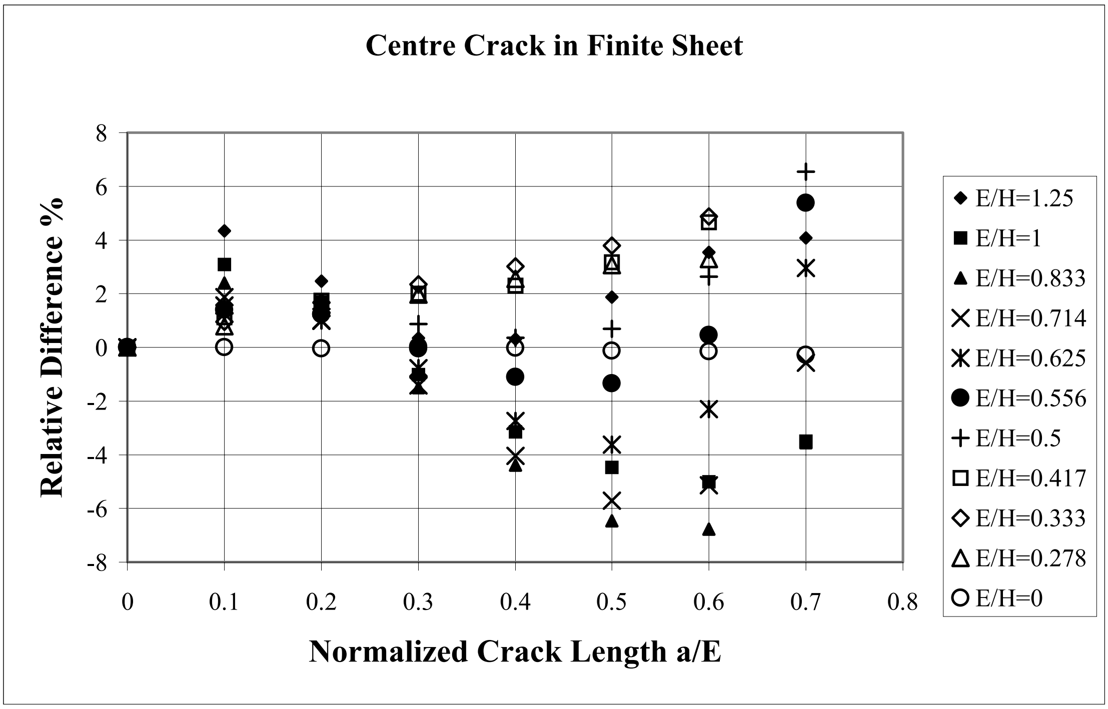

Figure 17. Accuracy of proposed equation for a centre crack in a sheet of finite dimensions.

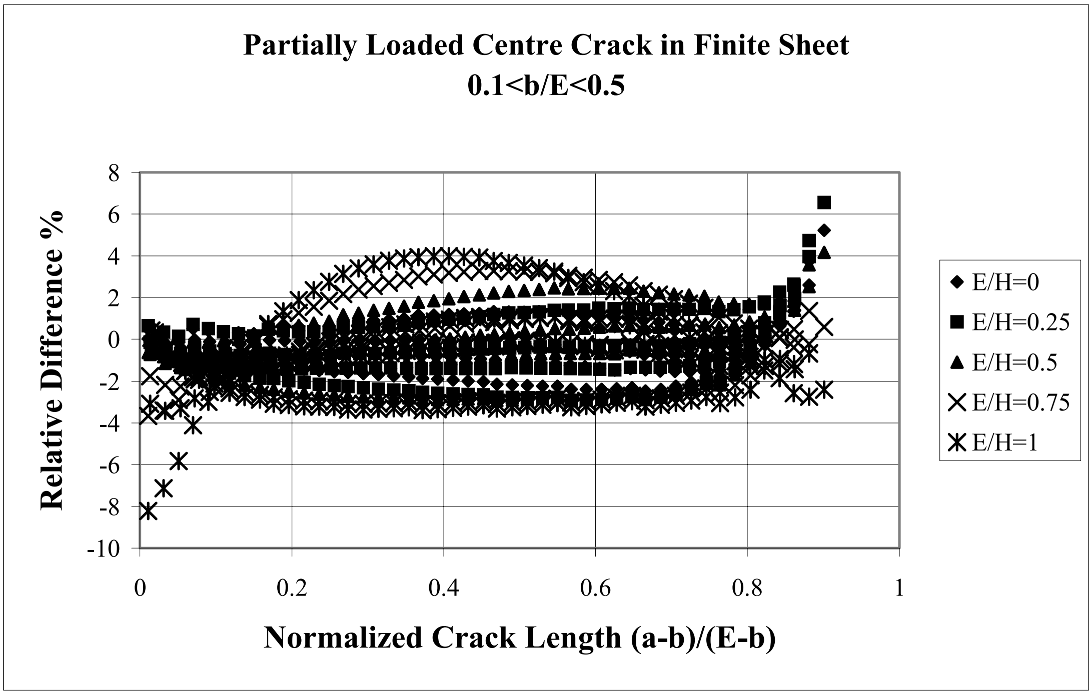

Figure 18. Accuracy of proposed equation for a centre crack, in a sheet of finite dimensions, subjected to a symmetric partial crack surface pressure.

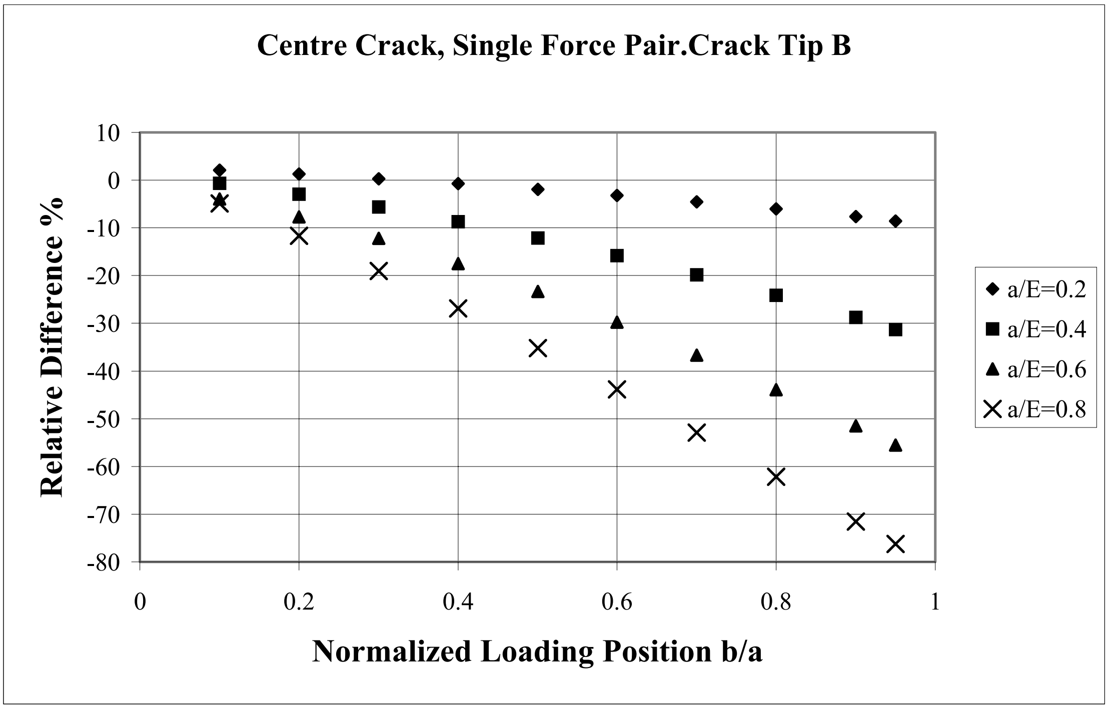

Figure 19. **Relative difference in stress intensity factor, at crack tip B, compared to finite element analyses for a centre crack subjected to a single force pair acting closest to crack tip A.**

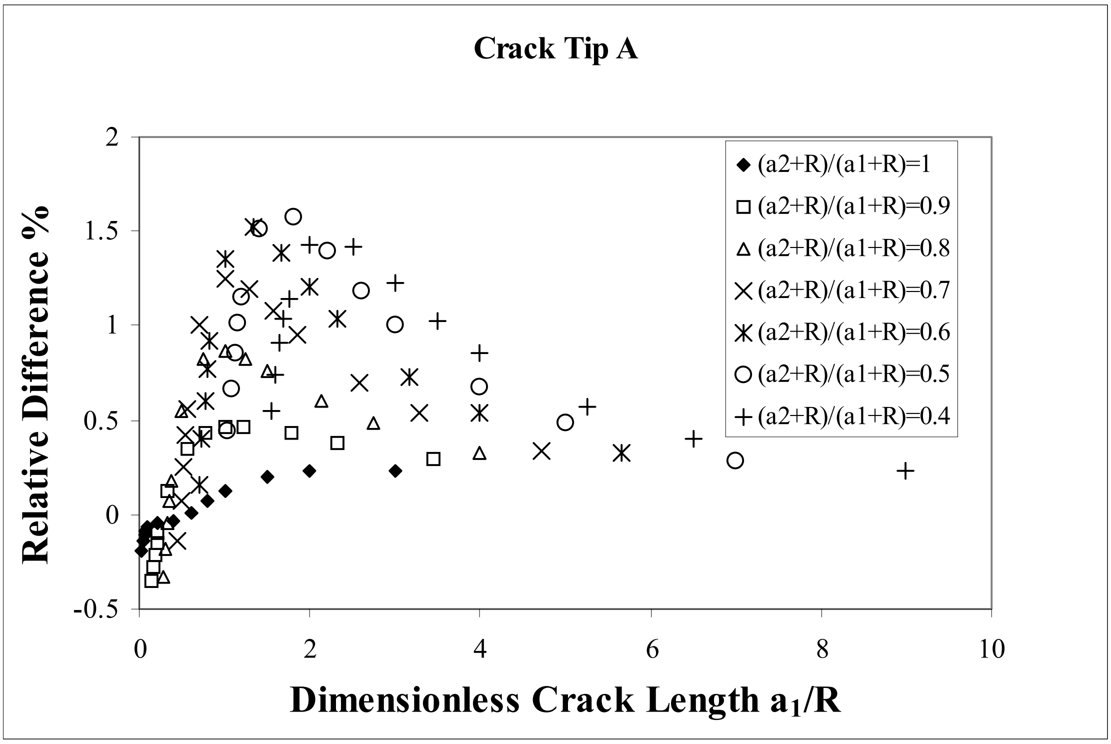

Figure 20. **Accuracy of the proposed equation for the stress intensity factor at crack tip A. Plate of infinite size containing a circular hole with two cracks of unequal lengths.**

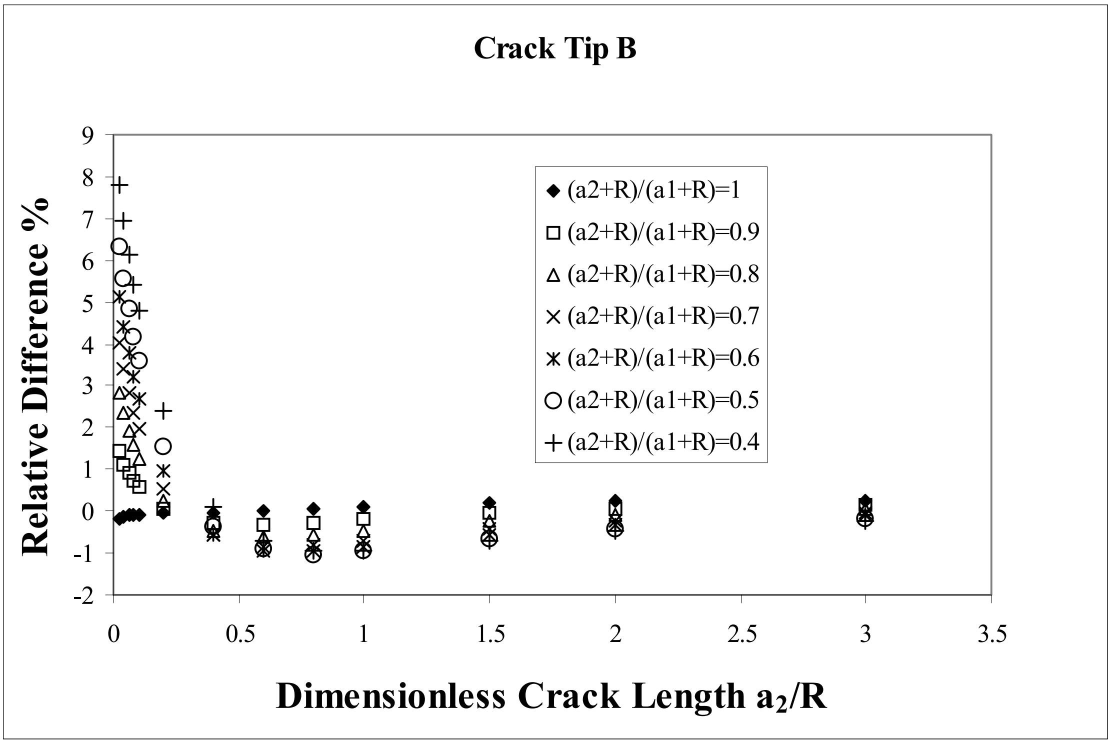

Figure 21. Accuracy of the proposed equation for the stress intensity factor at crack tip B. Plate of infinite size containing a circular hole with two cracks of unequal lengths.

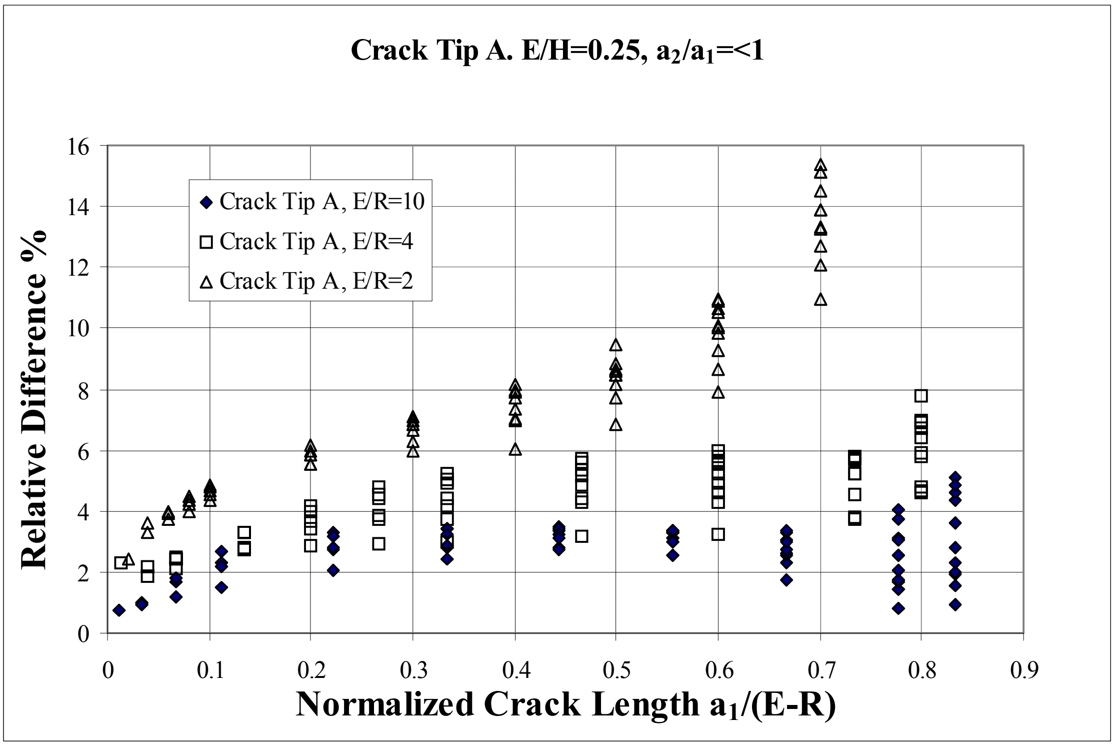

Figure 22. Accuracy of proposed stress intensity factor at crack tip A, when a2/a1□1, for two cracks of unequal lengths at a circular hole in a sheet of finite dimensions.

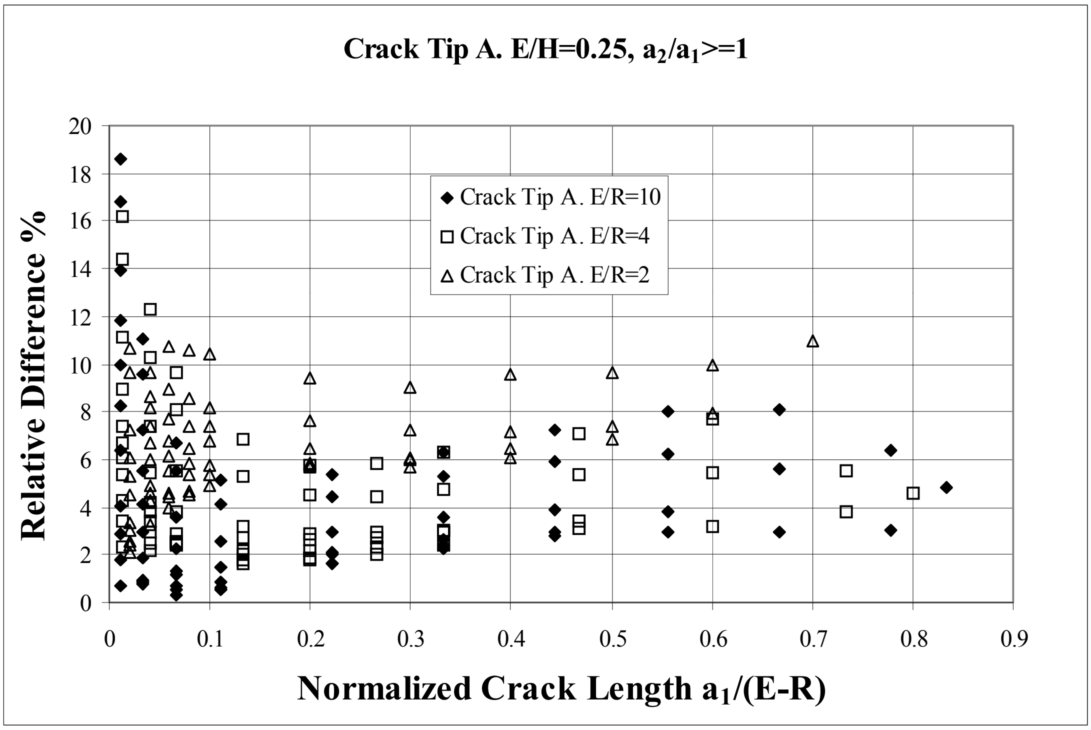

Figure 23. Accuracy of proposed stress intensity factor at crack tip A, when a2/a1□1, for two cracks of unequal lengths at a circular hole in a sheet of finite dimensions.

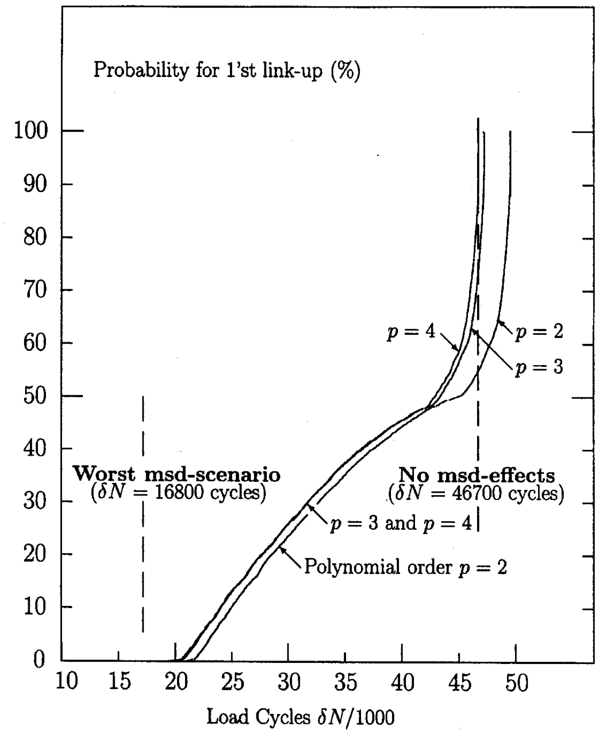

**Figure 24. Distributions for Scenario 2 showing the minimum number of load cycles δ_N from detection of first 1 mm crack in the plate until first link-up.
The solutions are for different polynomial orders p=2, 3 and 4, respecatively.**

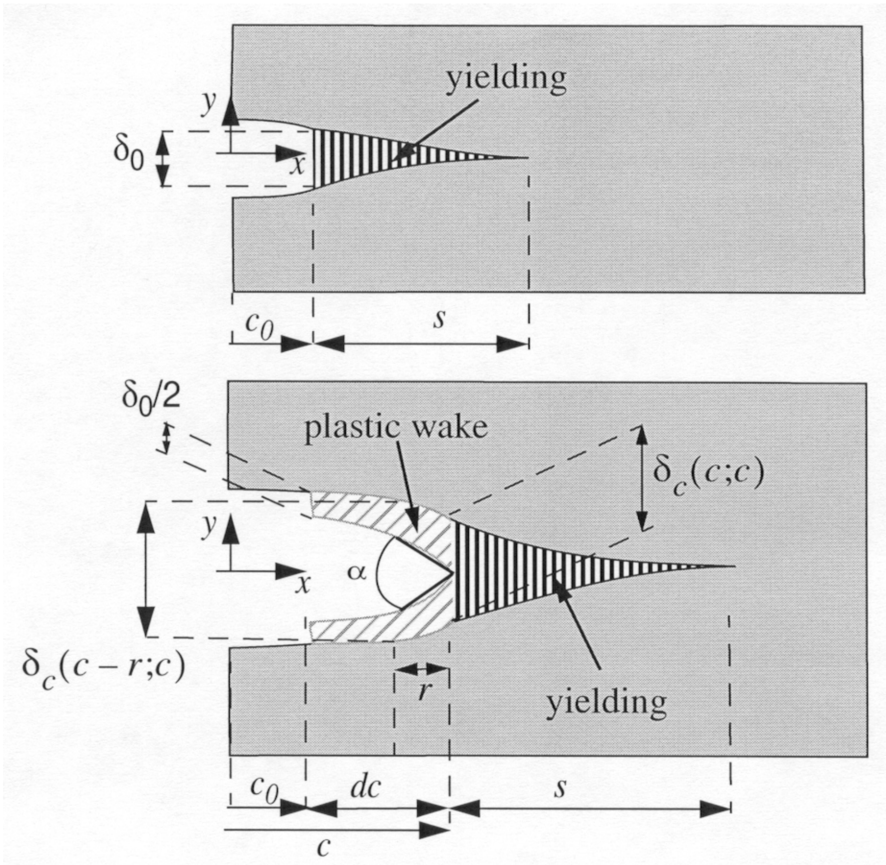

Figure 25 The crack profile at a) initiation, and at b) propagation with definition of crack growth parameters α and δ_0. The hatched area depicts the plastic stretch behind the crack tip.

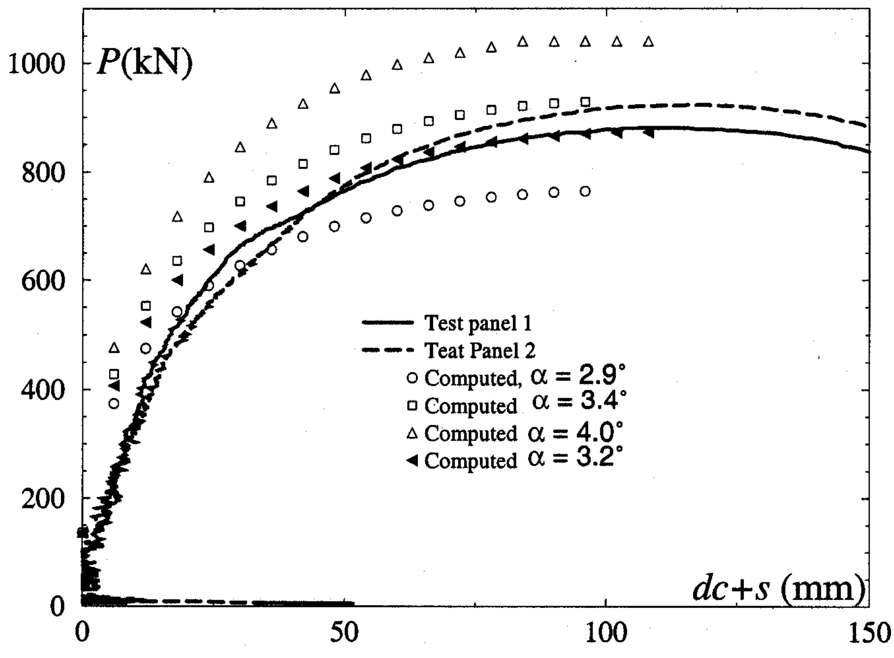

Figure 26. Applied load, *P*, versus physical half crack length plus plastic zone, *c+s*, from tests and Corresponding computed values for δ_0 =0.05 mm, α = 2.9°, 3.2°, 3.4°, 4.0°.

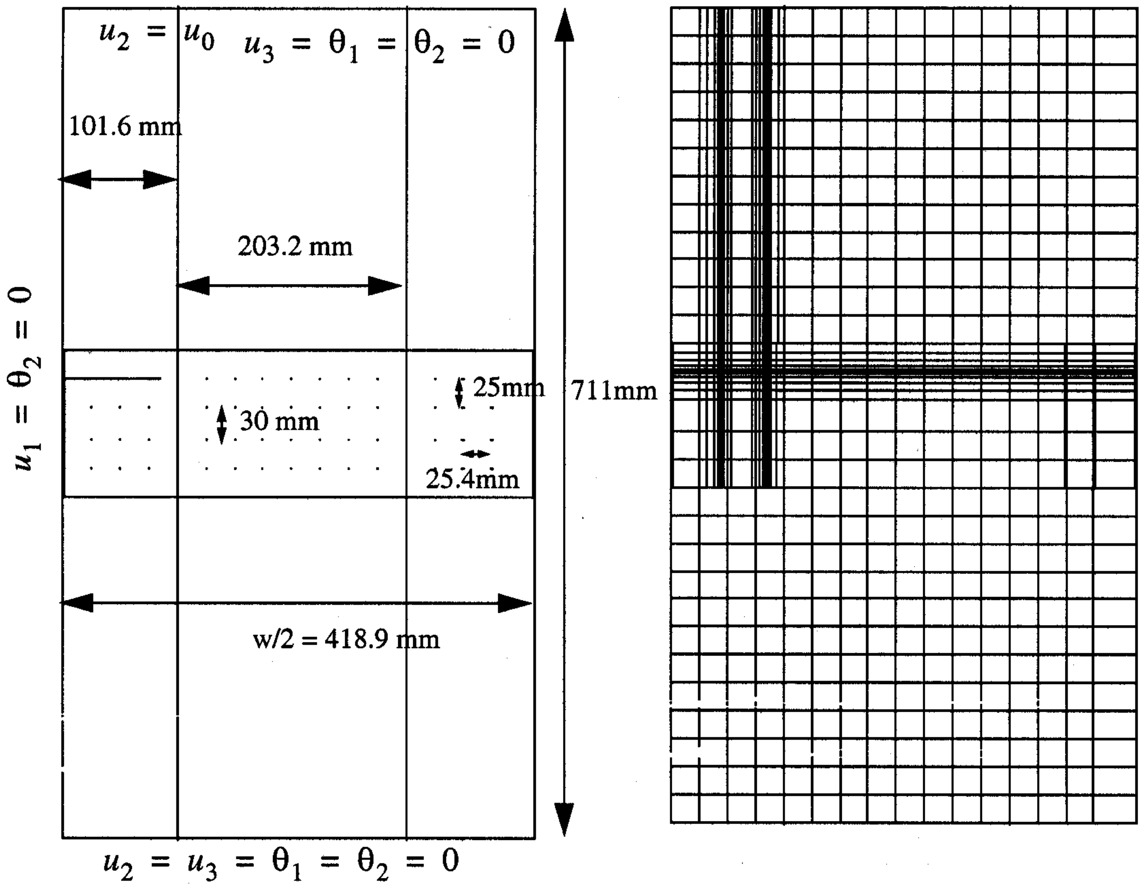

**Figure 27. FE-mesh used for residual strength analysis of panel.
Due to assumed symmetry only half of the panel is analysed.**

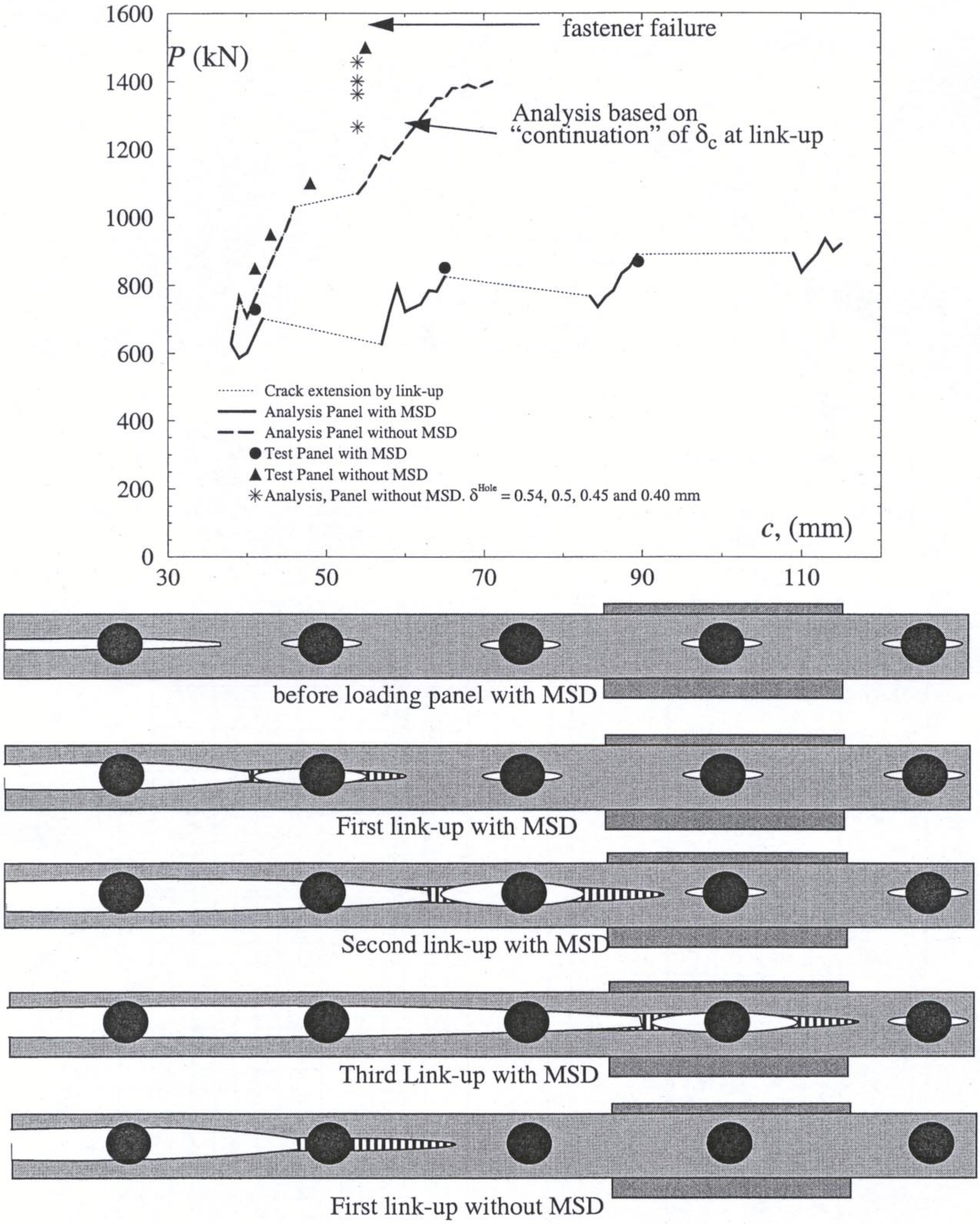

Figure 28 **Applied load *P*, versus position of lead crack *c* for stiffened scarf joint with and without artificially introduced MSD. The crack tip positions and plastic zones at link-ups are schematically illustrated.**

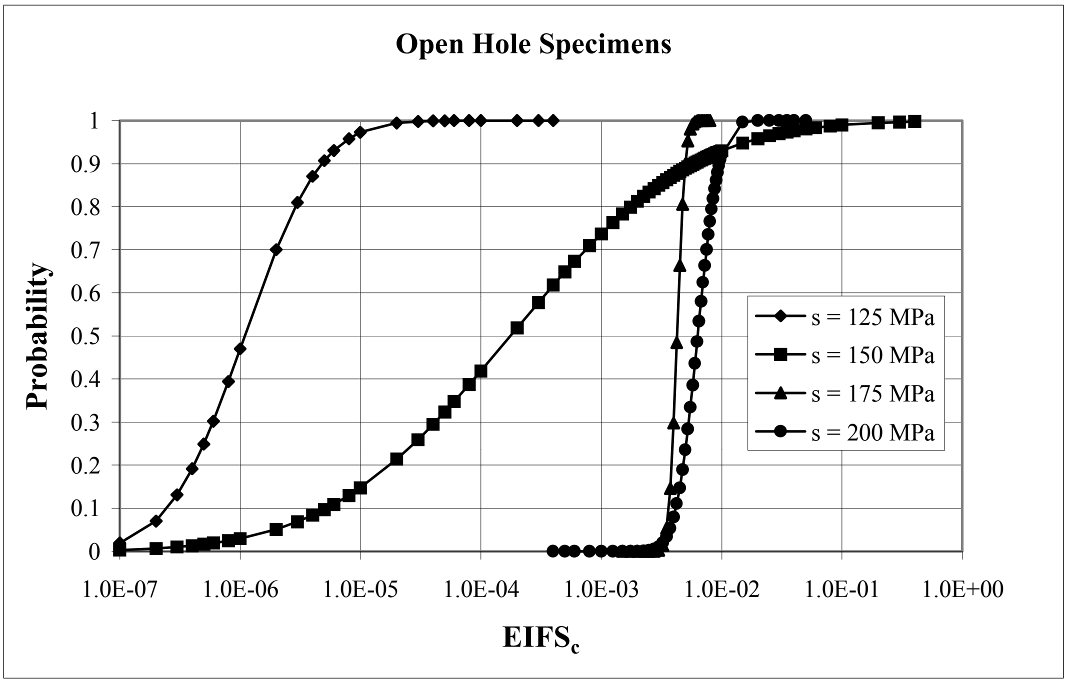

Figure 29. Cumulative EIFS distributions obtained for different stress levels using Paris´ law.

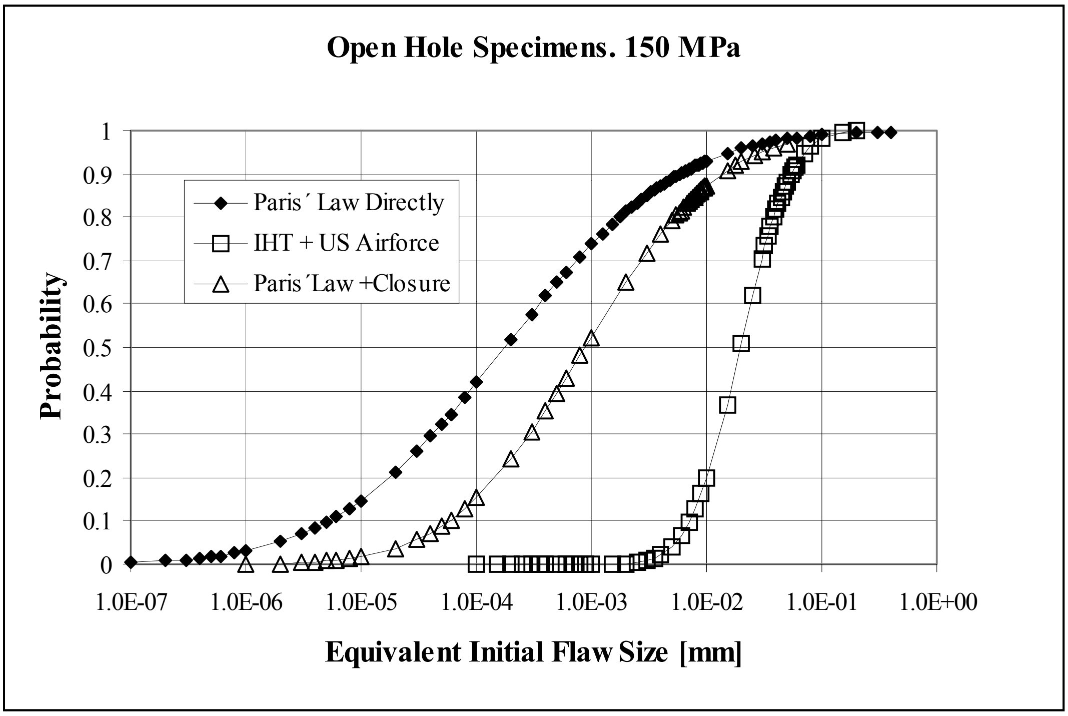

Figure 30. Cumulative EIFS distributions obtained using different methods for the same stress level.

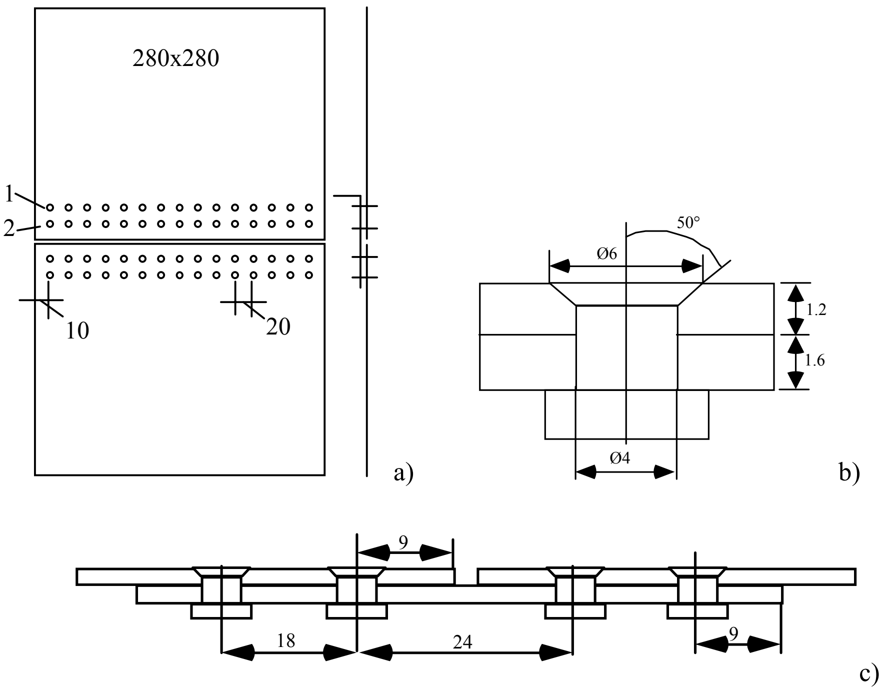

Figure.31: MSD test panel for the BRITE-EURAM co-operation program

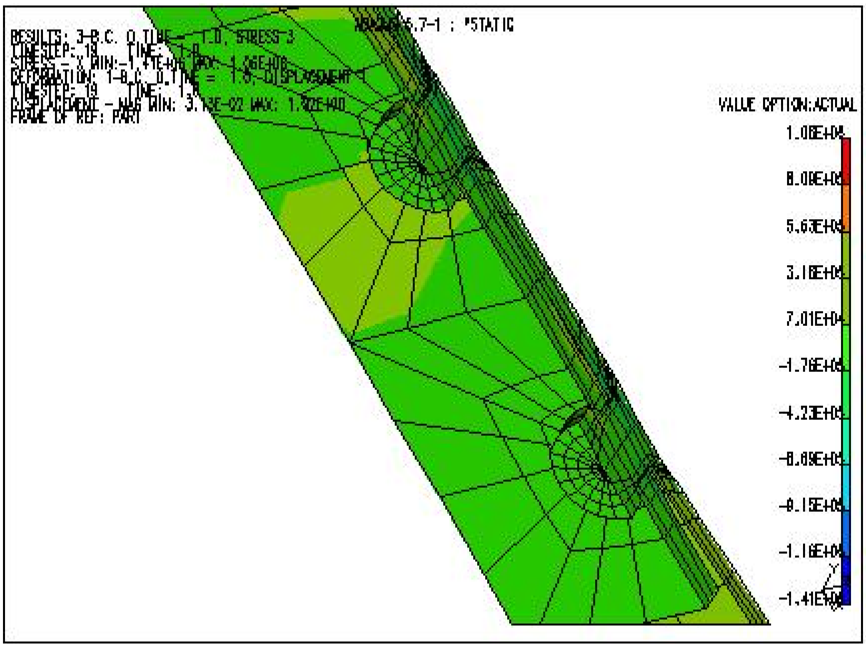

Figure.32: Example of detailed finite element model of the MSD specimens.

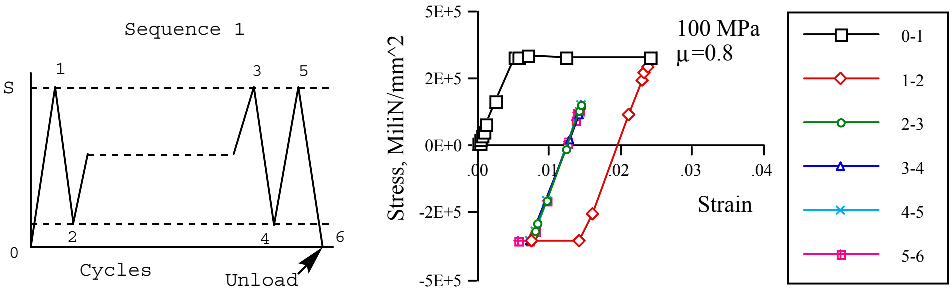

Figure 33. Stress-strain response at the critical location under the fatigue sequence at 100MPa maximum load.

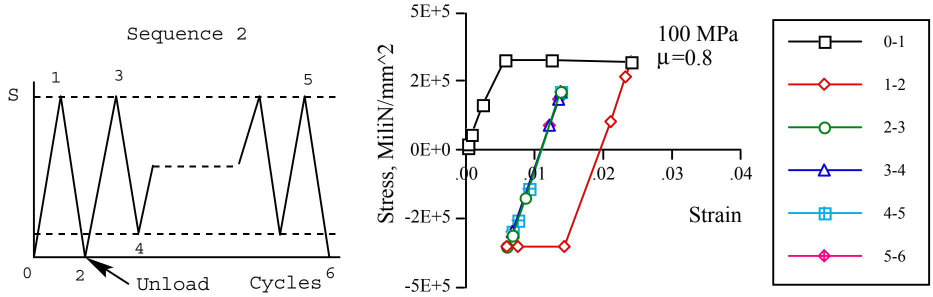

Figure 34: Stress-strain response at the critical location after the first full load cycle.

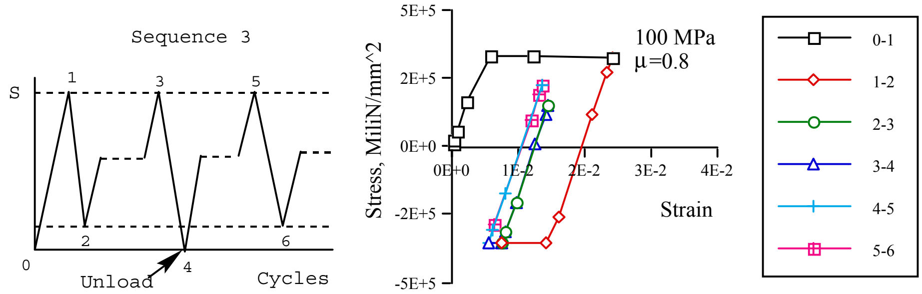

Figure 35. Stress-strain response at the critical location for the fatigue load sequence containing interruption.

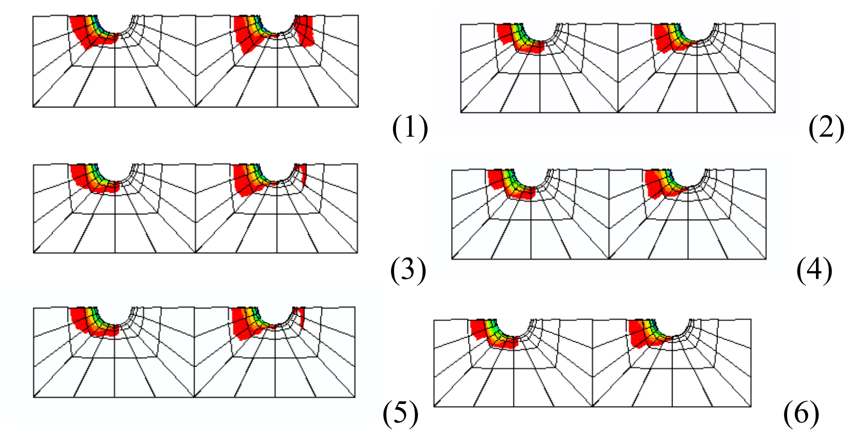

Figure 36. Contacts between sheet and splice for the load sequence as shown in Fig.34.

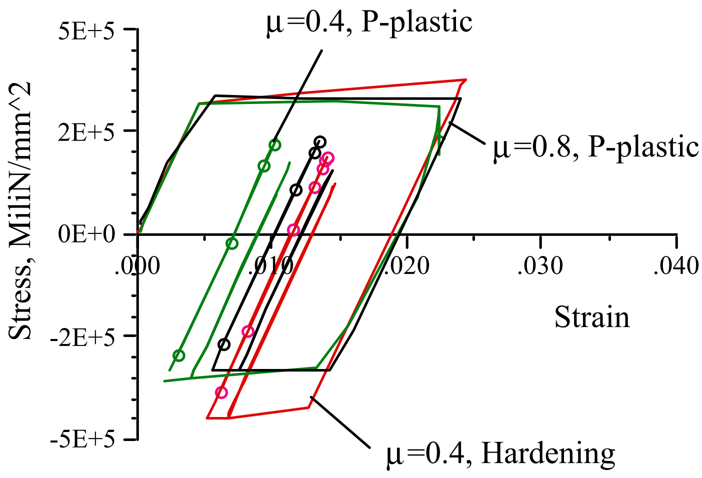

Figure 37. Effect of friction on the critical stress-strain response.

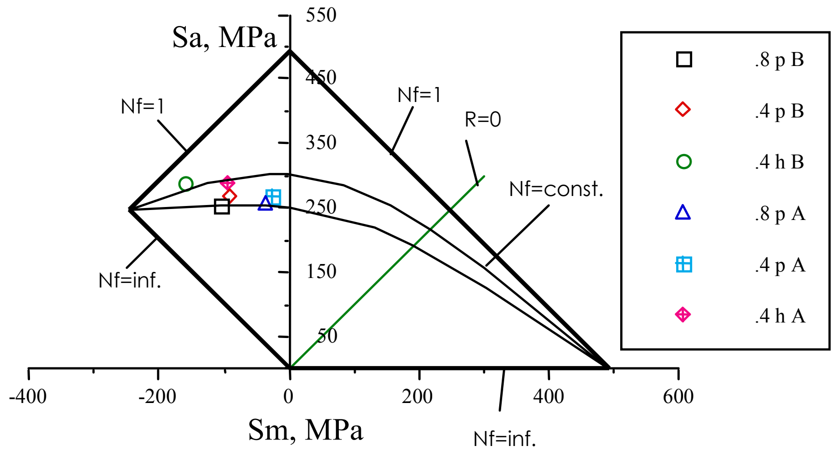

Figure 38. Schematic of fatigue map for finite element analyses under different considerations.

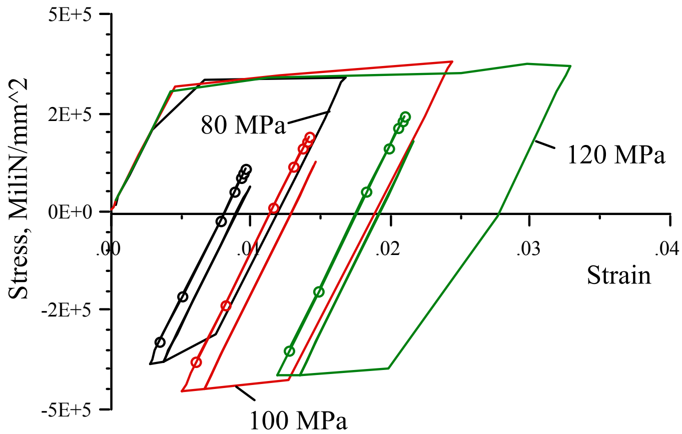

Figure 39. Stress-strain response for different remote stress levels.

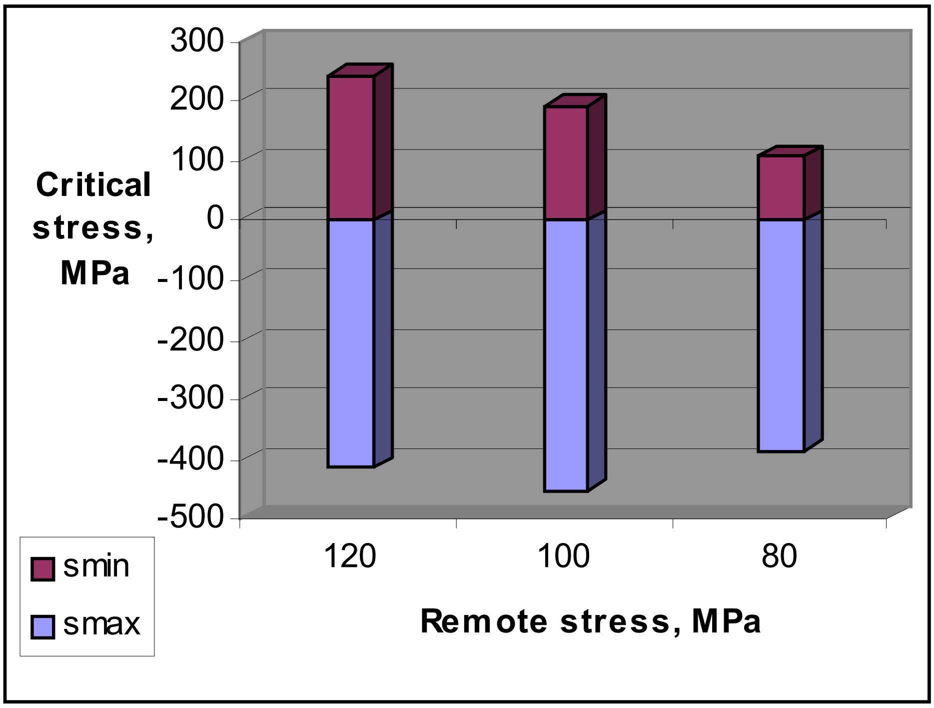

Figure 40. The shakedown stress state at the critical location for various load levels.

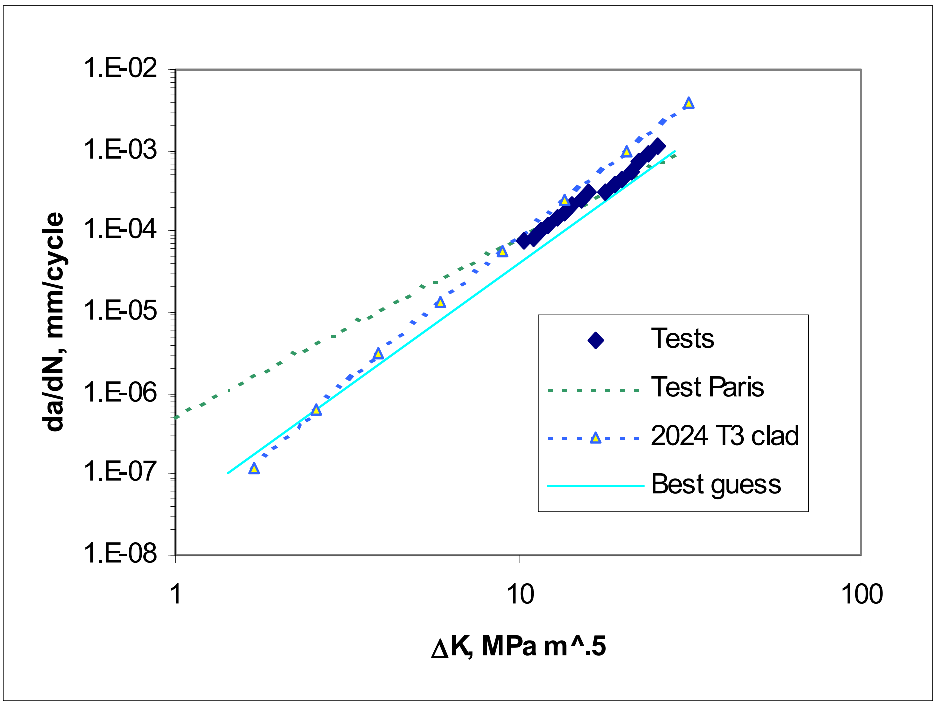

Figure 41. Comparison of various baseline data of fatigue crack growth rate.

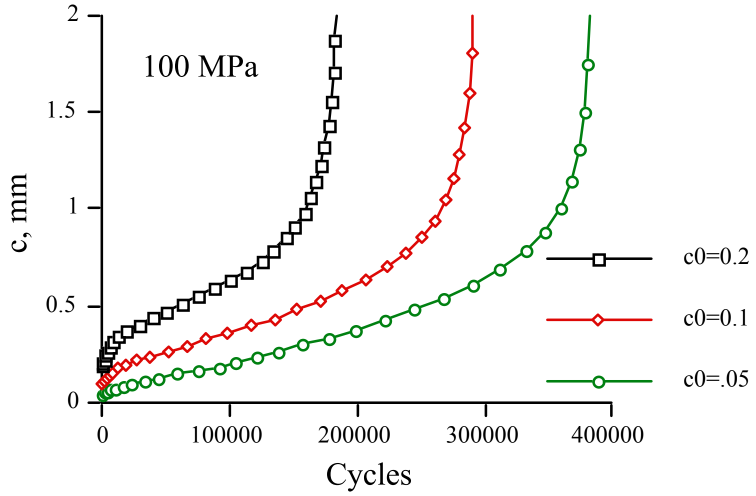

Figure 42. **Analytical crack growth for 100MPa remote stress for cracks initiated at different initial crack sizes.**

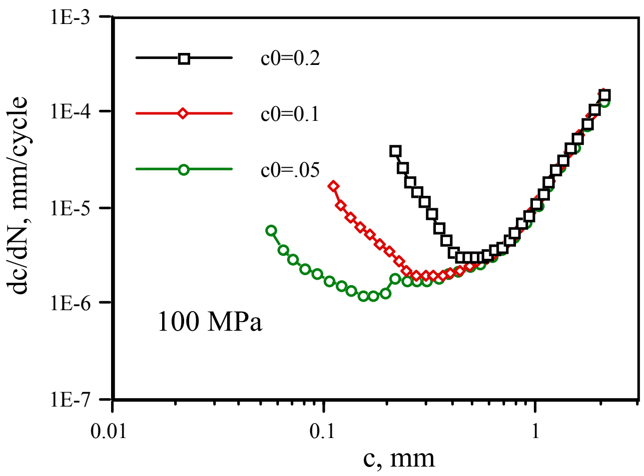

Figure 43. **Computed crack growth rate as a function of the initial crack sizes for 100Mpa stress**

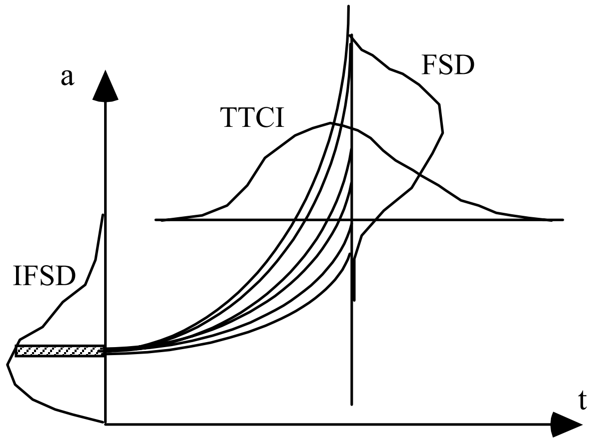

IFSD = Initial Flaw Size Distribution

TTCI = Time To Crack Initiation

FSD = Flaw Size Distribution

Figure 44. Schematic of the stochastic fatigue crack growth conditional to the initial crack distribution

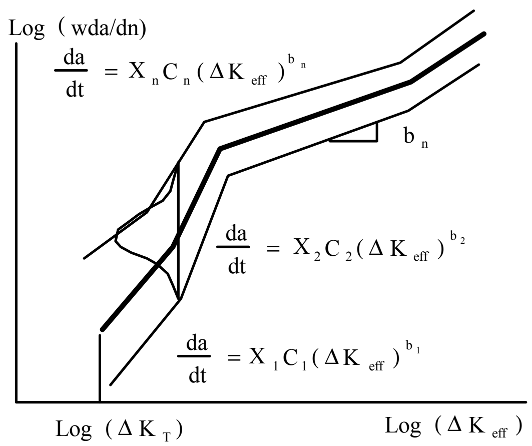

Figure 45. Stochastic description of baseline rate of the whole range fatigue crack growth from threshold regime up to quasi-static regime.

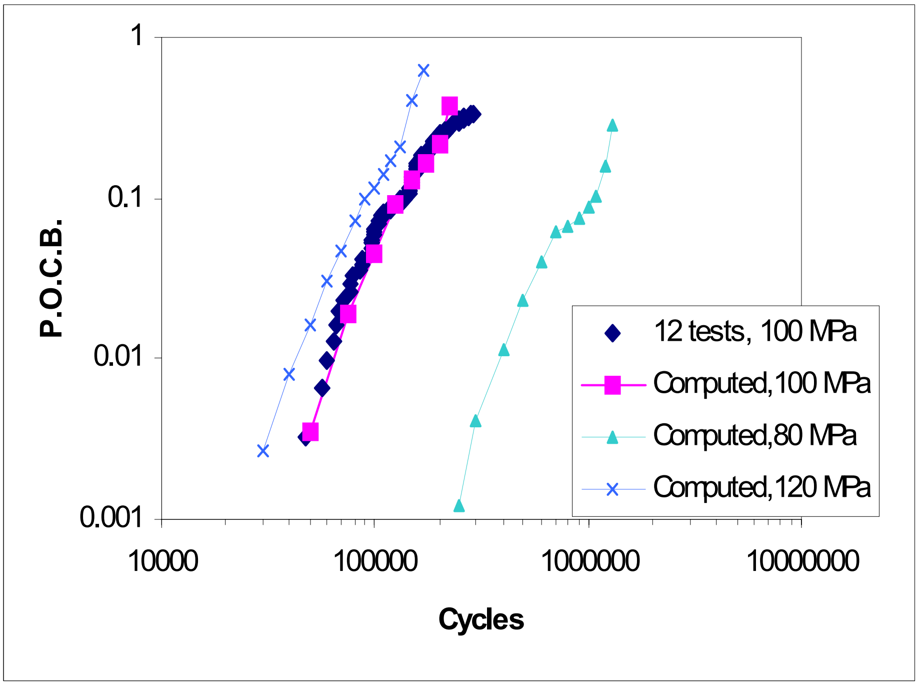

Figure 46. Prediction of probability of crack breaking for MSD panels for various fatigue levels as a function of load cycles.

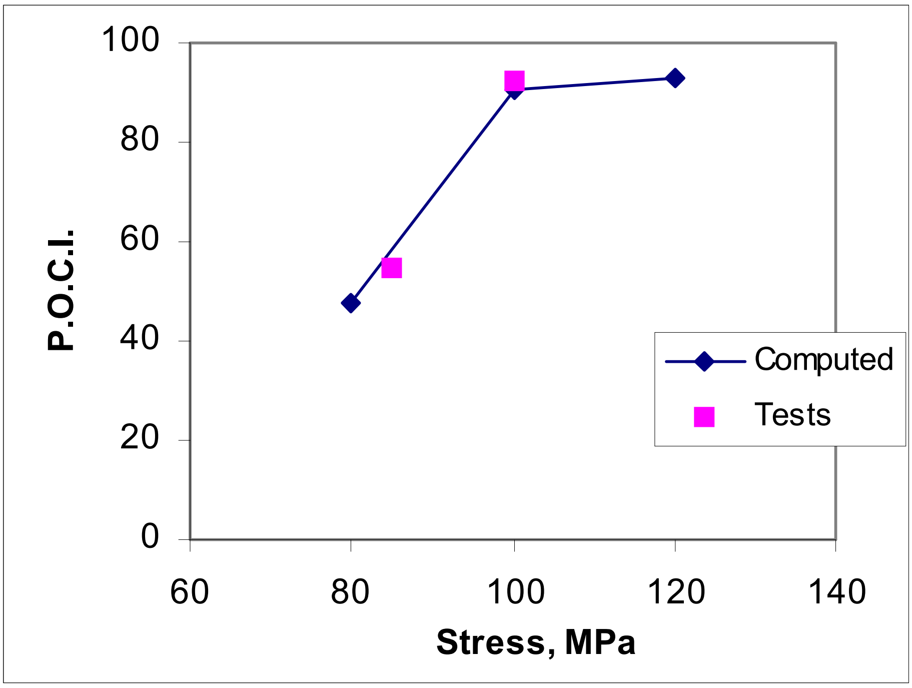

Figure 47. Comparison of test and analytical results for the probability of crack initiation as a function of the load level.

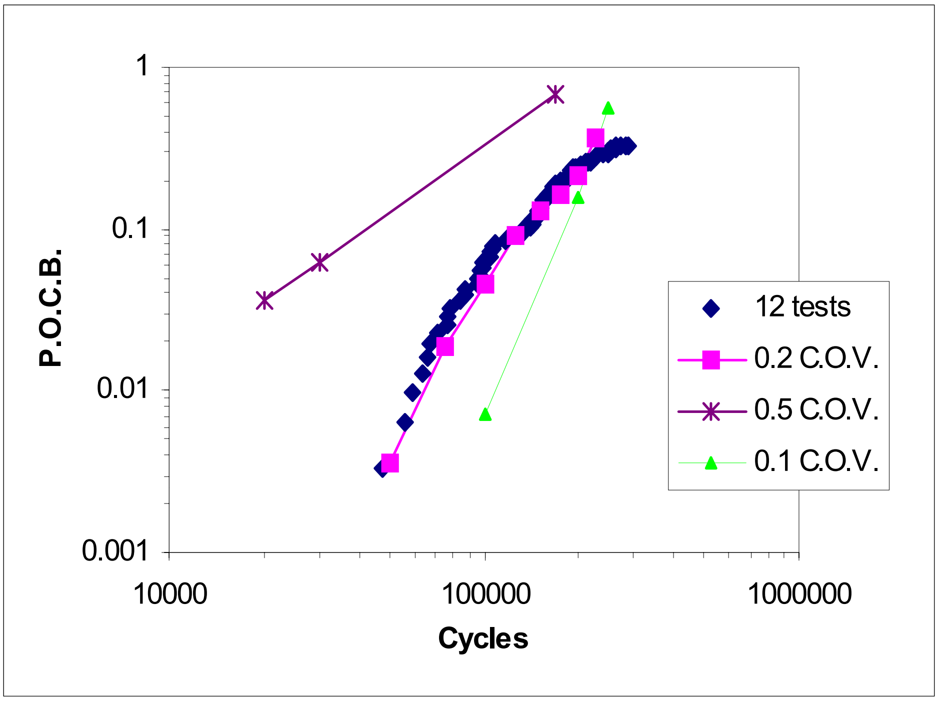

Figure 48. Evaluation of the effect of production quality on the reliability of the MSD panels.

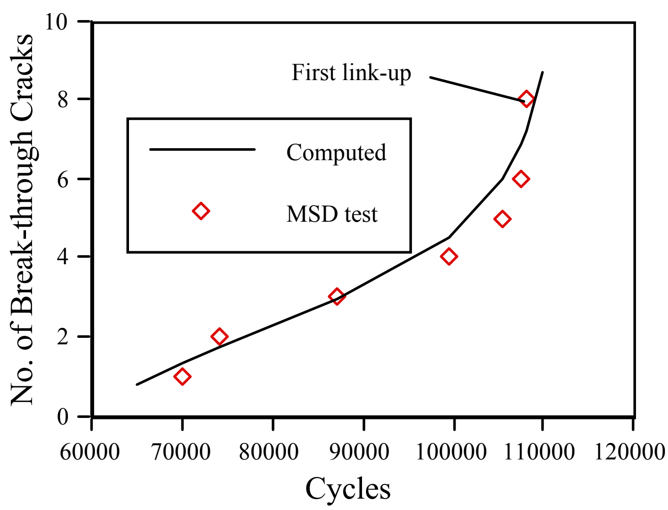

Figure 49. Comparison of the number of break-through cracks between analyses and the test for specimen MSD 4.

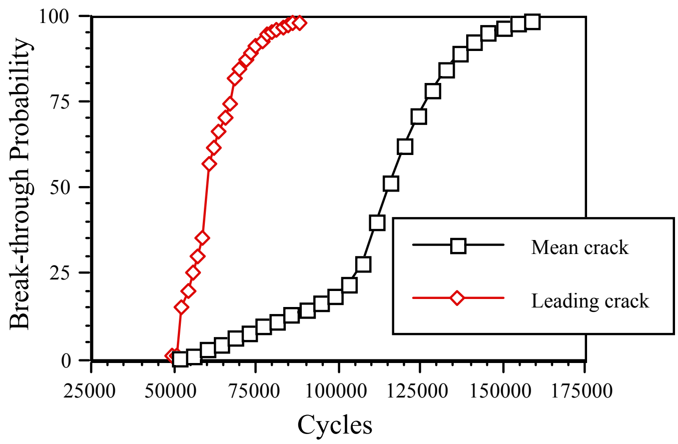

Figure 50. Mean and leading break-through probability for MSD 4 specimen.

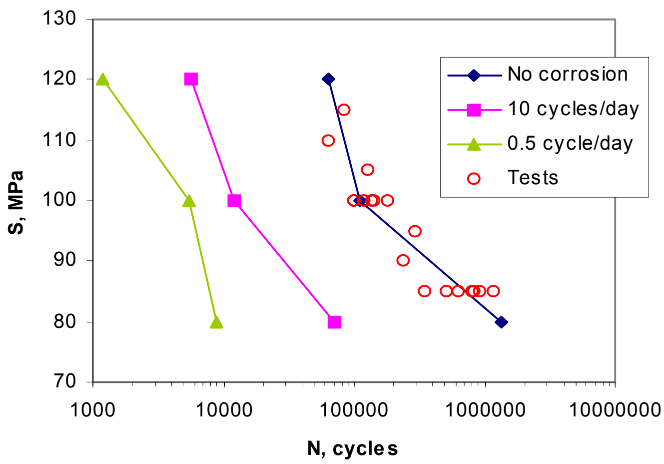

Figure 51. Comparison of fatigue lives when environmental attacks are considered.

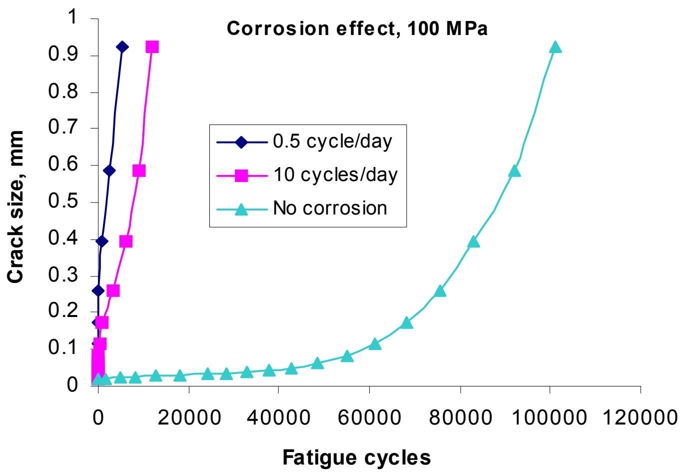

Figure 52. Fatigue crack growth under environmental attacks.

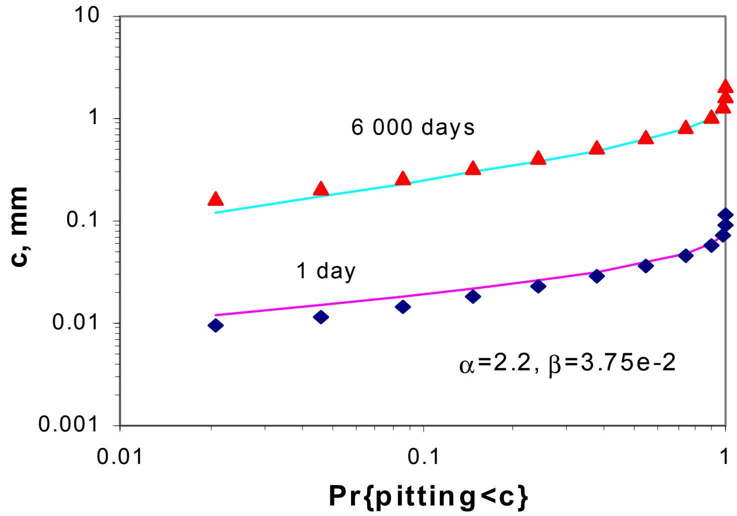

Figure 53. **Pitting crack initiation model for aluminium alloys in environmental attacks.**

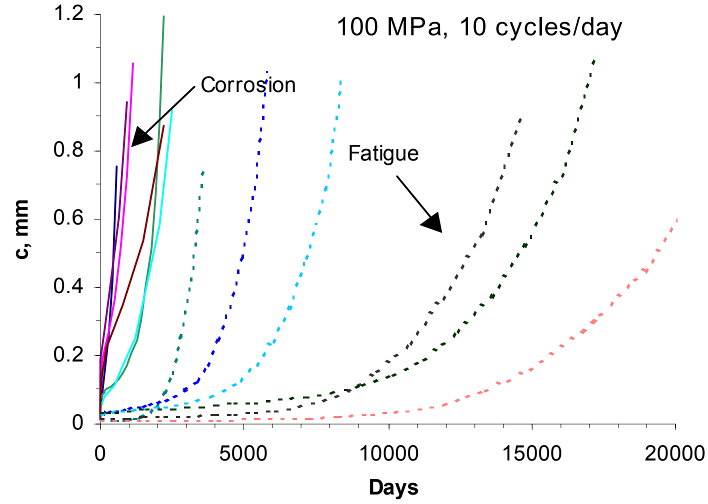

Figure 54. **Monte-Carlo simulation of crack growth under different conditions.**

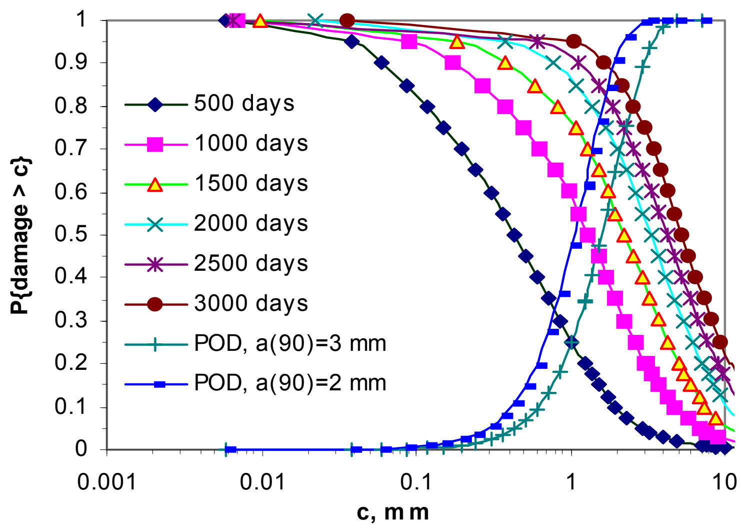

Figure 55. Distribution of fatigue damage compared to the probability of detection.

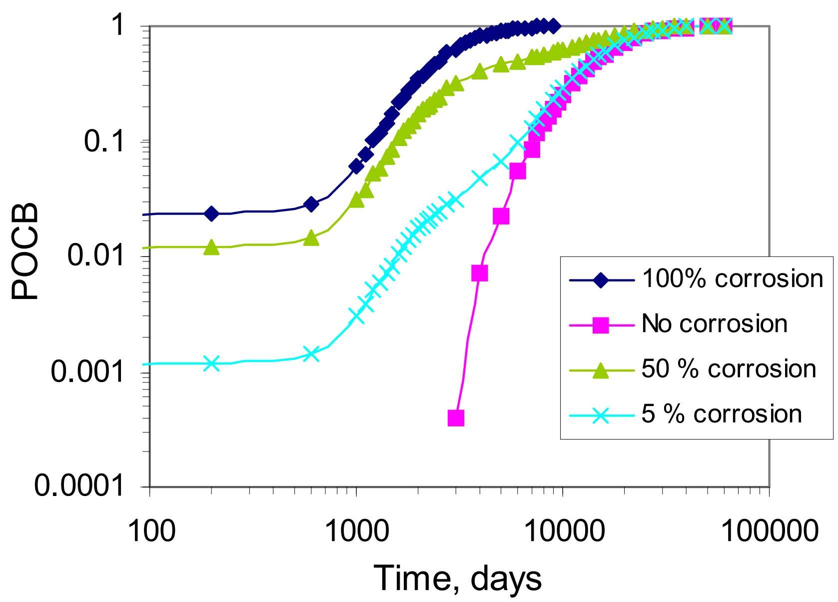

Figure 56. Probability of crack breaking when various degrees of corrosion are presented.

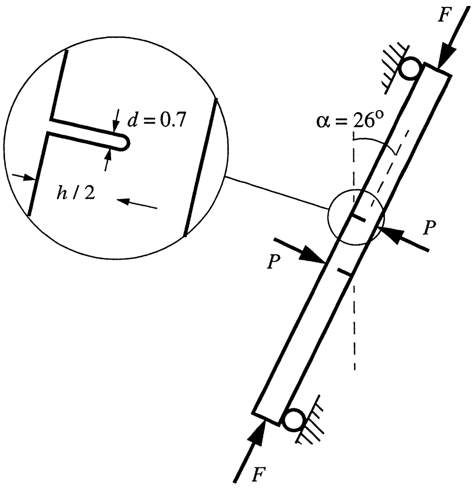

Figure 57. Schematics of the IDNS test specimen including loading arrangement.

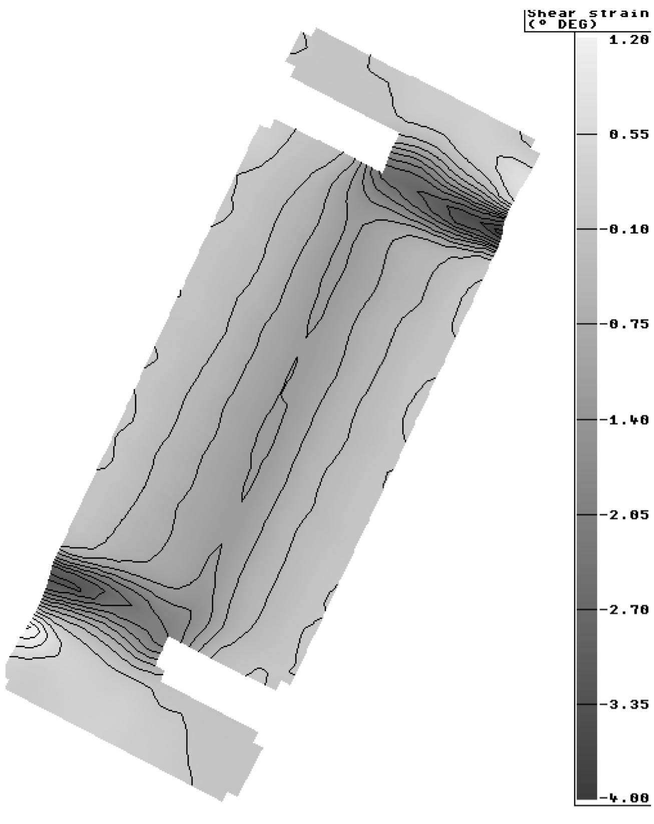

Figure 58. Experimentally determined strain field at a load close to failure for the IDNS-test.

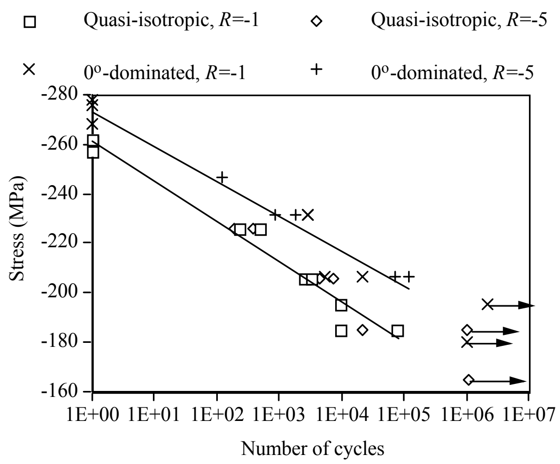

Figure 59. Fatigue results for specimens with quasi-isotropic and 0°-dominated layup; minimum stress vs. number of cycles.

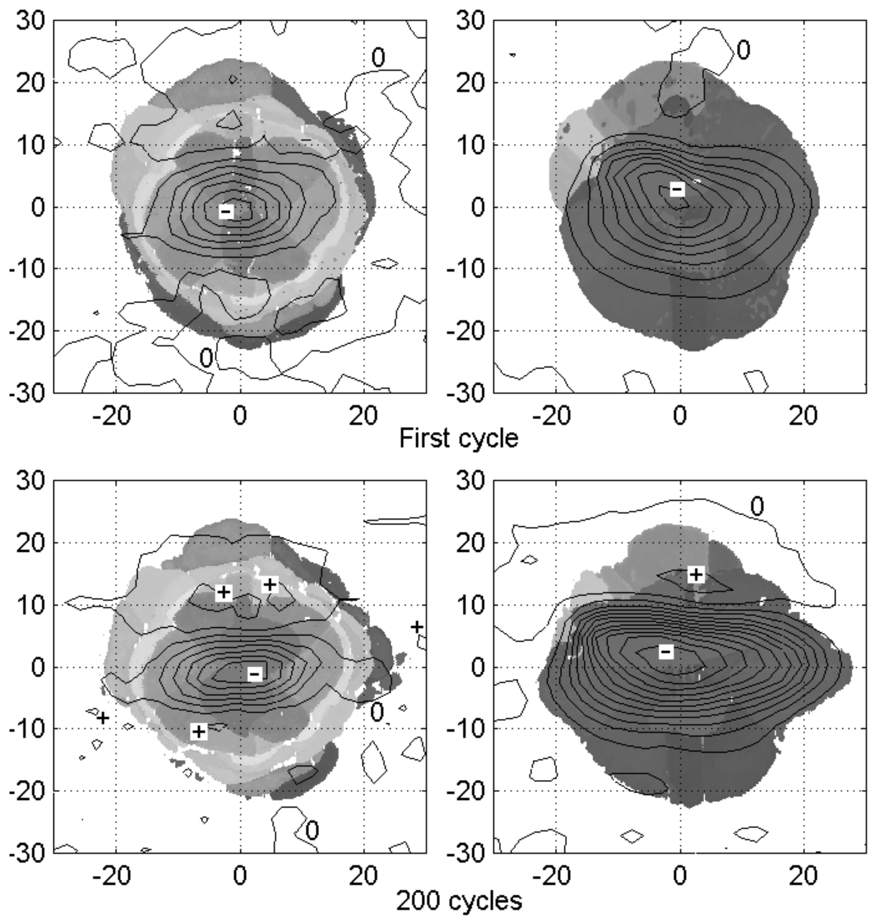

Figure 60. DSP-measurements of z-displacement superposed to C-scan maps for a quasi-isotropic specimen. Left column: frontside, right column: backside. The specimen failed after 230 cycles.

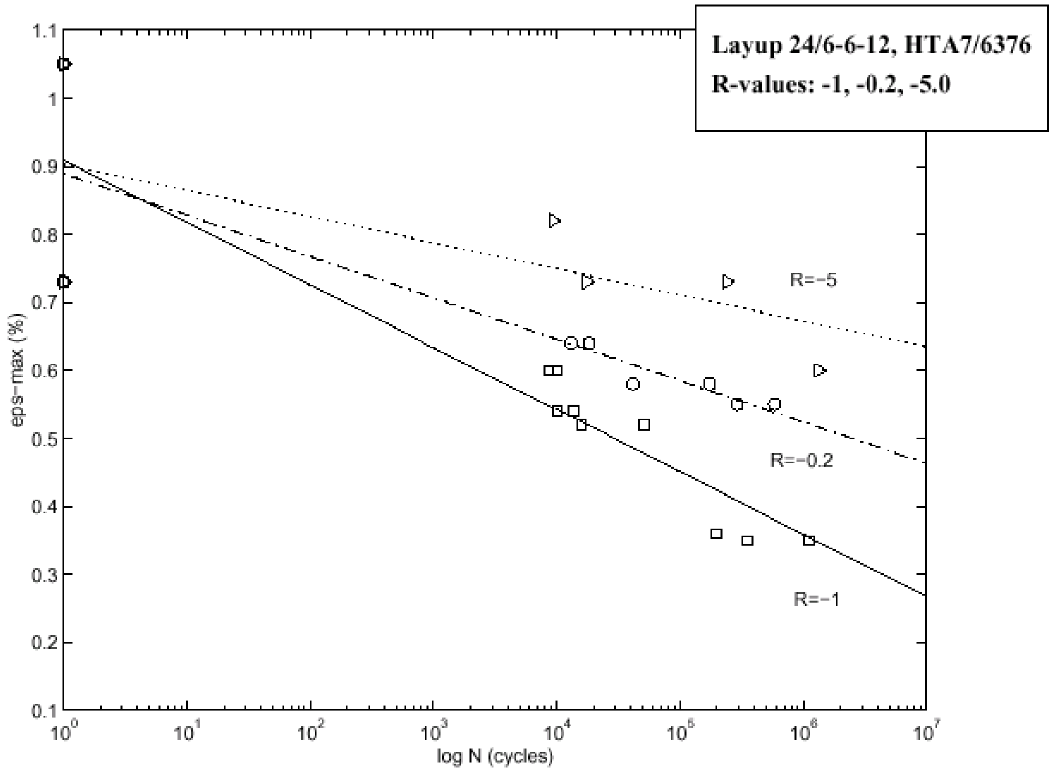

Figure 61. Fatigue testing of bolted joints at constant amplitude loading, R=-1, 0.2 and -5.

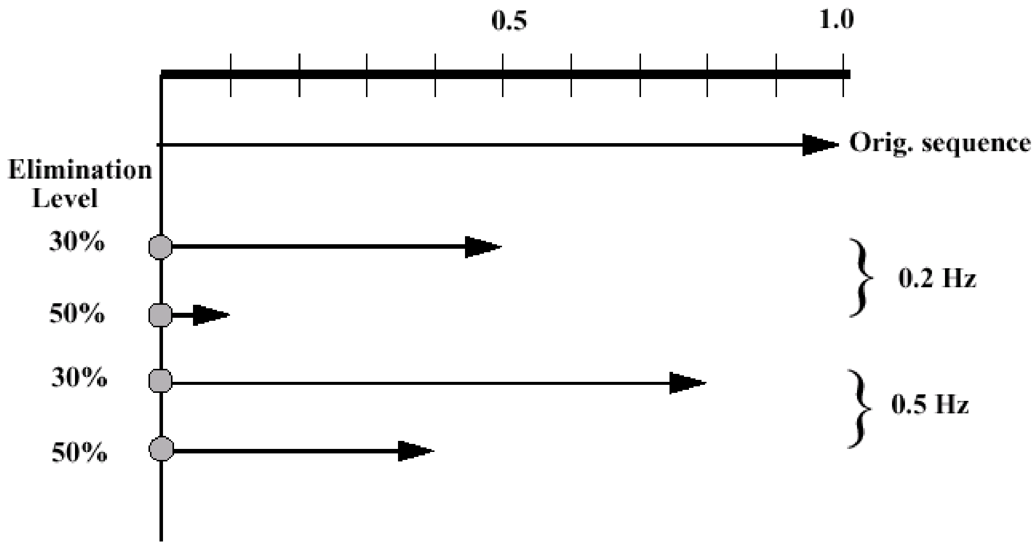

Figure 62. Reduction in normalised time depending on frequency and elimination level.

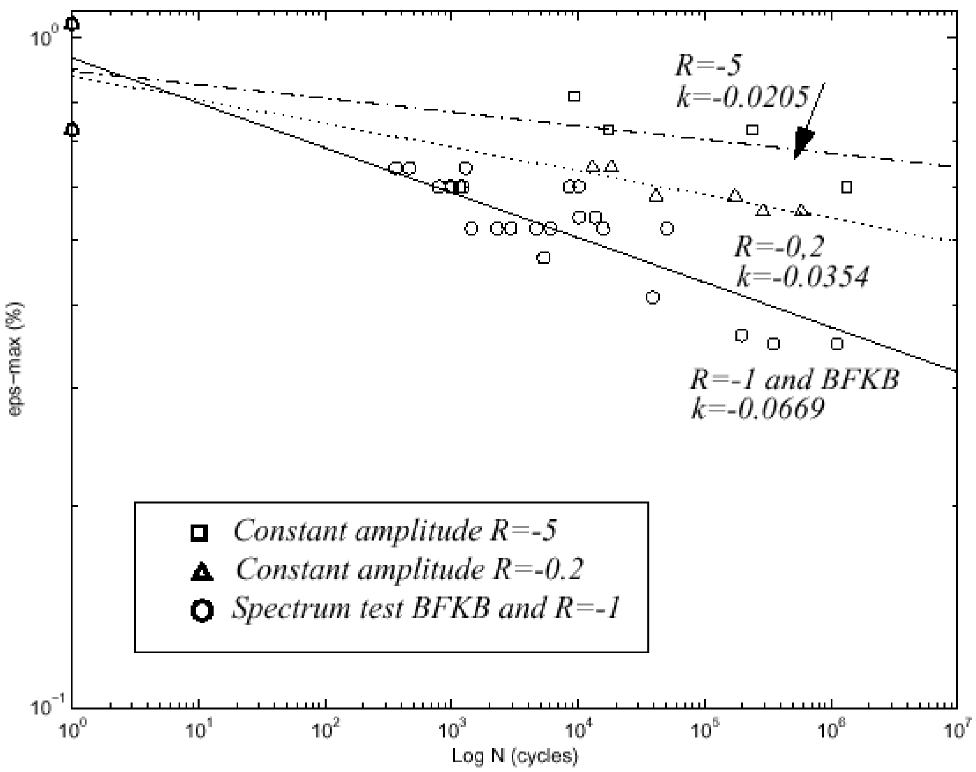

Figure 63. Determination of the slope for all test results, constant amplitude and spectrum loading also covering elimination for bolted joints.

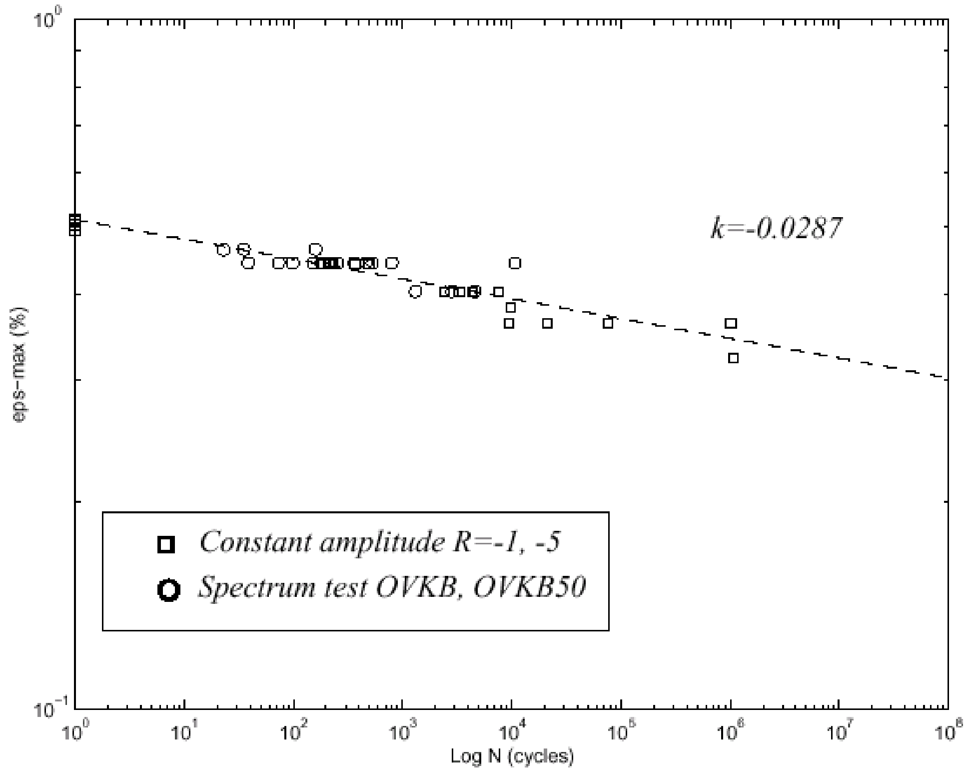

Figure 64. Determination of the slope for all test results, constant amplitude and spectrum loading including testing with elimination for FAI-specimens.

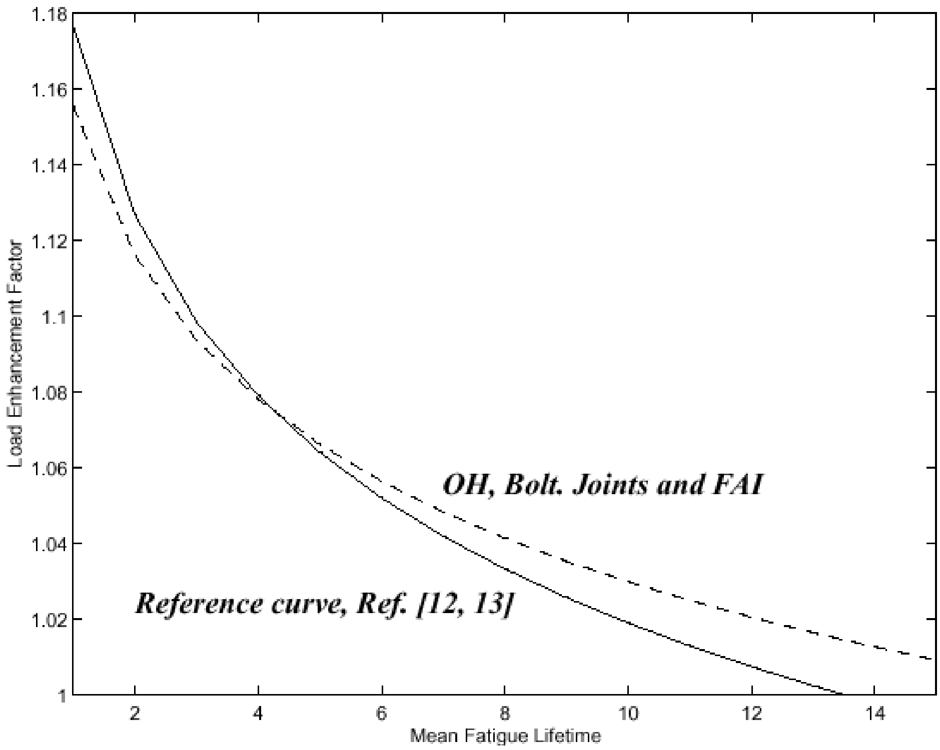

Figure 65. Load enhancement factor as function of mean fatigue test time. All test results included but with a limited data base. Reference curve, Ref. [32, 33].

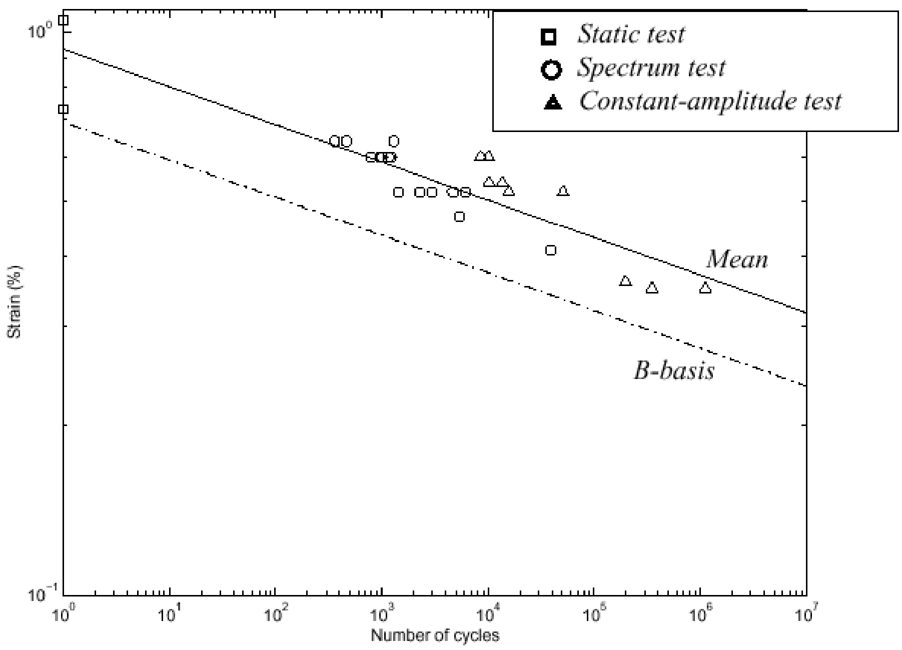

Figure 66. Strain as function of cycles for bolted joints specimens, Sendecky model Ref. [30].

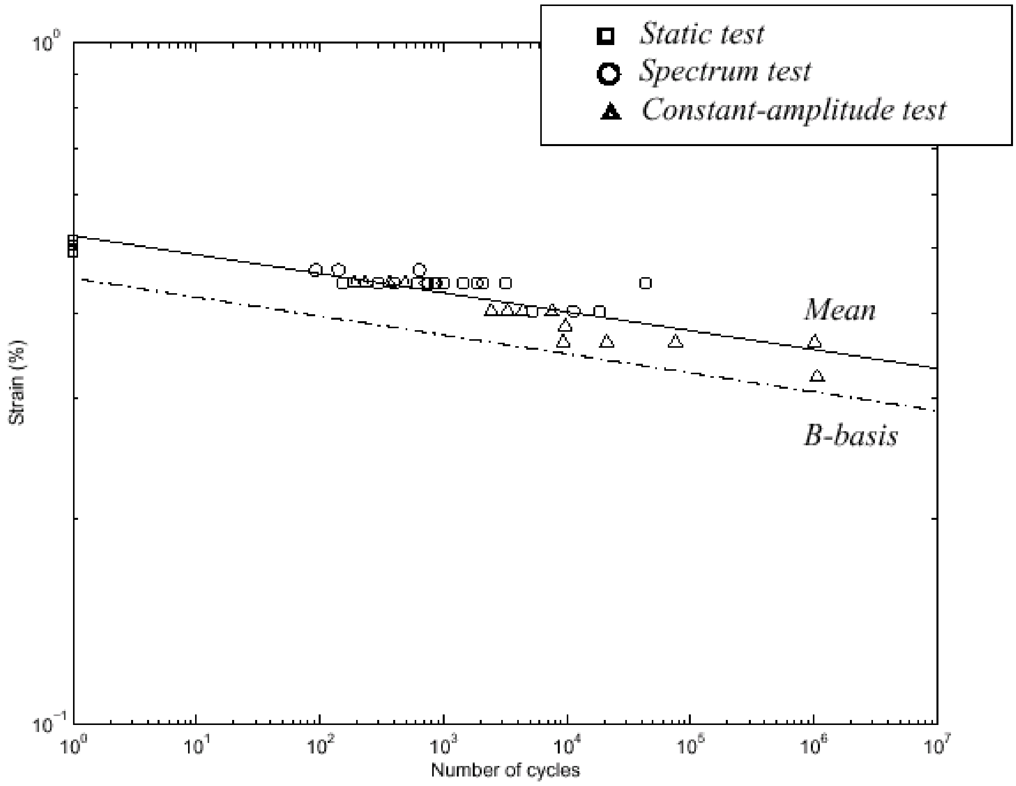

Figure 67. Strain as function of cycles for FAI-specimens, Sendecky model Ref. [30].

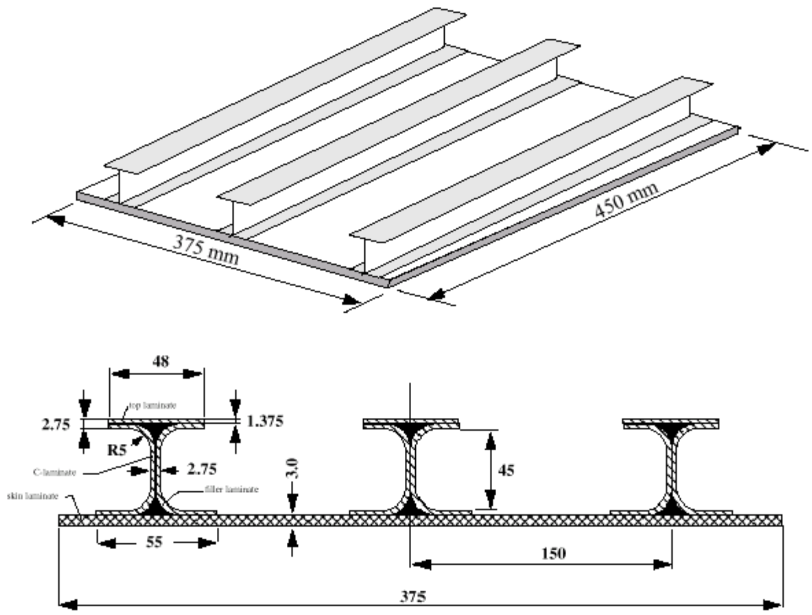

Figure 68. General overview of the EDAVCOS stiffened wing panel.

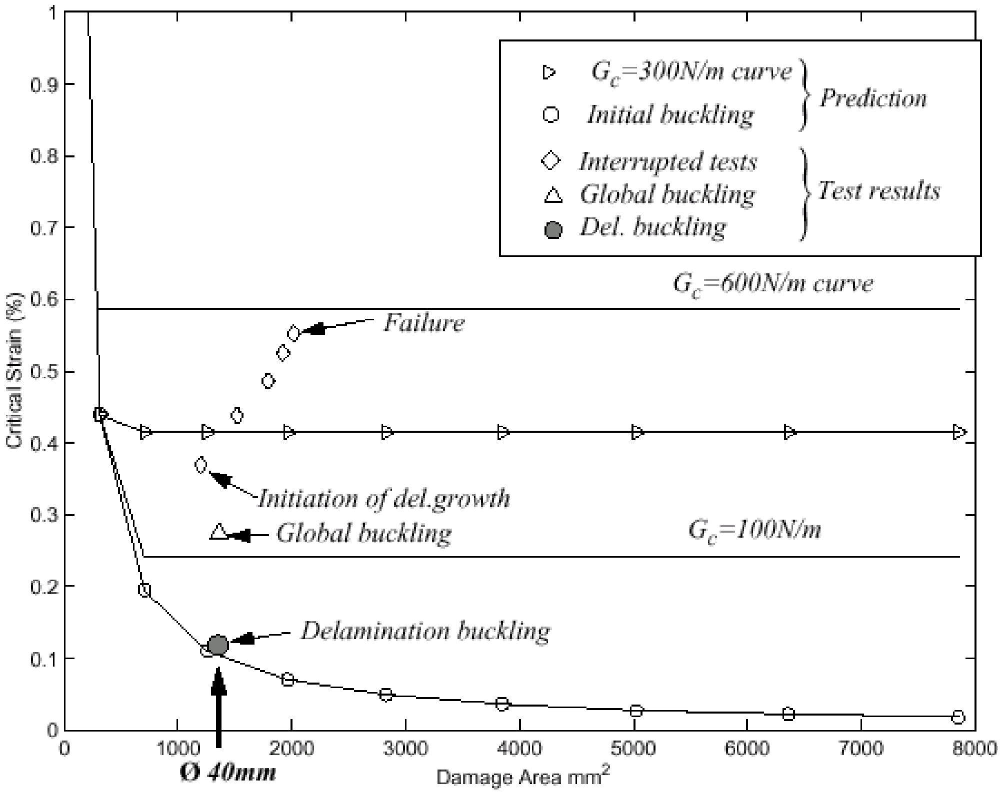

Figure 69. Comparison of predicted and experimental residual strength for panel SFN3 with an artificial defect, Ref. [35].

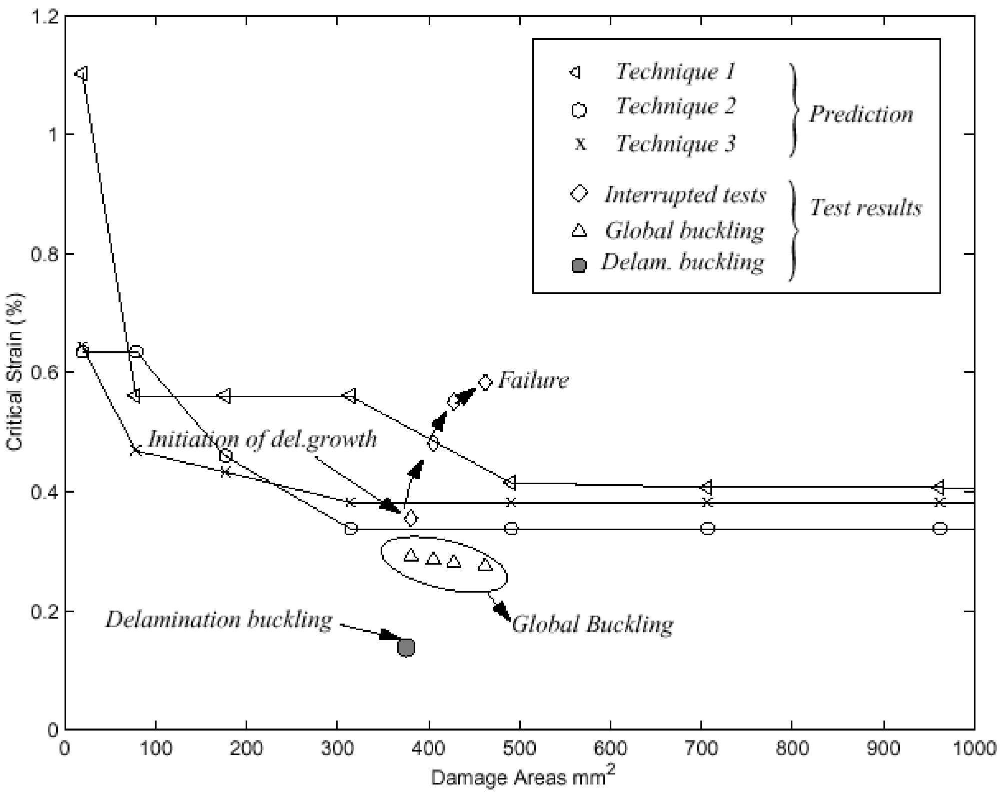

Figure 70. Prediction of impact strength for the EDAVCOS panel SFN1, Ref . [35].

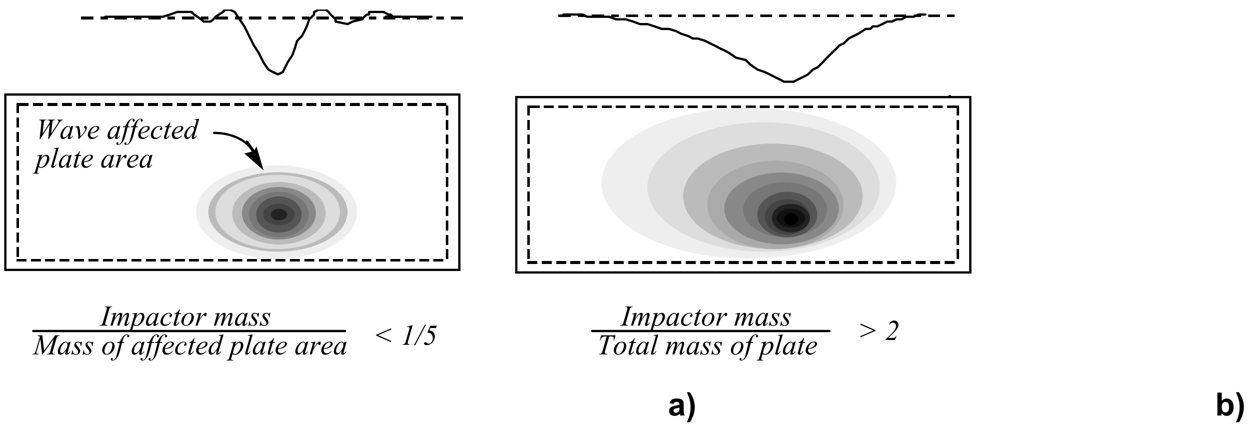

Figure 71. Mass criteria for response types in impacted plates.

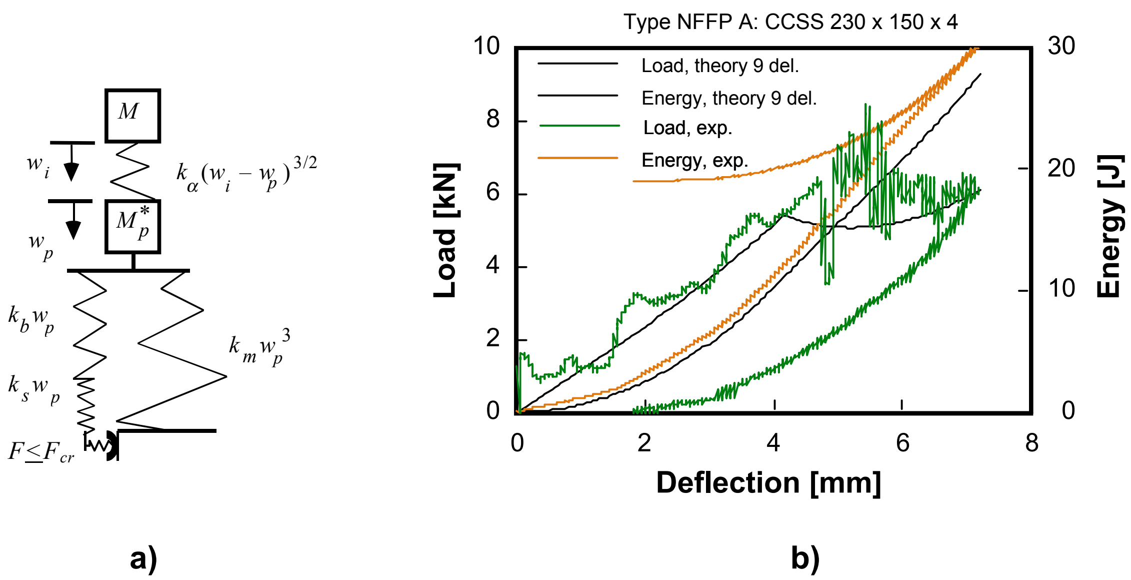

Figure 72. Model for large mass impact and comparison between predictions and experiments.

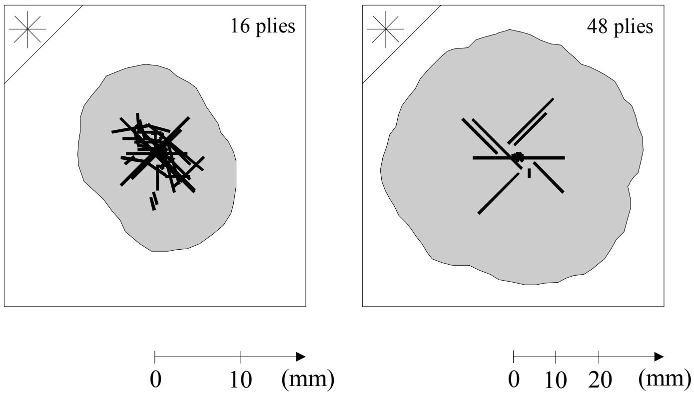

Figure 73. Projected delamination area and fibre damage in two quasi-isotropic laminates.

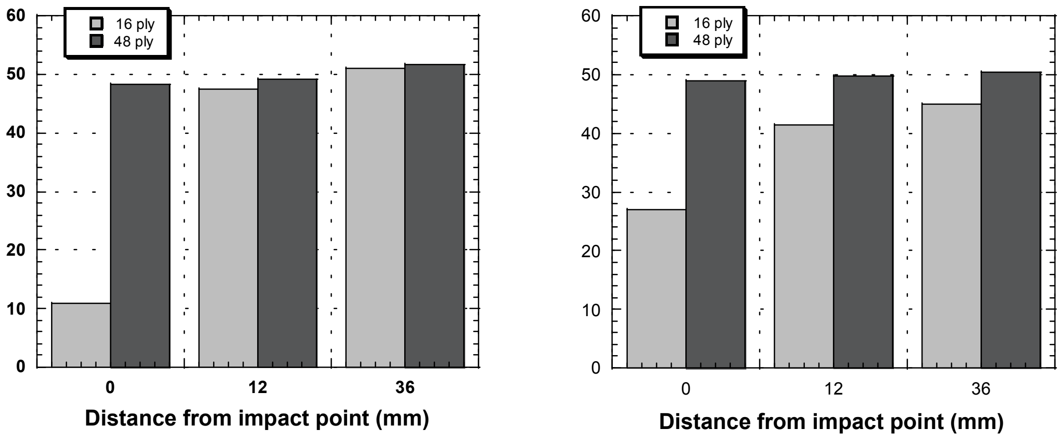

Figure 74 Measured axial modulus as a function of distance from the impact point.

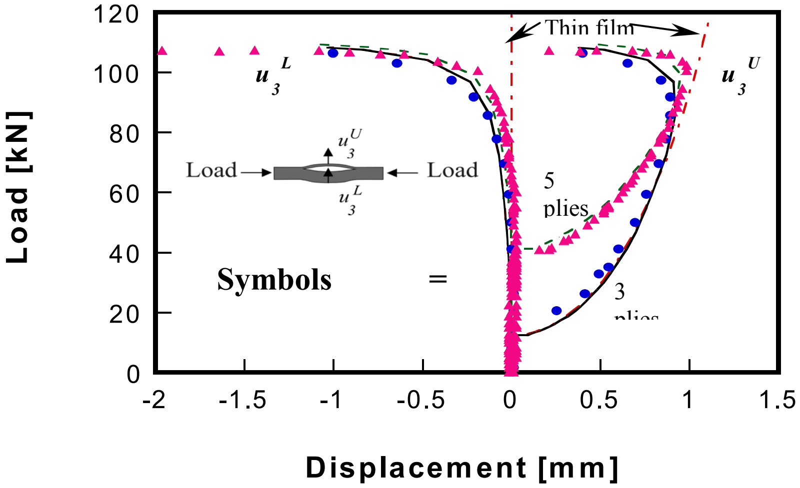

Figure 75. Predicted and measured load during buckling with delaminations at two depths.

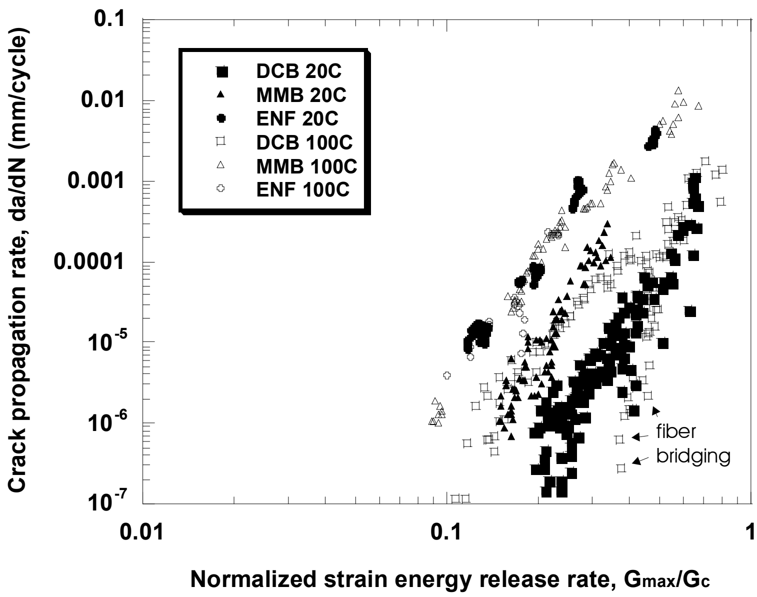

Figure 76. Crack propagation rates for delamination growth in fatigue.

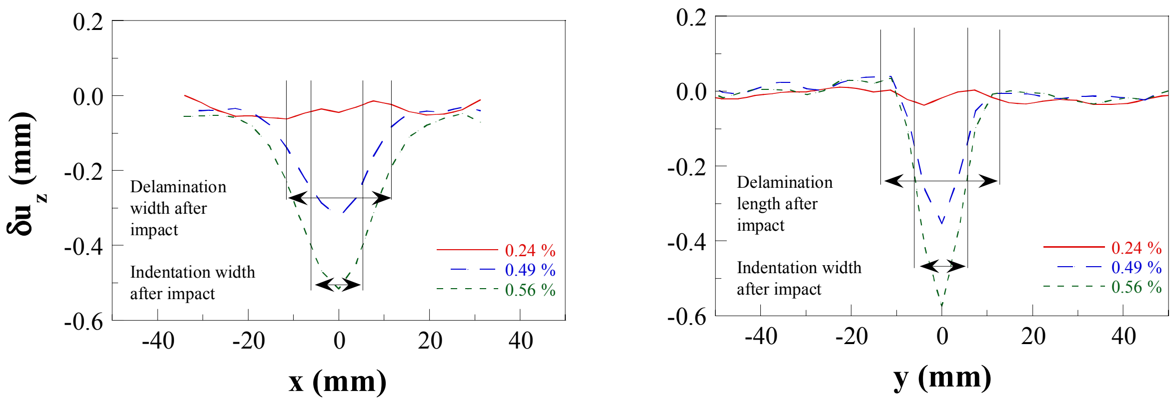

Figure 77. Indentation depth, δu_z, during compressive test of a panel with Nomex core and 1 mm face thickness. x-axes transverse the load direction.

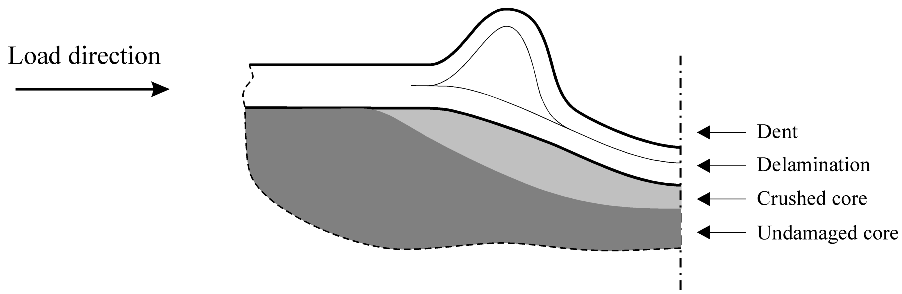

Figure 78. Sketch of delamination buckling.

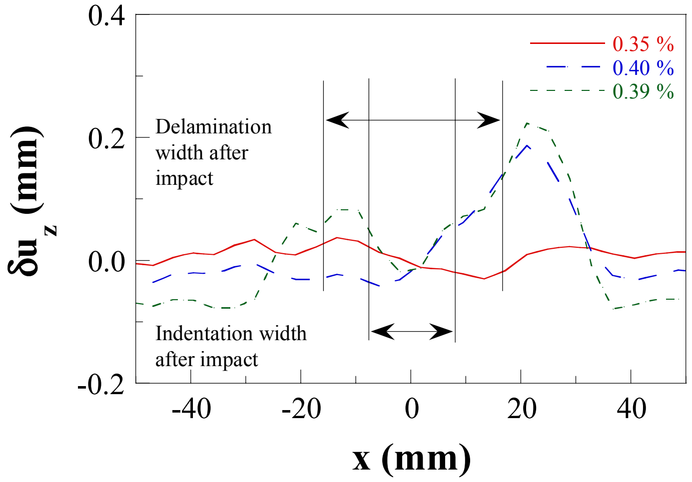

Figure 79. Delamination buckling at a line 10 mm above the centre of the indentation, δu_z, during compressive test of a panel with Nomex core and 1 mm face thickness.

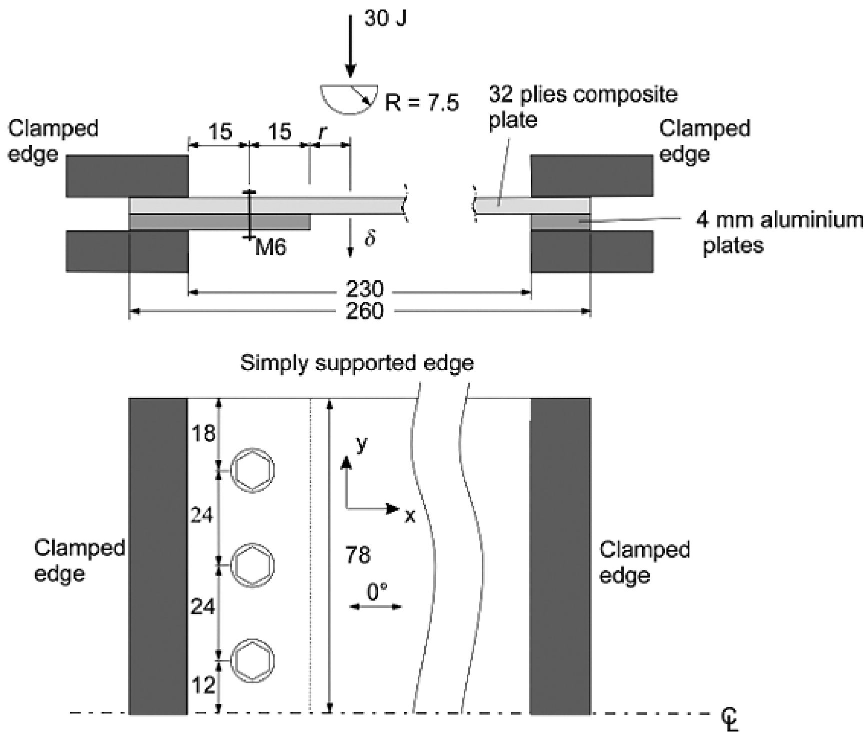

Figure 80. Bolted joint impacted with 30 J.

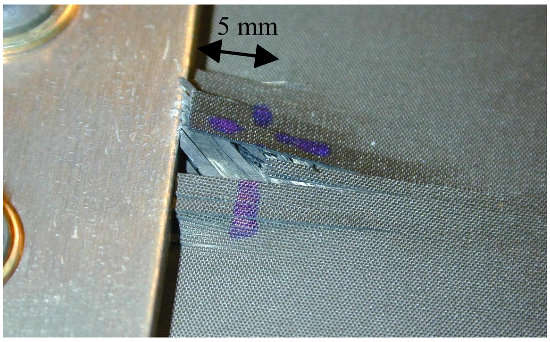

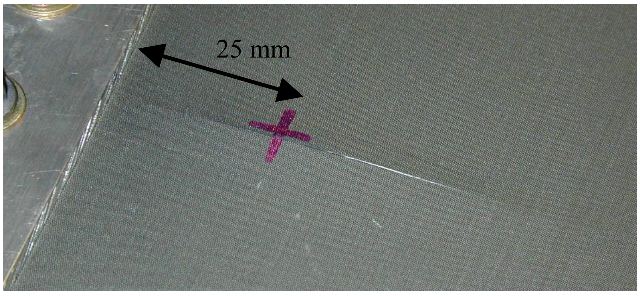

Figure 81. Damage on the back face after impact with r = 5mm and r = 25 mm respectively.

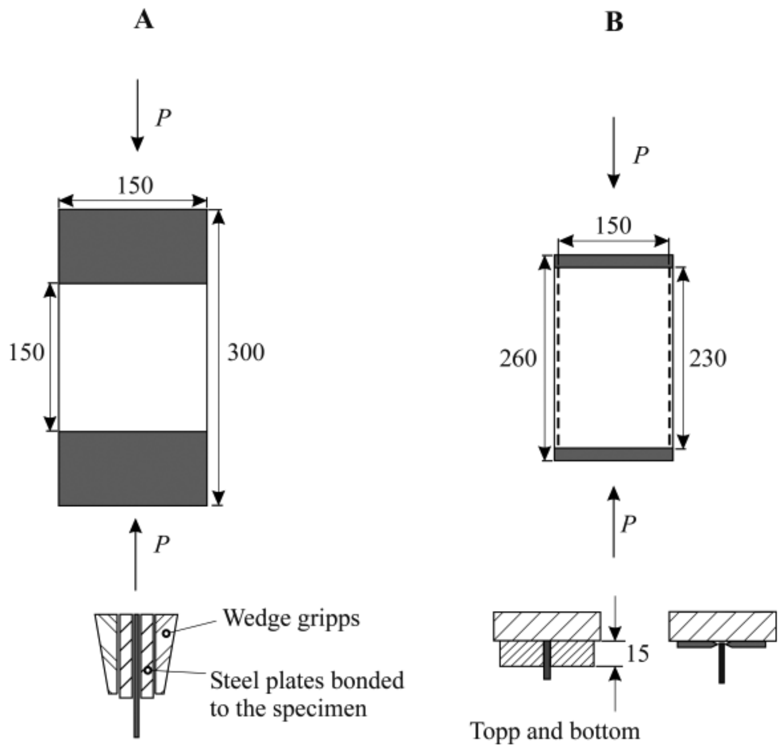

Figure 82. Specimen dimensions and boundary conditions.